



JOHANNES KEPLER

Universität Linz

Netzwerk für Forschung, Lehre und Praxis



Sensitization of Low Bandgap Polymer Bulk Heterojunction Solar Cells

DIPLOMARBEIT

zur Erlangung des akademischen Grades

DIPLOMINGENIEUR

in der Studienrichtung

Technische Chemie

Angefertigt am Linzer Institut für Organische Solarzellen LIOS

Betreuung:

Prof. Dr. Serdar Niyazi Sariciftci

Eingereicht von:

Christoph Winder

Mitbetreuung:

Dr. Christoph Brabec

Linz, September 2001

I want to thank all the people who supported and helped me to prepare this work:

- All the member of the “Linzer Institut for Organic Solar Cells” LIOS, Andrej Andreev, Elif Arici, Eugen Baumgartner, Antonio Cravino, Harald Hoppe, Markus Koppe, Maria Antonietta Loi, Gebhard Matt, Dieter Meissner, David Mühlbacher, Helmut Neugebauer, Markus Scharber, Niko Schultz and Gerald Zerza, all of them for many fruitful discussions and suggestions
- The staff of QSEL Patrick Denk, Franz Padinger and Roman Rittberger for pleasant atmosphere in the laboratory and the good collaboration.
- Specially my supervisors Dr. Christoph Brabec and Prof. Serdar N. Sariciftci for their great support and helpful advices
- The international collaborators, who provided the materials, A. Dhabanalan and R. Janssen from the TU Eindhoven, I. Perepichka and J. Roncali from the univertité d’ Angers, H. Meng and F. Wudl from the University of Los Angeles and J.K. Hummelen from the University of Groningen.

Personally I want to thank my family for their support during my studies.

Thank You

*I dedicate this work to my wife
Tatjana
And thank her for her personal support.*

Abstract

For increasing the power conversion efficiencies of polymer based solar cells, efficient harvesting of the terrestrial solar spectrum is necessary. In this work, two approaches are presented. Firstly, low bandgap polymer, with bandgaps < 1.8 eV, are used for a better match of the solar spectrum. Secondly, the admixture of small molecule dyes into the photoactive polymer matrix increase the amount of absorbed light.

Low bandgap polymers and their photophysical interaction with a fullerene type electron acceptor are characterised by a combined spectroscopic and device study.

Sensitization of low bandgap solar cells with organic dyes and conjugated polymer is demonstrated. Possible sensitization mechanisms are discussed.

Pristine low bandgap polymer solar cells as well as sensitized solar cells are characterised by I-V and photocurrent measurements. The device performance is analysed in terms of schematic energy level diagrams and diode response.

Zusammenfassung

Für höhere Effizienzen polymerbasierender Solarzellen wird ein effektives Einfangen des irdischen Sonnenlichtes benötigt. In dieser Arbeit werden zwei neue Zugänge präsentiert. Erstens, Polymere mit Bandlücken kleiner 1.8 eV führt zu einer besseren Überlappung mit dem Sonnenspektrum. Zweitens, die Zumischung organischer Farbstoffe erhöht die Lichtabsorption.

Die Polymere und ihre Wechselwirkung mit fulleren-basierenden Elektronenakzeptoren wird sowohl spektroskopisch als auch in Solarzellen Anwendungen untersucht.

Sensitivierungsmechanismen von Polymersolarzellen mit Polymeren und organischen Farbstoffen wird präsentiert.

Sensitivierte wie auch nichtsensitivierte Solarzellen werden mittels I-V und Photostrommessungen charakterisiert. Die Leistungsparameter der Solarzellen werden anhand von Energiediagrammen und des Diodenverhaltens diskutiert.

TABLE OF CONTENTS

1	INTRODUCTION	4
1.1	MOTIVATION.....	4
1.1.1	<i>Necessity of alternative energy sources</i>	<i>4</i>
1.1.2	<i>Advantages of Organic Semiconductors</i>	<i>5</i>
1.1.3	<i>Limitation of Today's Polymer Solar Cells – Necessity of Low Bandgap Polymer and Dyes</i>	<i>5</i>
1.2	ORGANIC SOLAR CELLS	6
1.3	PRINCIPLES OF BULK HETEROJUNCTION SOLAR CELLS.....	8
1.4	BANDGAP ENGINEERING	16
1.5	SENSITIZATION OF SOLAR CELLS –ANTENNA EFFECT	21
2	EXPERIMENTAL	25
2.1	MATERIAL CHARACTERIZATION	25
2.2	DEVICE PREPARATION.....	26
2.3	DEVICE CHARACTERIZATION	28
3	MATERIAL SCREENING - RESULTS AND DISCUSSION	30
3.1	PEDOT- DERIVATIVES.....	30
3.1.1	<i>pEDOT-C10</i>	<i>31</i>
3.1.2	<i>pEDOT-DOP.....</i>	<i>35</i>
3.2	ISOTHIONAPHTALENE-DERIVATIVES.....	39
3.2.1	<i>EHI-PITN</i>	<i>40</i>
3.2.2	<i>PME-EHI-PITN.....</i>	<i>43</i>
3.2.3	<i>pEDOT-EHI-ITN.....</i>	<i>46</i>
3.3	PTPTB.....	49
4	SENSITIZATION OF SOLAR CELLS – RESULTS AND DISCUSSION.....	60
4.1	SENSITIZATION WITH MDMO-PPV	60
4.2	SENSITIZATION WITH NILE RED	64
5	GENERAL DISCUSSION.....	72

6	CONCLUSION	75
7	REFERENCES	77
	CURRICULUM VITAE	82
	LIST OF PUBLICATIONS	84

1 Introduction

1.1 Motivation

1.1.1 Necessity of alternative energy sources

Mankind is still searching for reliable, cheap and environmentally friendly energy sources. The classical energy sources cannot provide these requirements for the future any more. The fossil energy sources coal, oil and gas cause air pollution and climate problems. Carbon dioxide, the final product of the combustion of all organic materials, is known to influence earth climate significantly. Also, the stock of these carbon-based fuels is limited and thought to run out in roughly 50 years [1].

The use of nuclear power as energy source is not accepted by wide section of the population any more because of security and health risk. Further, the disposal of nuclear waste is still an unsolved problem, worldwide.

Over the last decades, there have been big efforts for developing new, alternative energy sources.

The sun, on the other hand, matches all requirements of an ideal energy source. It is reliable, ubiquitous and for free. The nature uses the sun as its nearly only energy source in photosynthesis since millions of years.

The direct conversion of sunlight into electricity by photovoltaic cells is known for many years. Monocrystalline silicon and galliumarsenide devices exceed efficiencies of 24 % energy conversion [2] of the terrestrial sunlight, but the production costs are too high for economic use in widespread energy production. Thin film technique should reduce material consumption and production costs. Typical materials, which are used in thin film photovoltaic devices, are inorganic semiconductors like amorphous and polycrystalline silicon, cadmium telluride and copper indium diselenide. Generally, all these inorganic semiconductors need high temperature operations in their production, which causes high cost, and are difficult to handle.

1.1.2 Advantages of Organic Semiconductors

Scientists and engineers are looking for new materials and systems. Organic semiconductors, including conjugated polymers, are promising materials for solar cells. They are cheap in production and purification. Furthermore, organic chemistry can tailor the materials for the demand. Organic devices are flexible, lightweight and easy to produce [3]. Polymer procession is done by spin casting [4], doctor blading [5,6] has been successfully applied for solar cells preparation, ink-jet printing or of even roll-to-roll processing are well known techniques for polymer processing and could be principally used for device fabrication. All this techniques are done at room temperature.

1.1.3 Limitation of Today's Polymer Solar Cells – Necessity of Low Bandgap Polymer and Dyes

Despite recent reports on improved efficiencies [7,8,9], current limitation of polymer solar cells is still their low efficiency and the limited lifetime of the devices. This work will mainly deal with efficiencies. Whereas the open circuit voltage V_{OC} and the fill factor FF are in the range of inorganic solar cells, the short circuit current I_{SC} is nearly a factor ten lower. The FF describes the cell at the maximum power point, for its definition see in the experimental part. The low I_{SC} is mainly caused by the low amount of absorbed light within the active layer. Light absorption is the primary step for conversion of light into electricity and the amount is p directly proportional to the I_{SC} . The low I_{SC} is mainly caused by the mismatch of the optical absorption of the used materials and the solar spectrum.

Figure 1.1 shows the terrestrial solar spectrum, AM1.5, and the integral spectral flux in comparison with the absorption spectrum of an MDMO-PPV/PCBM blend, which is used in the most efficient polymer solar cell today [8,10]. The maximum of the spectral flux is between 700 and 900 nm, whereas the MDMO-PPV/PCBM blend absorbs between 300 and 500 nm. Furthermore, the light absorption, measured in reflection geometry, is less than 50 %, even at wavelength of the MDMO-PPV maximum. Film thickness cannot be increased further at this moment because of the limited charge carrier mobility in this type of conjugated polymers.

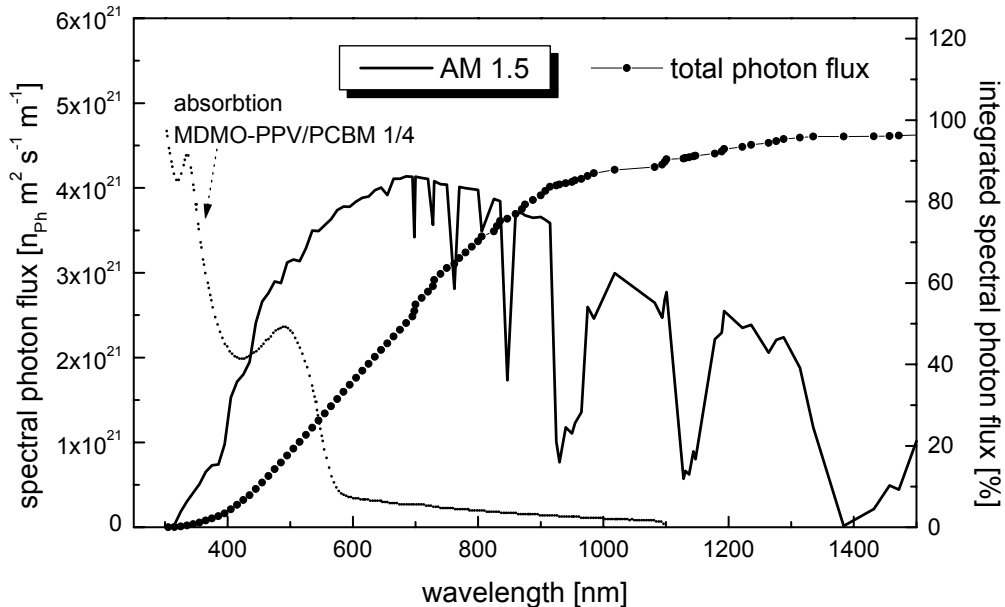


Figure 1.1: The terrestrial AM1.5 sun spectrum (—) and the integrated spectral photon flux (starting from 0 nm) (-•-) in comparison with the absorption of the active layer (---) of an MDMO-PPV/PCBM solar cell.

The aim of the presented work is to study two ways to overcome these limitations of polymer bulk heterojunction solar cells by two new approaches.

- (i) The usage of low bandgap polymers, i.e. polymers with a bandgap below 2 eV, which match the terrestrial solar spectrum better [10];
- (ii) The admixture of organic dyes with high absorption coefficients. Afterwards, the dye should transfer the absorbed energy to the low bandgap polymer [11]. The absorption coefficients of the dyes exceed the polymer one's. The light absorption can therefore be increased and the active layer can be made thinner.

1.2 Organic Solar Cells

Today, three different types of solar cells using organic molecules are existing: Dye sensitized nanocrystalline TiO₂ solar cells, molecular organic solar cells and polymer solar cells [3]. The highest efficiencies among these solar cells (11%) have been reported for the dye sensitized nanocrystalline TiO₂ solar cells, which are based on photo-electrochemical principles. It was originally invented by Gerischer and Tributsch [12], but it is named after M.

Grätzel, who reported the highest efficiency of 11 % using nanocrystalline TiO₂ to achieve high interface area electrodes [13].

Molecular Organic Solar Cells use organic dyes [14]. The active layers are cast by vacuum evaporation techniques. The organic dyes show high absorption coefficients and a good match of the solar spectrum. But their efficiencies are limited by the low exciton diffusion length and the low charge mobility of the materials. Efficiencies of 1 % were already achieved in 1986 by Tang, using copper-phthalocyanine and a perylene-tetracarboxylic derivative [15]. Doping with C₆₀ could slightly improve the power efficiencies [16]. Recently, the use of doped pentacene, which shows much higher mobilities, pushed up the efficiencies up to 2 % for thin film and 4.5 % for single crystalline devices [17,18,19].

The third type of organic solar cells, the polymer solar cells, should be discussed in more details since they are the basis for this work. Pristine polymer cells, sandwiched between asymmetric contacts, show low efficiencies because the inefficient charge generation in the polymer layer [20,21]. The discovery of the photoinduced charge transfer from π -conjugated polymer to fullerene [22,23] opened a new way for solar cells and photodiodes [24]. The efficiency for this process is near unity, i.e. this process is much faster than any competing radiative and non-radiative relaxation pathways. Bilayer devices from conjugated polymers and C₆₀ fullerene shows improved efficiencies. But as for molecular cells, only the light absorbed within the distance of the diffusion range of excitons to the heterojunction contributes to the current [25].

A breakthrough for polymer solar cells was the introduction of the bulk heterojunction [26,27]. Mixing of the conjugated polymer and C₆₀, respectively a better soluble derivative of fullerenes [28], leads to a three-dimensional heterojunction and therefore to efficient charge generation within the whole bulk. Very soon, power efficiencies up to 1 % could be reached. Morphology [29,30,31] and improving the electrical contact interfaces have been shown to be crucial parameters for device efficiencies. Intensively engineering and improvement of the contacts pushed up the power efficiency over 3 % [8,9,10].

1.3 Principles of Bulk Heterojunction Solar Cells

Three steps are essential for the conversion of light into electricity, how it is done by solar cells [32]:

- (i) absorption of light,
- (ii) charge carrier generation
- (iii) and selective transport of the opposite charges to the opposite contacts.

The general principles are the same for all solar cells, but should here be described in reference to polymer -fullerene solar cells.

Light with an energy $\hbar\omega \geq$ the band gap E_g can excite electrons over the bandgap from the valence band to the conduction band. In conjugated polymer, this excitations are the π - π^* or HOMO-LUMO [33] excitations. These excited electrons can be converted to current. Hence, the amount of absorbed light is directly related to the short circuit current. Absorption spectrum and thickness of the active layer are the important parameter. The thickness cannot be increased over a certain limit because of the limited mobility of the charge carriers.

The charge carrier generation takes place at interfaces, either at p-n junctions or Schottky junction. P-n junctions are typically polymer-polymer or polymer-fullerene blends, Schottky junctions are semiconductor-metal interfaces. Only the light absorbed at the depletion layer of the interface or the exciton diffusion range of the material to the junction can create charge carriers.

The photoinduced charge transfer from conjugated polymer to fullerene is an efficient way for charge generation [34]. For a schematic picture is shown in figure 1.2. The photoinduced charge transfer at polymer fullerene interfaces has been shown to happen in the subpicosecond range. Newest results even show a time constant of 15 fs [35]. This process is much faster than any radiative or non-radiative relaxation pathways for excitation in conjugated polymers and its quantum efficiency is therefore near unity.

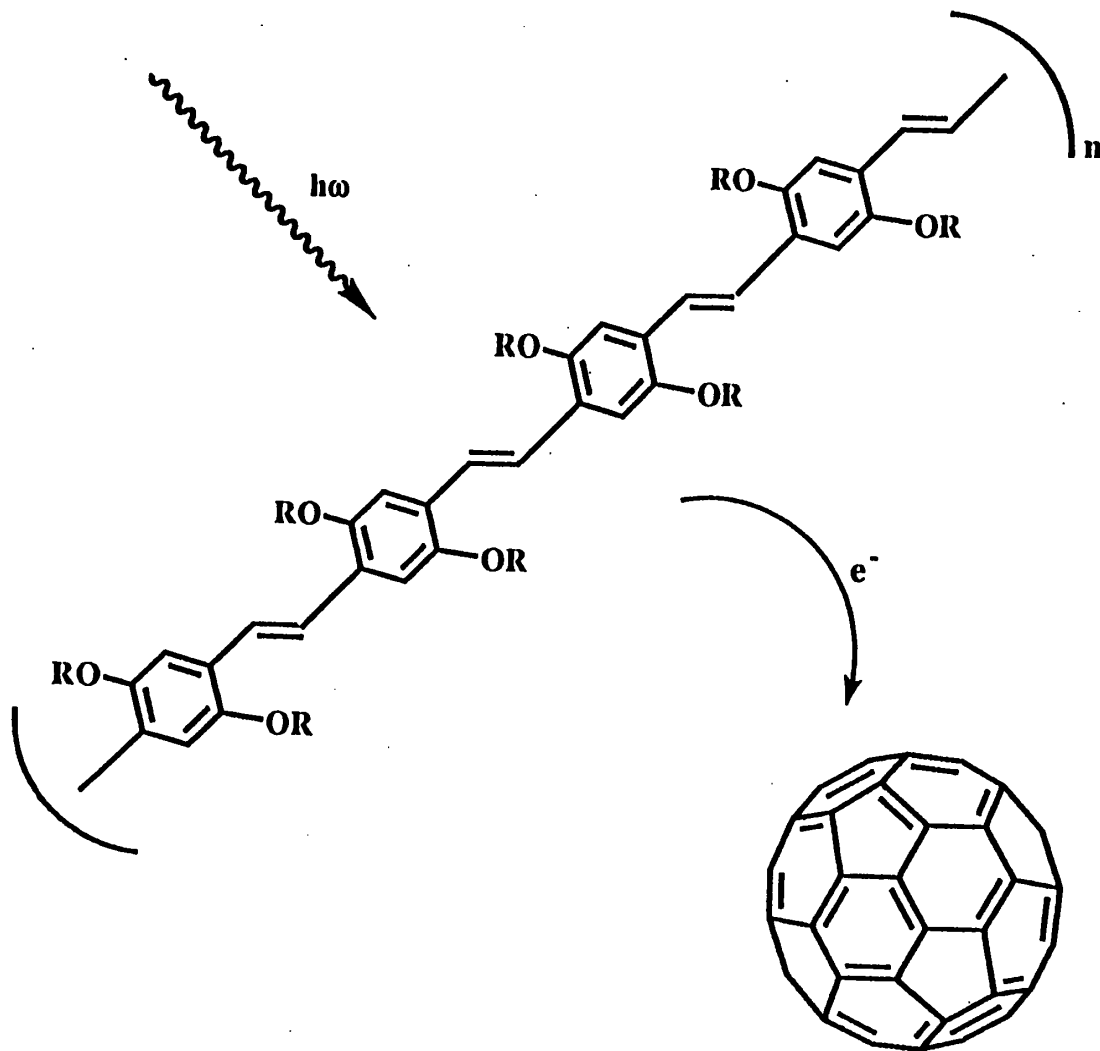
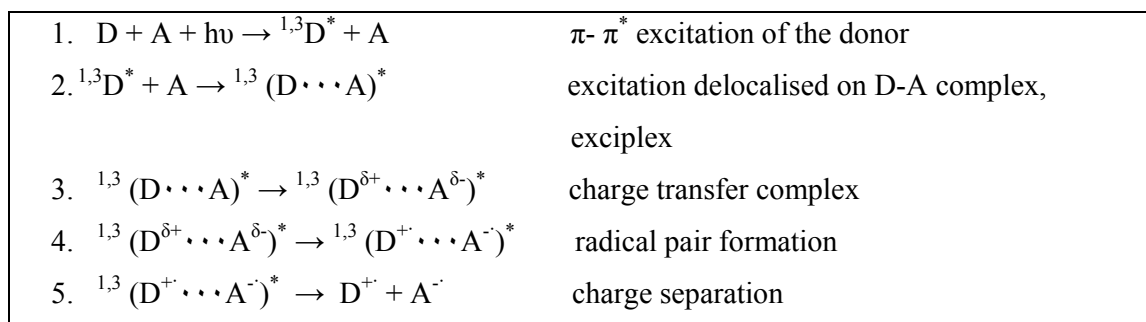


Figure 1.2: Photoinduced charge (electron) transfer from photoexcited PPV to C₆₀ fullerene

The charge transfer takes place in a multistep process as described by the scheme 1.1.



Scheme 1.1: Reaction cascade for ultra fast electron transfer from a donor (π -conjugated polymer) to an acceptor (fullerene derivative); the corresponding hole transfer from an acceptor to a donor takes place in similar steps.

D and A are donor and acceptor, respectively. The indices 1,3 denote singlet and triplet excited states.

From thermodynamic principles, it is necessary that the ionisation potential of the excited donor state I_D^* is lower than the electron affinity of the acceptor and the coulombic interaction between the charge separated states, see equation 1.1.

$$I_D^* - A_A - U_c \leq 0 \quad 1.1$$

The I_D^* can be estimated by the inverse electron affinity. Energetically, this simply means that the donor LUMO lies above the acceptor LUMO, neglecting the coulombic interaction.

The back transfer is slow. The charges are therefore metastable and show lifetimes up to the millisecond range at 77 K [36]. The corresponding hole transfer from photoexcited fullerene to polymer takes place after the same principles.

The ultrafast charge transfer is a good biomimetic model for the primary photoexcitation in green plants. Whereas in photosynthesis the light energy is converted into chemical energy, solar cells are intended for the generation of electricity.

In the third step, the created charges have to be transported selectively to the contacts. The holes are transported by the polymer to the ITO contact and the electrons to the Al. Conjugated polymers show high mobilities along the chains, but the mobility is limited by the hopping between the chains. The electrons are transported by the fullerene via a hopping

process. The most efficient charge separation is found for a cell containing 80 % fullerene [8,32]. Similar values are found for polymer solar cells with perylene acceptors [37,38]. For charge generation, a few percent would be sufficient. But the interconnection of all acceptor molecules in the bulk is of importance for efficient charge collection. Isolated fullerene molecules or clusters are charge traps and the electrons are captivated there.

An easy and good model to describe a polymer diode is the metal-insulator-metal diode (MIM), introduced by Parker for light emitting diodes [39]. The polymer is assumed to have a negligible amount of intrinsic charge carriers and can therefore be seen as an insulator. It should be pointed out here, that this assumption is insufficient under illumination. For the contacts, tunnelling injection diodes are assumed.

Figure 1.3 shows a pristine polymer device under different working conditions within the MIM picture. Figure 1.3a shows short circuit case, where photo created holes are transported to the ITO contact electrons the Al. The driving force for the separation is the electric field across the polymer layer. The electric field is constant over the whole layer and is provided by work function difference of the contacts. Under open circuit conditions and illumination, this case is shown in figure 1.3b, the created charges show no preferred direction. The open circuit voltage cancels the potential difference of the contacts. The maximal observed open circuit voltage V_{oc} should be the workfunction difference between the two contacts. In the case of ITO and Al it should be roughly 0.4 V.

In the case of a negative applied bias, i.e. positive contact to the Al and negative contact to the ITO, the diode works as photodetector [40,41,42]. It is presented in figure 1.3c. Photoinduced charges are selectively transported, assisted by the external field, to the contacts, holes to the ITO and electrons to the Al. Polymer diodes are known as very sensitive photodiodes. As example, polythiophenes show quantum yields of 80 % under -15 V bias [43].

Under forward bias, electrons are injected from the Al to the conduction band and holes from the ITO to the valence band. The observed net current is dominated by the recombination of the two charge carriers. If electrons and holes recombine radiatively, electroluminescence can be observed. This effect was observed first time for conjugated polymers in 1990 by the group of R. Friend in Cambridge [44]. This discovery induced a big research efforts over the last decade and polymer based LEDs are now on the step to the market [45].

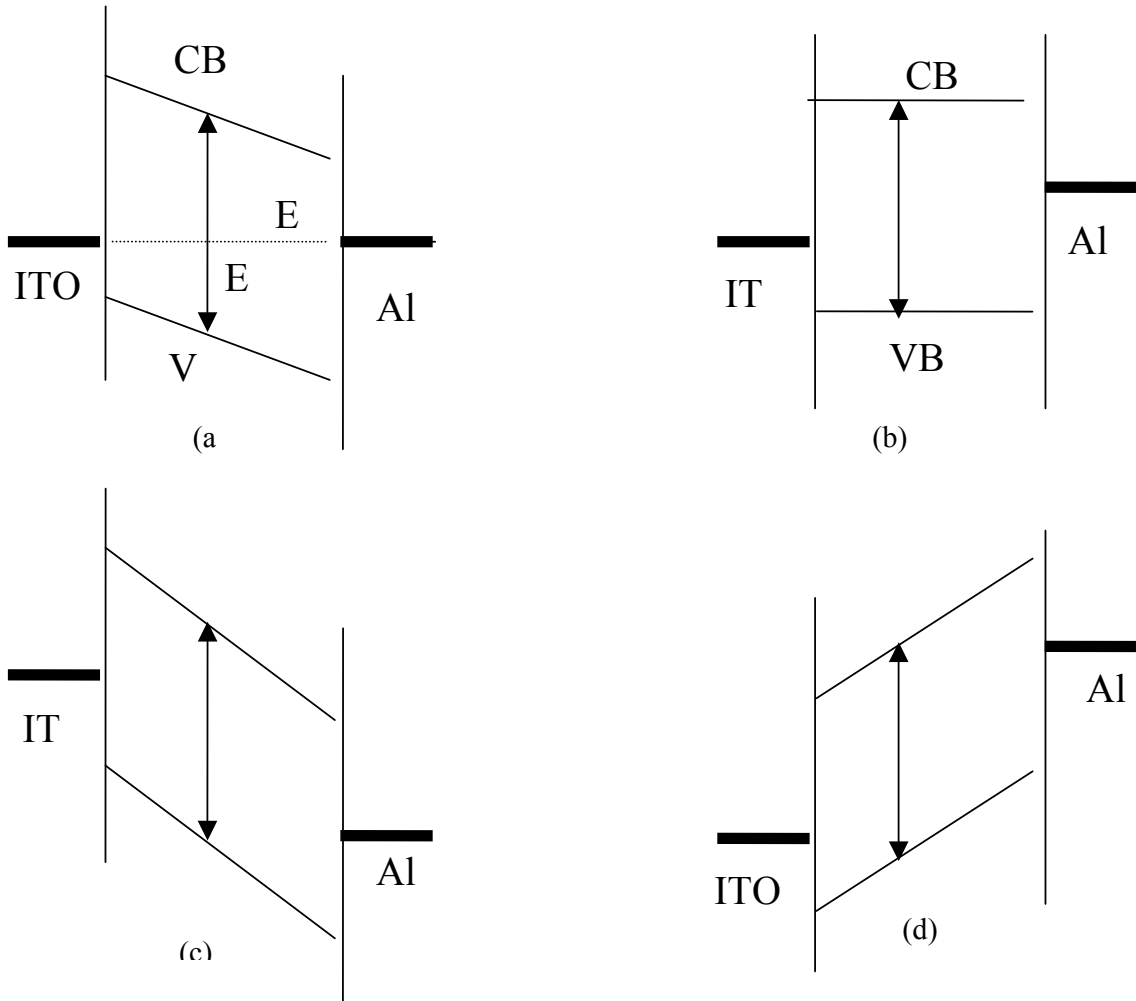


Figure 1.3: MIM picture for a polymer diode under different working conditions (a) short circuit, under illumination the holes are transported to the ITO contact, the electrons to the Al contact, (b) open circuit condition under illumination, the V_{OC} in the MIM picture is the workfunction difference between the two contacts, (c) diode under reverse bias, diode work as photodetector, and (d) diode under forward bias, diode can work as light emitting diode.

The MIM picture explains well the diode behaviour of the devices as well as the solar cell activity of single layer devices. However, in bulk heterojunction devices the observed V_{OC} of MDMO-PPV/PCBM device > 0.8 V is not in accordance with the work function difference of ITO and Al of 0.4.

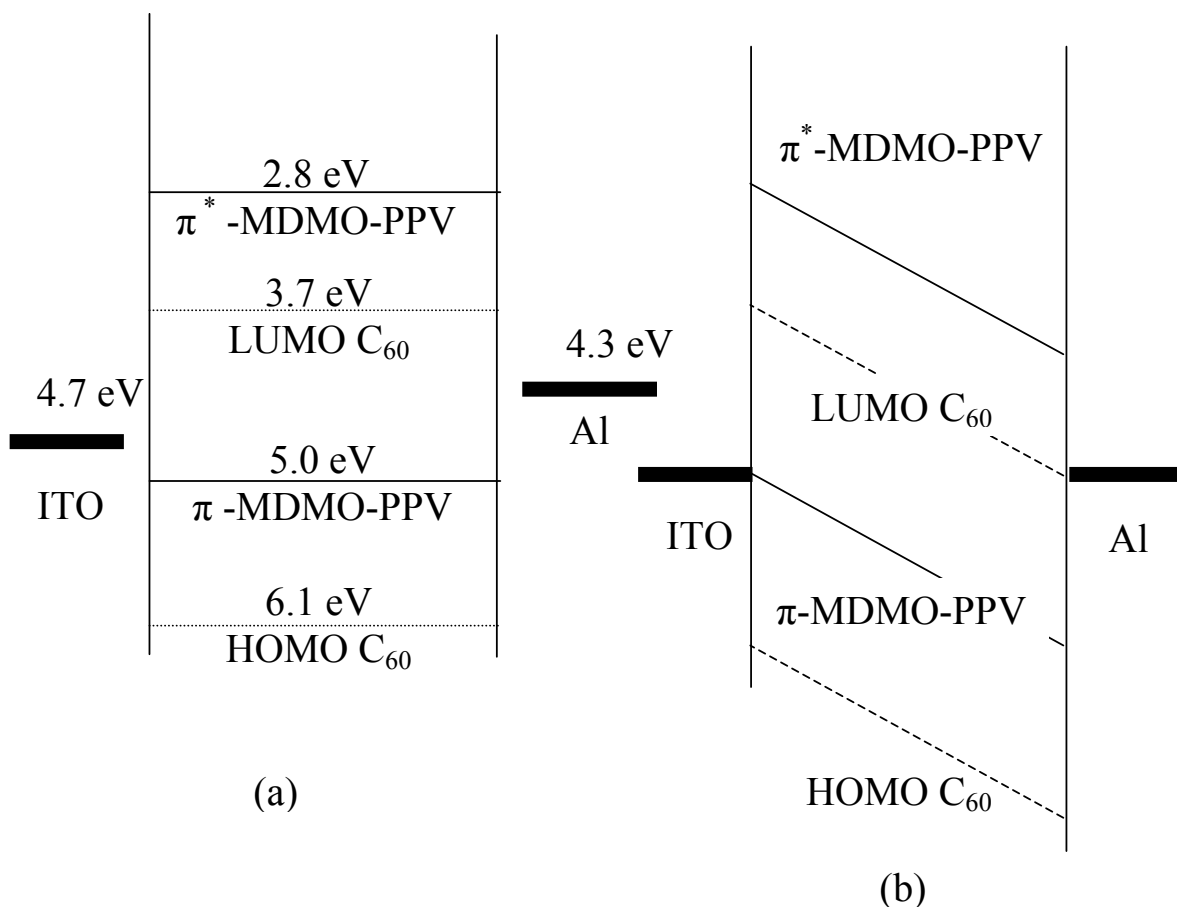


Figure 1.4: band diagram of a MDMO-PPV/PCBM bulk heterojunction under flat band conditions,(b) under short circuit conditions, assuming no interfacial layer at the metal contacts and pinning of the Al and ITO to the energy states of the polymer and C₆₀, respectively.

Latest results [46] show a slight dependence of the V_{OC} to the cathode metal workfunction. The open circuit voltage is varying 200 mV after changing the contact from Ca (2.8 eV), Al (4.3 eV) and even Au (5.2 eV) as cathode.

On the other hand, the open circuit voltage is highly dependent on the LUMO level of the acceptor. The metals seem to make an ohmic contact to the fullerene by Fermi level pinning to the LUMO level. For the anode, no such investigation are done up to now.

For classical p-n junction, the maximal open circuit voltage is the splitting of the quasi-fermi-levels of holes and electrons. In the case of a polymer fullerene cell, these levels can be estimated for the hole with the polaron level of the conjugated polymer and for the electrons the LUMO level of the fullerene. In figure 1.4, the energy levels of MDMO-PPV and PCBM are shown in a) flat band conditions and b) short circuit. In this picture, pinning of the metals to the corresponding fermi energies in the bulk is assumed. For a clear picture of action of a polymer/fullerene bulk heterojunction solar cell, further investigations have to be done.

Several improvements of the contacts have been done over the last several years.

On the anodic side, the ITO contact is improved with a thin PEDOT:PSS layer. It flattens the rough surface of the ITO contact and ensures good hole contact between polymer and ITO. On the cathodic side, a thin insulating layer of LiF is incorporated between the Al contact and the organic layer. This technique improves the efficiency of LEDs [47,48]. Increased power conversion efficiency could be recently also shown for polymer type solar cells [8,9]. In both cases, the devices show improved diode behaviour. The underlying mechanism is still under investigation.

Figure 1.5 shows the equivalent circuit for a solar cell, modelled with one diode.

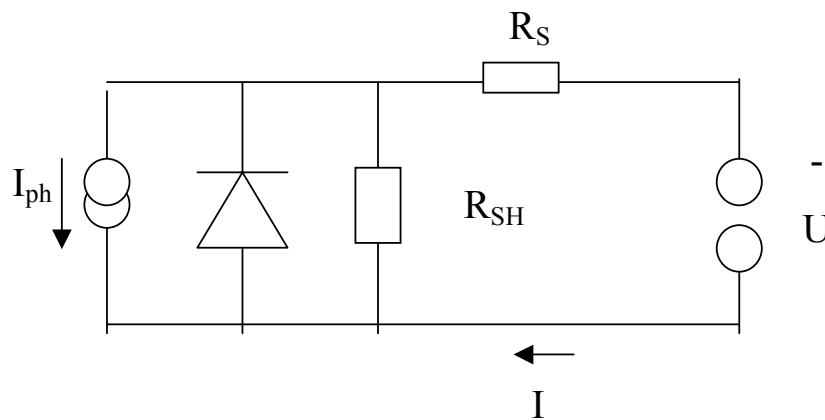


Figure 1.5: Equivalent circuit for a single junction solar cell. The photo generated current I_{ph} shows in the inverse direction of the forward one of the diode. Shunt resistance R_{SH} and series resistance R_S are important for the fill factor. Ideally, series resistance should be low and shunt resistance high.

The I-V curve of this circuit is described by equation 1.2.

$$I = I_0 \left(\exp\left(\frac{q}{nkT}(U - IR_S)\right) - 1 \right) + \frac{U - IR_S}{R_{SH}} - I_{PH} \quad 1.2$$

The current I consist of following three parts.

- (i) The diode is described by the Shokley equation, whereas I_0 is the saturation current of the diode, q the elementary charge, n the diode ideality factor, k the Boltzmann constant and T the temperature. The applied voltage U is reduced by the series resistance R_S
- (ii) The current through the shunt resistance R_{SH} , the applied voltage is again reduced by the series resistance.

(iii) The photo generated current I_{PH} , representing the activity of the solar cell under illumination.

For an ideal solar cell, the series resistance should be small and the shunt resistance ideally high. The figure 1.6 and 1.7 shows the influence of these two parameters on the I-V curve [49,50]. For the parameters, typical values for organic solar cells are taken.

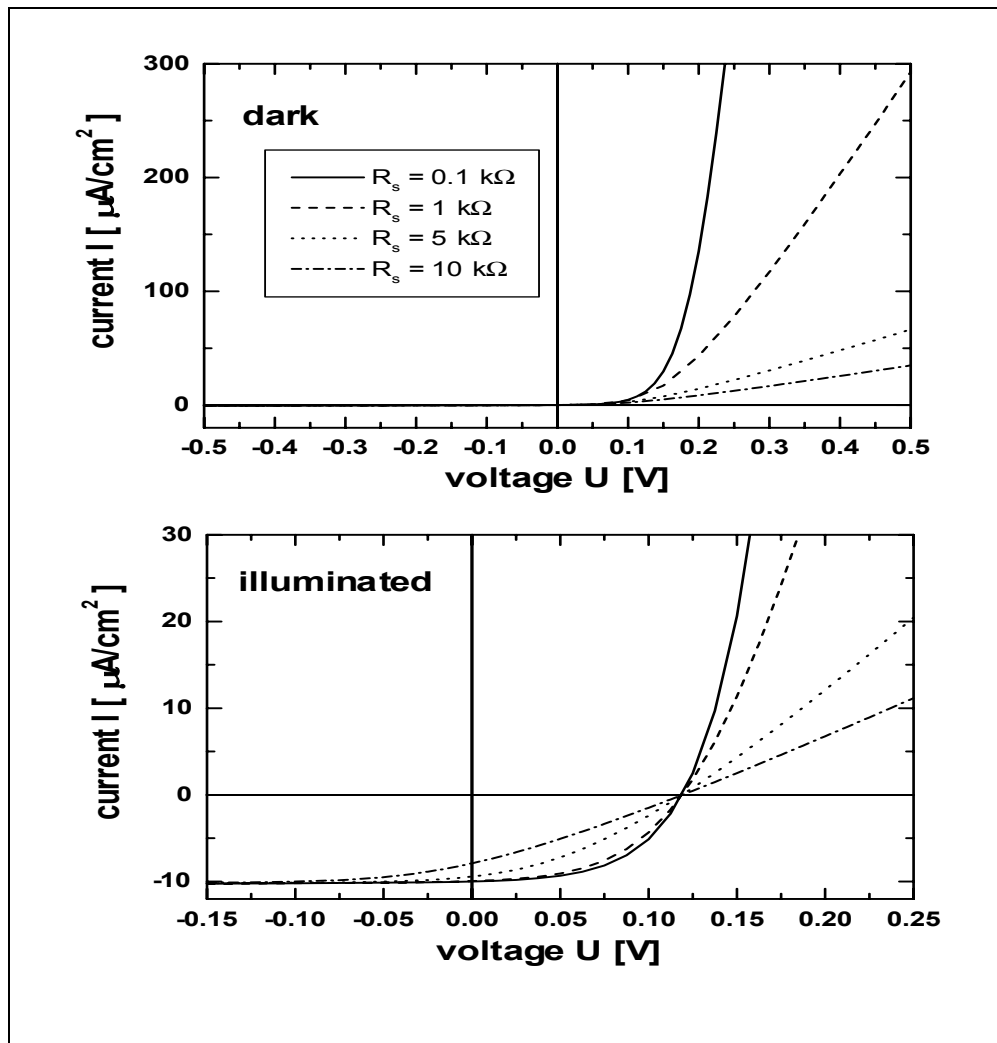


Figure 1. 6: Influence of the series resistance on the I-V curve of an organic solar cell, I_0 is chosen with 100 nA cm^{-2} , $n=1$, $R_{SH} = 1\text{M}\Omega$ and $I_{PH} = 10\mu\text{A cm}^{-2}$.

In the dark, the influence of the series resistance can be seen in the forward direction, the curves become flat and the injection currents are lower. Under illumination, the increasing series resistance lowers the short circuit current, because a part of the photo generated current is lost via the diode. Further, the FF is reduced significantly. The open circuit voltage is not influenced by the series resistance.

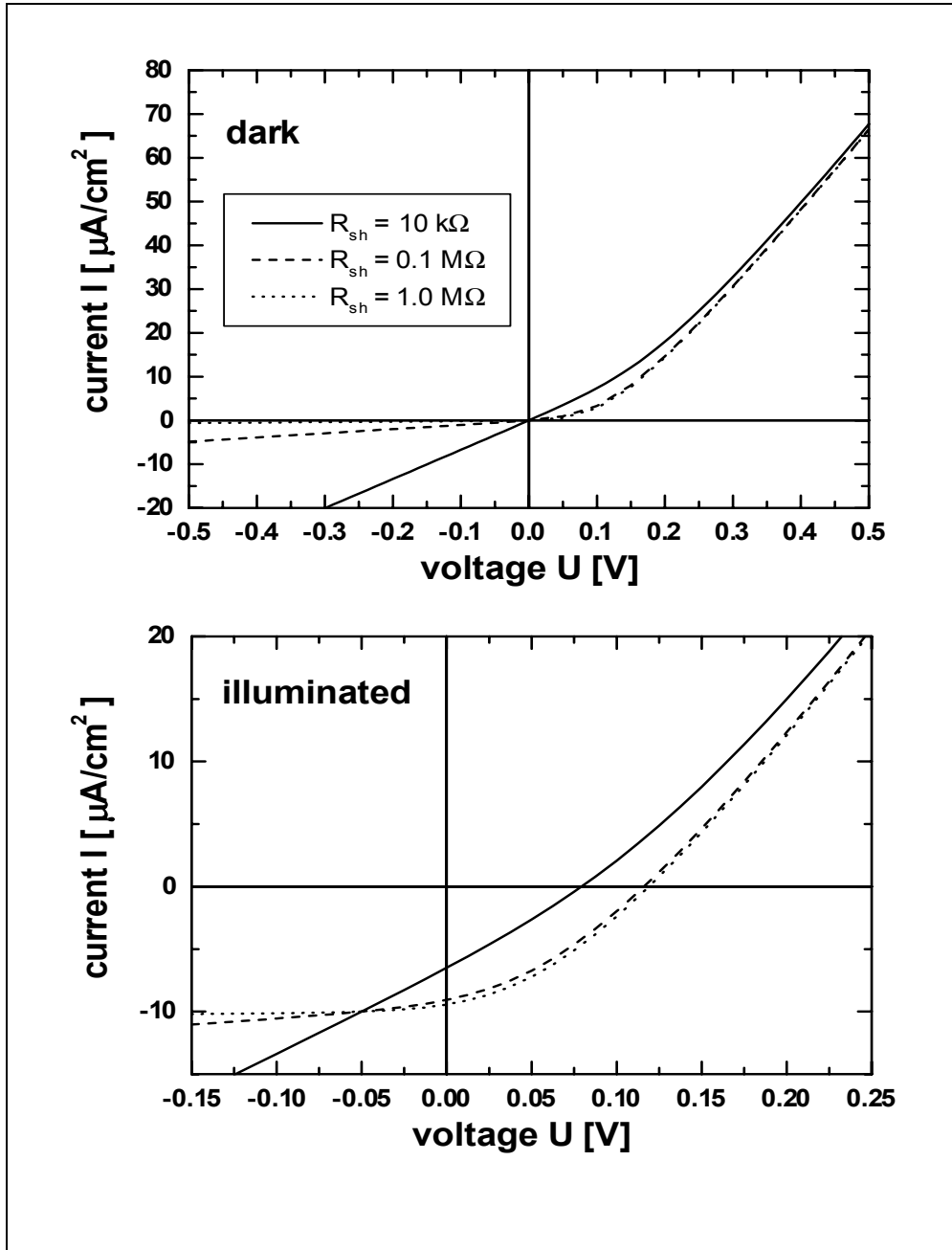


Figure 1. 7: Influence of the shunt resistance on the I-V on the I-V curve of an organic solar cell, I_0 is chosen with 100 nA cm^{-2} , $n=1$, $R_S=5\text{k}\Omega$ and $I_{PH}=10\mu\text{A cm}^{-2}$.

The I-V curves are influenced by a non-infinite shunt resistance in the dark as well as under illumination. In the dark, an ohmic contribution is added on the diode curve. Under illumination, the V_{OC} as well as the I_{SC} are reduced by the shunt resistance. For lower shunt resistances, the FF is reduced dramatically.

1.4 Bandgap Engineering

The bandgap of semiconductors is defined as the energy difference between the edges of the conduction band and valence band. In terms of molecular chemistry these are LUMO and HOMO levels of the individual molecules broadened up by the van der Waals interactions in the organic solid state. In an intrinsic semiconductor, there aren't any states in the gap.

After the Hückel approximation, an infinite *all trans* polyacetylene chain with equivalent C-C bonds [51] should not have any bandgap at all. The π - electrons are delocalised along the chain and all bonds are of equal length. Peierls predicted the instability of such a structure and the localisation of alternating double and single bonds [52]. Figure 1.8a show the potential energy of polyacetylene vs. bond length alternation. Exchange of single and double bond leads to an equivalent structure of the same energy, these two structures are denominated as phase A and phase B. This equivalency of the two phases is denoted as “degenerate ground state” in *trans*-polyacetylene. The bandgap E_g of *trans*-polyacetylene is roughly 1.5 eV.

For a non-degenerate conjugated polymer, two different ground states, the aromatic form and the quinoid form, exist. The two forms differ in the position of the double bond. The aromatic form is energetically the more stable one. The potential energy diagram is shown in figure 1.8b. In Polythiophene, the zero bandgap lies at a slightly quinoid structure [53]

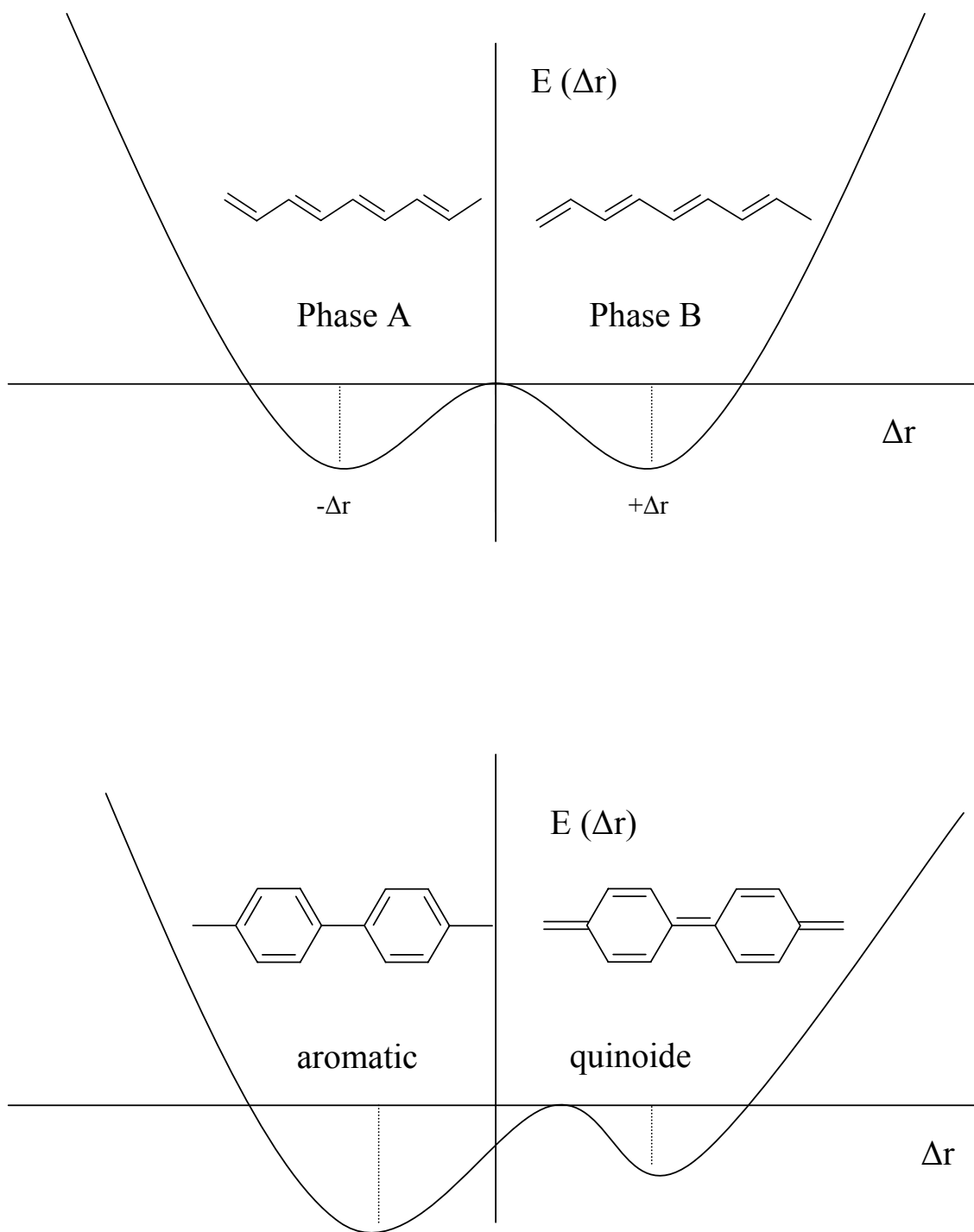


Figure 1.8: Potential diagram vs. bond length alternation for (a) trans-polyacetylene as conjugated polymer with degenerate ground state; (b) for polyphenylene as conjugated polymer with non-degenerate ground state.

Several factors influence the bandgap of non-degenerate ground state polymers. They should be discussed here for non-degenerate ground state polymers [54, 55]. For an isolated chain, the bandgap is the sum of four contributions, after equation 1.3. Their structural meaning is shown in figure 1.9 for polyphenylene, as example. In comparison, the corresponding quinoid form is drawn.

$$E_G = E_{\Delta r} + RE + E_{\Theta} + E_{SUB} \quad 1.3$$

$E_{\Delta r}$ is the energy contribution from bond length alternation to the bandgap, RE is the resonance energy, E_{Θ} the energy caused by the inter ring torsion angle and E_{SUB} the influence of the substituents. In the solid phase, additional intermolecular effects between the chains have to be taken into account, which generally leads to broader bands and a lower bandgap.

For the isolated chain, the bond length alternation is the most important factor. The influence of the bond length alternation on the bandgap has been discussed above. Generally, the aromatic form shows higher stabilisation energy and therefore the higher bandgap.

The resonance energy is defined as the difference of the π -energy of the conjugated polymer and a reference structure, with located double and single bonds without any resonance. Resonance energy leads to an energy stabilisation and so to an increased splitting of the HOMO-LUMO energy.

Conjugation along the chain is an important factor for the charge carrier mobility, but also for the bandgap. The more orbitals interact, the broader the bands become and the smaller is the HOMO-LUMO gap. Torsion between the ring plain interrupts the conjugation and therefore increases the bandgap.

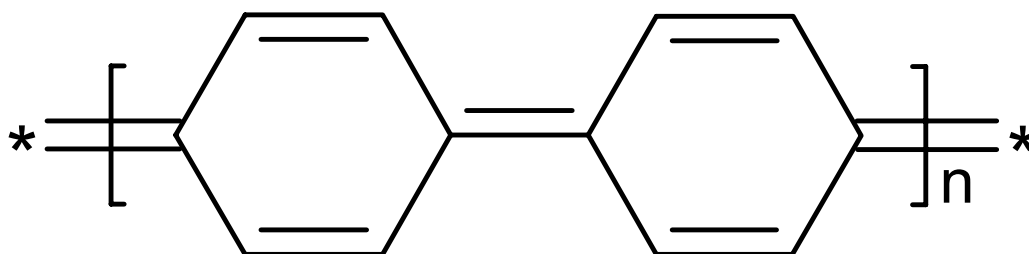
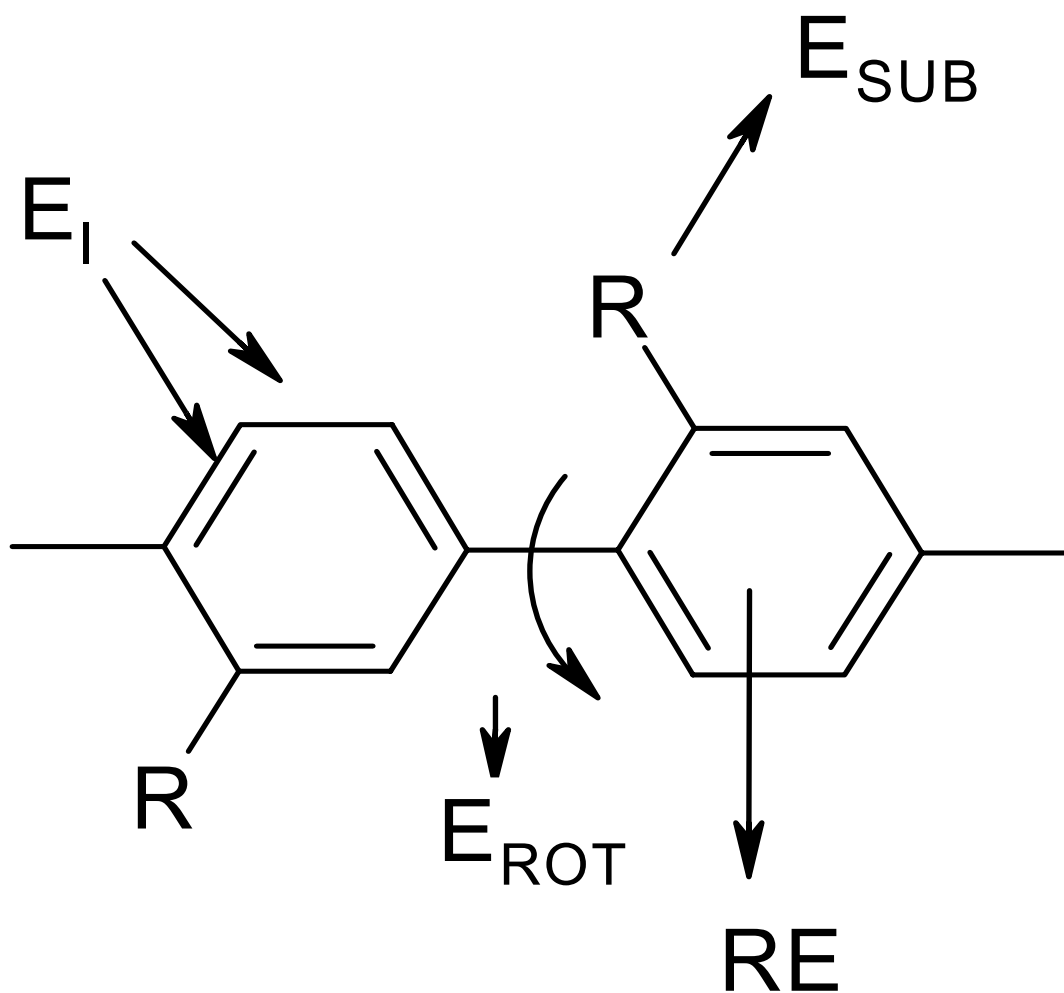


Figure 1.9: The upper part shows the aromatic form of poly-paraphenylene with the different parameters determining the bandgap of conjugated polymers: bond length alternation, resonance energy, inter ring torsion angle and substituent effects, the lower part shows poly-paraphenylene in the quinoid form.

Substituents can influence the energetic position of the HOMO and LUMO position vs. vacuum itself.

Electron donating groups raise the HOMO level and electron withdrawing groups lower the LUMO.

Several synthetic approaches can be used to influence the bandgap. The easiest way to manipulate the bandgap of a given polymer is the introduction of side groups. They can influence the bandgap via mesomeric and induced electron effects, i.e. increase or decrease the electron density in the aromatic unit. Side groups are also important for the solubility of the polymer. Furthermore, their effect on the structure in solid phase has to be taken into account. For example, bulky side groups can hinder crystallinity and interrupt interchain effects, which causes an increase of the bandgap.

Alternating of electron rich and electron poor compounds lead to so called push-pull polymers. The bandgap of such copolymers can decrease significantly. The electronic feature of the individual compounds can be determined either by side groups or by the monomer itself.

A third popular way to minimize the bandgap is the introduction of methine groups between the ring systems. By this approach, every odd unit becomes an increased quinoid character. These influences the bandgap by two ways. First, the bond length alternation is reduced and so the Peierls stabilisation. Secondly, the quinoid form minimize the inter annular rotation by the double bond character of the bridge bonds. The structure becomes more flat and the resonance between the rings is increased.

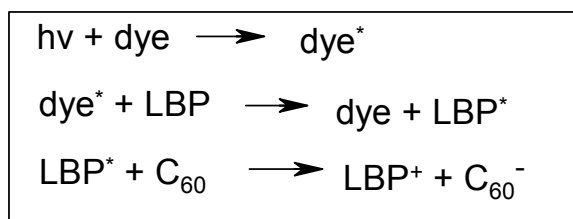
All this three approaches can be used separately or in combination. It will be seen that the approaches do not necessarily lead to a reduced bandgap due to other effects that counteract on the original strategy.

1.5 Sensitization of Solar Cells –Antenna Effect

One part of this work is to increase light absorption in polymer solar cells by blending with high absorbing dyes and thereby improve the short circuit current. The task of the dye is to absorb light and to transfer the collected energy to the conjugated polymer and fullerene. The charges are transported by the polymer and the fullerene. For polymer blend/ C₆₀ bilayer devices, an enhancement of the photocurrent was observed [56]. Several studies were done on polymer/dye mixtures for solar cells [38,57,58]. Multilayer heterojunction solar cells with a dye for light harvesting has been proposed [59] and realised [60] by the group of K.Yoshino.

Two different mechanisms for the sensitization are proposed: (i) energy transfer from the dye to the low bandgap polymer LBP and subsequent charge transfer and (ii) separate electron transfer from the dye to the fullerene and hole transfer to the LBP. Which mechanism occurs depends mainly on the level of the energy states and the exciton binding energy, which was shown by Halls et.al [61].

For the energy transfer, the reaction cascade following excitation of the dye is presented in scheme 1.2.



Scheme 1.2: Sensitization mechanism for bulk heterojunction solar cells by energy transfer. The dye transfer the absorbed energy radiation less to the low bandgap polymer, afterwards makes the polymer the charge transfer to the fullerene.

After the excitation of the dye, this excitation energy is transferred to the LBG. From there, charge transfer occurs. The electron is transferred form the LBP to the fullerene. The holes and electrons are transported by the LBP and fullerene, respectively. The dye does not take part in the charge transport. Excitations of the LBP are contributing separately to the current. A schematic energy level diagram with flow of charges is shown in figure 1.10.

Energy transfer is often described by the Foerster mechanism [62]. The rate constant k_{FET} for the Foerster transfer, shown in equation 1.4, depends on the distance r to the inverse sixth power.

$$k_{\text{FET}} = \tau_d^{-1} (R_0 / r)^6 \quad 1.4$$

τ_d is the lifetime of the excited state and R_0 the characteristic transfer radius. R_0 is given by equation 1.5.

$$R_0 = \alpha \int_0^{\infty} F_h(\nu) \epsilon_g(\nu) (\nu)^{-4} d\nu \quad 1.5$$

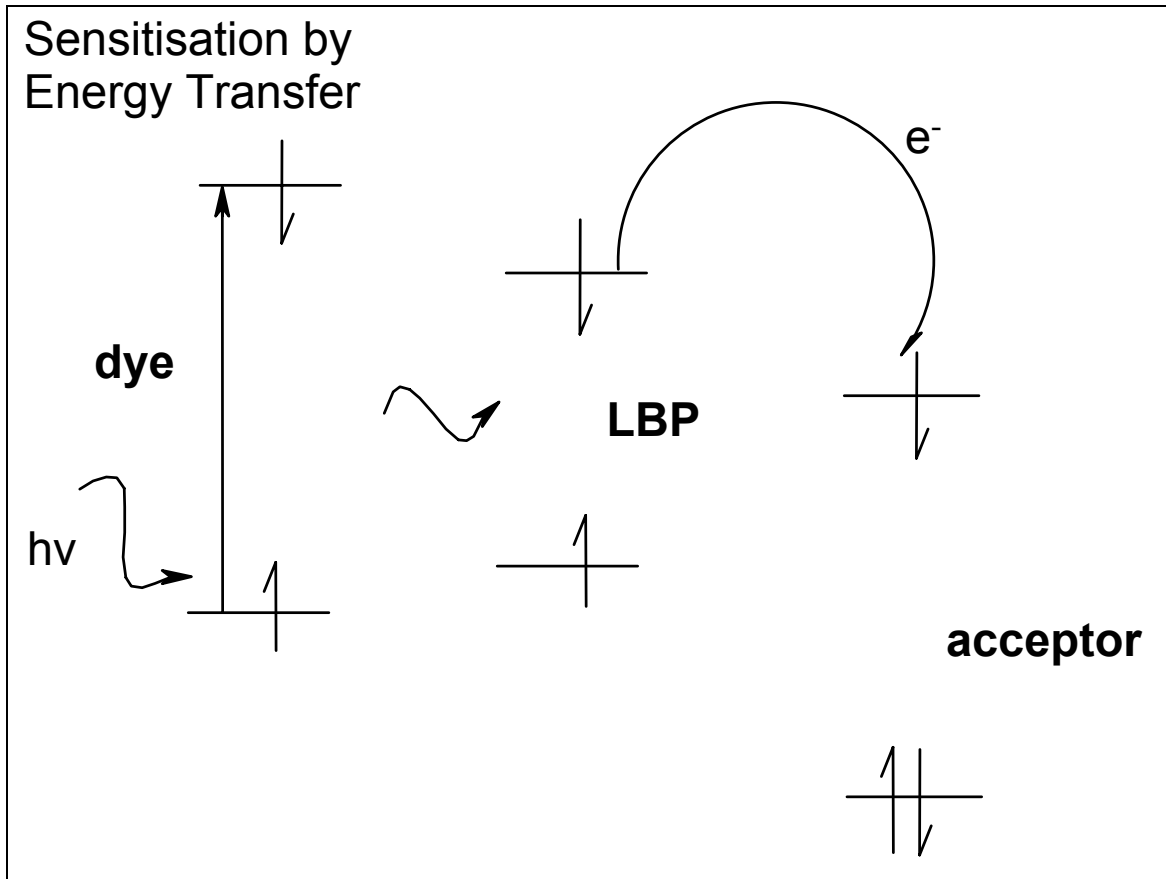
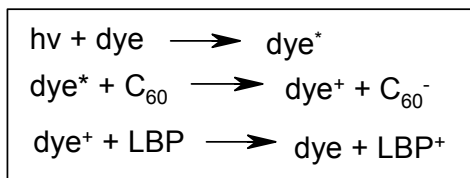


Figure 1.10: sensitization of low bandgap polymer solar cells by energy transfer from the dye to the LBP with subsequent charge transfer.

F_h and ϵ_g are describing the host (dye) emission and guest (LBP) absorption spectra, respectively. α is a proportional constant. Spatial closeness and overlap of host emission and guest absorption are seen as crucial parameter for efficient energy transfer. Mechanistically, Foerster energy transfer takes place radiation less i.e. without emission and re-absorption.

Alternatively, sensitization takes place via charge transfer; the reaction cascade is shown in scheme 1.3.



Scheme 1.3: Sensitization of bulk heterojunction solar cells via charge transfer mechanism. The excited dye transfers an electron to the fullerene and a hole to the LBP.

Unlike for the energy transfer, the dye makes a separate charge transfer to the C_{60} , resulting in a positively charged dye molecule and a negatively charged fullerene. Subsequently, the positive charge is transferred to the higher lying HOMO of the LBP. The charge transport to the electrodes occurs like usual, via the conjugated polymer for the holes and via the fullerenes for the electrons. For energy levels and charge flow see figure 1.11.

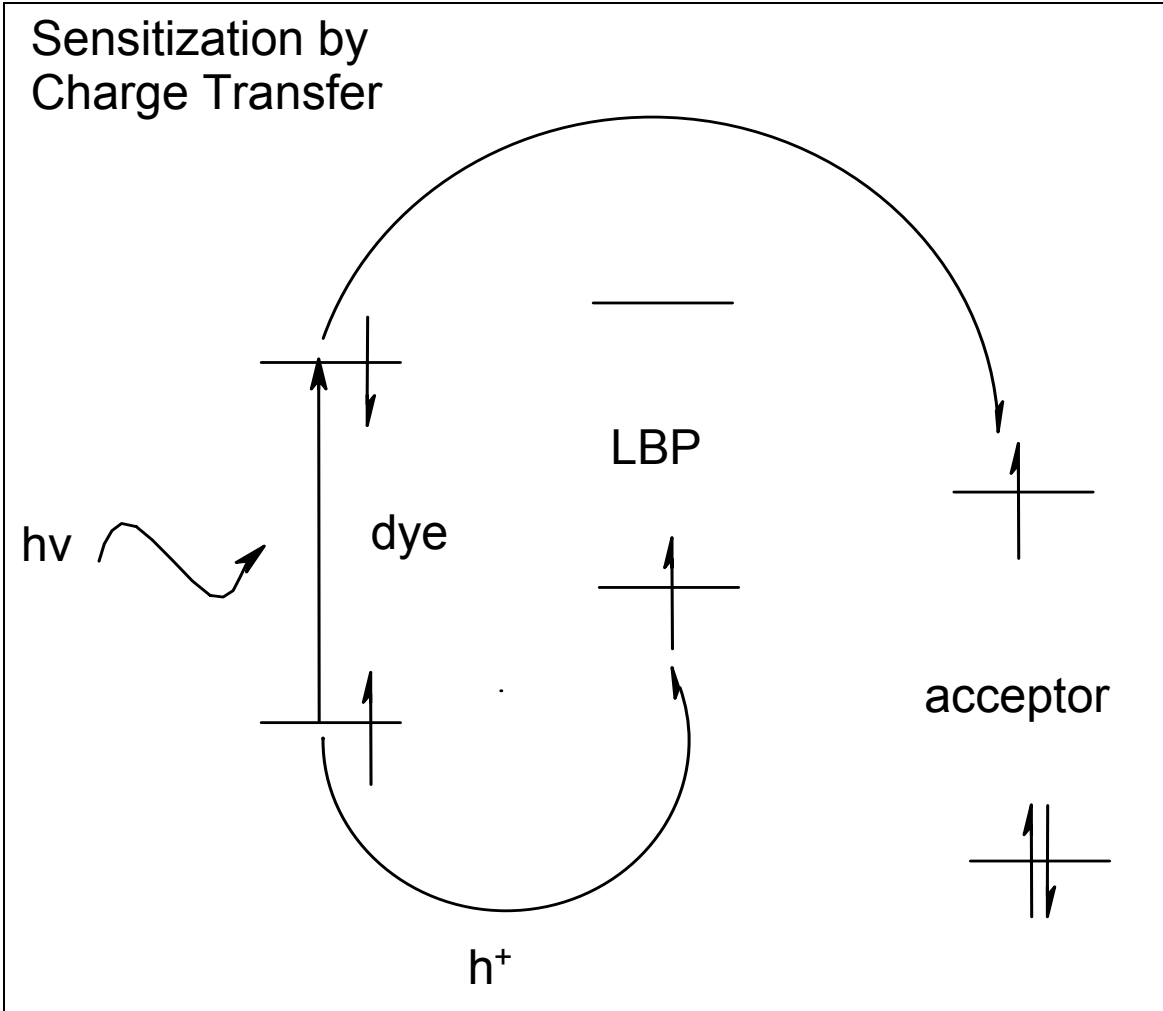


Figure 1.11: Sensitization of low bandgap polymer solar cells by separate charge transfer from the dye and the LBP to the acceptor.

The aim of this work is to sensitize low bandgap solar cells via the energy transfer mechanism. But up to now, by which mechanism sensitization occurs under which conditions is still under debate and experimental distinguishing is difficult.

2 Experimental

2.1 Material Characterization

The materials were characterised by absorption and emission spectroscopy in solution and as thin films, spin cast on glass. The absorption of the solutions and thin films was measured on a HP 8453 spectrometer. Background correction was done with the pure solvent and a clean glass substrate, respectively. The photoluminescence in solution was measured with a Hitachi F 4010 spectrometer. The photoluminescence of the thin films was measured in a homemade setup. Excitation was done with an argon laser at 476 or 514 nm; the luminescence was measured in a backscattering geometry by a Silicon detector, the spectra were corrected for the detector sensitivity.

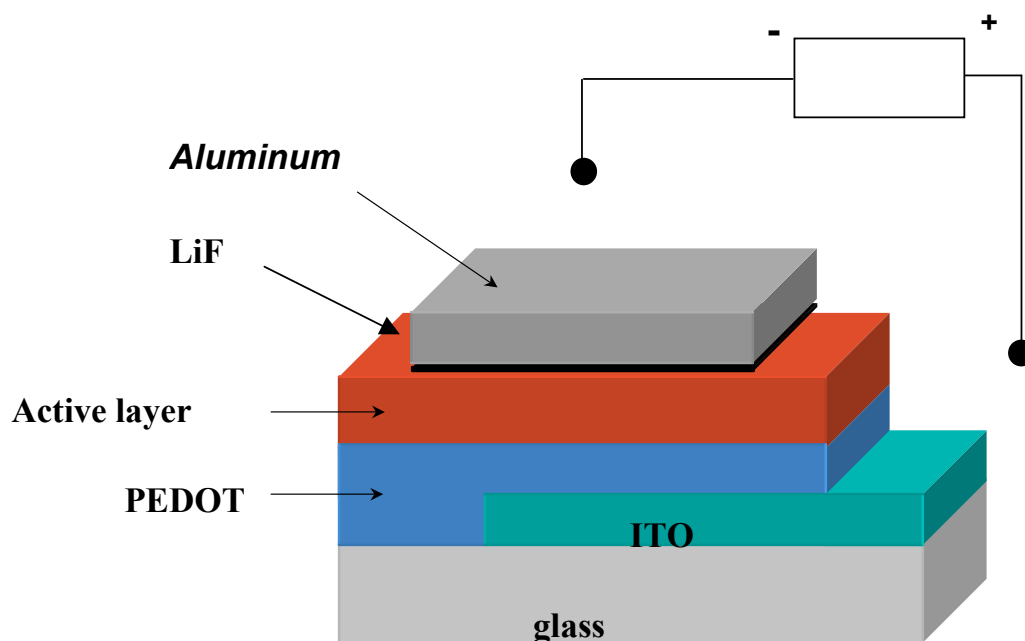


Figure 2. 1: The device configuration for solar cells (SC) and light emitting diodes (LED).

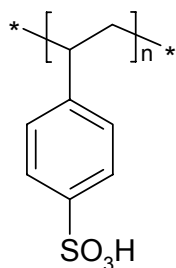
2.2 Device Preparation

The structure that was used for solar cells as well as for light emitting diodes LED is shown in figure 2.1. The devices were fabricated in a sandwich geometry. As substrates, glass sheets of 1.5x1.5 cm² covered with ITO were used. ITO (indium tin oxide) is transparent and conductive and therefore often used as electrode in PV and LED.

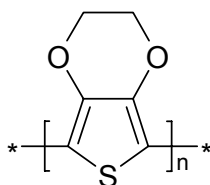
The ITO was structured by etching with an acidic mixture of HCl_{konz.}:HNO_{3 konz.}:H₂O 4.6:0.4:5 for 15 minutes. Half of the substrate was coated with a commercial varnish to protect the active ITO area against the etching acid. The varnish was removed afterwards by acetone in an ultrasonic bath. Then, the ITO was cleaned in an ultrasonic bath again with acetone and following isopropanole as cleaning solvents.

On the ITO substrate, PEDOT:PSS, poly (ethylene-dioxythiophene) doped with polystyrene-sulphonic acid, purchased by the Bayer AG, was spin cast twice from an aqueous solution (0.5 w%, PEDOT: PSS 2:3) on the ITO substrate, giving an average thickness of ~100 nm. The PEDOT:PSS layer improves the quality of the ITO electrode. The surface roughness of ITO is minimized and the electric contact to the polymer is improved. Further, the work function of the electrode is changed.

Then, the substrates were dried in vacuum. The chemical structures of PEDOT and PSS are shown in figure 2.2.



PSS



pEDOT

Figure 2. 2: Chemical structure of pEDOT-PSS (poly (3,4 ethylenedioxythiophene):polystyrene-para-sulfonic acid).

The active layers were also spin cast. Solution were prepared and stirred and heated up for at least twelve hours. For the spin casting, the substrate was mount in the spincoater, Spincoater

Model P 6700 Series from SCS Inc. For all spin casting processes a two-step program was used, if not otherwise referred. After 40 sec rotating with 1500 rpm, 30 sec at 2000 rpm followed. The spin cast process was done in ambient conditions unless otherwise referred. The following evaporations and the basic characterisation of the devices were done in an argon glovebox, MB 204 from Mbraun.

The top electrode was a two-layer deposition of Lithiumfluorid-Aluminium. The deposition was done by thermal deposition at a pressure better than 10^{-5} mbar. As source, tungsten boats were used. The average thickness of the LiF and Al layer is 0.6 nm and 60 nm, respectively. The thickness of the layers is monitored by a quartz balance, intellemetrics IC 600. The evaporation was done through a shadow mask in order to define a device area of $1.5 \times 3 \text{ mm}^2$.

A reference device with MDMO-PPV/ PCBM was made within each series in order to control the correct fabrication. The structure of the two components is shown in figure 2.3.

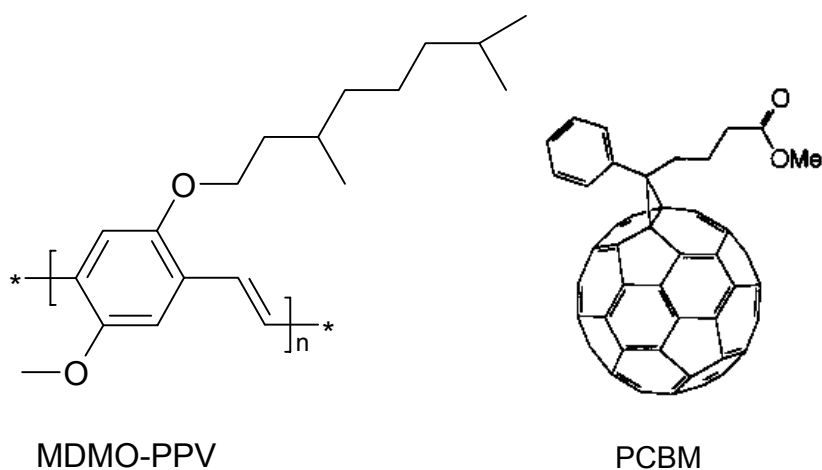


Figure 2.3: Chemical structure of MDMO-PPV (poly-(2-methoxy, 5-(3,7 - dimethyloctyloxy)) para phenylene-vinylene) (cited as PPV) and PCBM ([6,6]-Phenyl C₆₁ butyric acid methyl ester).

2.3 Device Characterization

Solar cells were characterised under 80 mW cm^{-2} white light illumination from a Steuernagel solar simulator (metal homogenise lamps with AM 1.5 filters). This simulates AM1.5 conditions. The I-V curves were measured with a Keithley 2400. ITO was connected to the positive electrode, Al to the negative. The curves were recorded by continuously sweeping from -2V to $+2\text{V}$ and recording data points in 10 mV steps.

Solar cells are described by several parameters like open circuit voltage, short circuit current and fill factor. The fill factor is defined after equation 2.1.

$$FF = \frac{V_{MPP} I_{MPP}}{V_{OC} I_{SC}} \quad 2.1$$

V_{OC} is the open circuit voltage, I_{SC} the short circuit current per area and V_{MPP} and I_{MPP} are the voltage and current per area at the maximum power point, respectively. The power conversion efficiency is given in equation 2.2.

$$\eta_{AM1.5} = \frac{P_{out}}{P_{in}} = FF \frac{V_{OC} I_{SC}}{P_{in}} \quad 2.2$$

P_{out} is the electric power at the maximum power point of the cell and P_{in} is the incident light power per area.

The spectral photocurrent was detected by a Lock In amplifier while the sample was excited with monochromatic light with $\sim 200 \mu\text{W cm}^{-2}$ and a FWHM of $\sim 4 \text{ nm}$. The incident-photon-to-collected-electron efficiency (IPCE) for a certain wavelength λ is calculated by formula 2.3.

$$IPCE(\%) = \frac{1240 * I_{SC}}{\lambda * P_{in}} \quad 2.3$$

The IPCE is the relation of the numbers of electrons generated by the cell under short circuit conditions to the number of the incident photons. I_{sc} is the short circuit current in $\mu\text{A cm}^{-2}$, λ the wavelength in nm and P_{in} the monochromatic light incidence in W m^{-2} . As light source, a

halogen lamp with 80 mW was used, followed by a monochromator. The spectrum of the halogen lamp was measured each time with a calibrated monocrystalline silicon diode.

The electroluminescence was measured with an Avantes spectrometer; the spectra are corrected for the detector sensitivity.

AFM measurements are done with a "Dimension 3100" instrument from Digital Instruments, Santa Barbara, CA, in the tapping mode.

For low temperature studies, cells with pristine MDMO-PPV and MDMO-PPV/PTPTB 1:1 (wt %) with Au electrodes were prepared. The cells were cooled down to liquid helium temperature and I-V curves were recorded during heating up. Room temperature curves were recorded before and after the cooling to monitor possible damage of the device, especially the contacts. The cells showed in all cases the same characteristic before and after the measurement.

The dependence of the short circuit current on the light illumination power was measured on the solar simulator with different optical density filters between the light source and the device. The dependence is fitted after a power law 2.4.

$$I_{sc} \propto P_{in}^{\alpha} \quad 2.4$$

The α -value is extracted as the gradient in the double logarithmic plot.

3 Material Screening - Results and Discussion

Different low bandgap materials were tested by spectroscopic characterisation and device application for their suitability in bulk heterojunction solar cells.

3.1 PEDOT- derivatives

These two materials were synthesized by Igor Perepichka in the group of Prof. Roncali at the university of Angers and provided the university of Linz for spectroscopic and device application testing.

PEDOT derivatives are promising candidates for bulk heterojunction solar cells. The HOMO-LUMO gap of the monomer is lower than for benzene. Their chemical similarity to the PEDOT:PSS should lead to a good contact to the hole transport layer. The two materials presented in this work are among the first PEDOT polymers soluble in organic solvents.

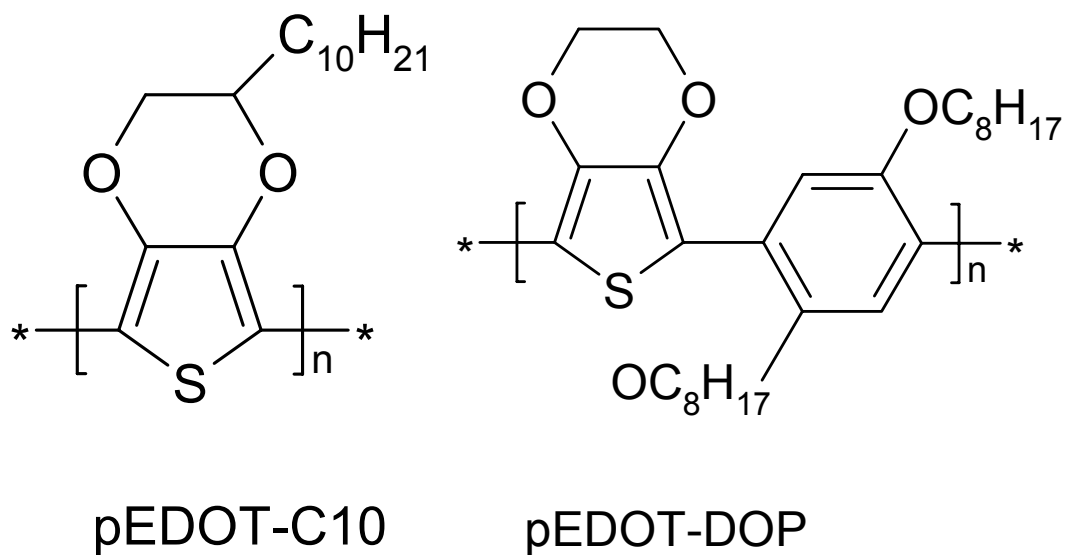


Figure 3. 1: Chemical structure of pEDOT-C10 (poly-[(1'-dodecyl)-3,4-ethylenoxythiophene]) and pEDOT-DOP (poly-[(3,4-ethylenoxythiophene)-para-(2,5-dioctyloxy-phenylene)]).

3.1.1 pEDOT-C10

Spectroscopy

Poly (1'-dodecyl-3, 4 ethylenoxythiophene), abbreviated as pEDOT-C10, is soluble in many organic solvents including chloroform, toluene and chlorobenzene. Its structure is shown in figure 3.1.

Absorption and luminescence spectra in chlorobenzene solution are presented in figure 3.2. The absorption maximum around 600 nm has a molar extinction coefficient of $3710 \text{ l mol}^{-1} \text{ cm}^{-1}$ *. This value corresponds to a specific extinction coefficient of $13 \text{ l g}^{-1} \text{ cm}^{-1}$. The onset of the absorption is estimated at 680 nm.

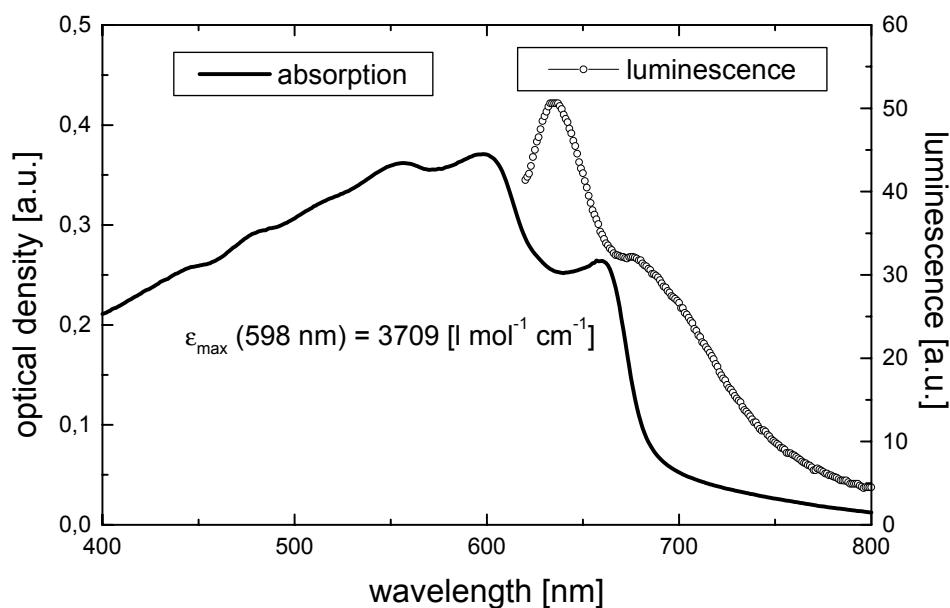


Figure 3. 2: Optical absorption (—) and luminescence (-o-) of pEDOT-C10 in a $10^{-4} \text{ mol l}^{-1}$ chlorobenzene solution, the excitation wavelength for the luminescence measurements is 600 nm.

Thin films of high quality can be made by spin casting. For the absorption and luminescence spectra, which are presented in figure 3.3.a, similar features like for the solution are observed in figure 3.2. The thickness of the film is measured by AFM with approximately 200 nm. The absorption coefficient of pEDOT-C10 in a thin solid film at the maximum at 600 nm is

* the monomer, drawn in figure3.1, is taken as molecular unit ($M= 280.2 \text{ g mol}^{-1}$)

calculated with $\alpha = 3500 \text{ cm}^{-1}$. The onset of the absorption is at 680 nm as in the solution. The bandgap, estimated from the absorption onset, is therefore 1.8 eV. It is interesting to note that the absorption and emission spectra undergo just a slight red shift after transferring from chlorobenzene solution into the solid state unlike most conjugated polymer, which exhibit significantly red shifted spectra in solid state.

For the blends with PCBM, in the spin cast films no large-scale phase segregation is observed. The absorption spectrum of the blend, see figure 3.3b. The photoluminescence of the polymer, shown also in figure 3.3b, is completely quenched in the blend with PCBM, indicating photoinduced charge transfer.

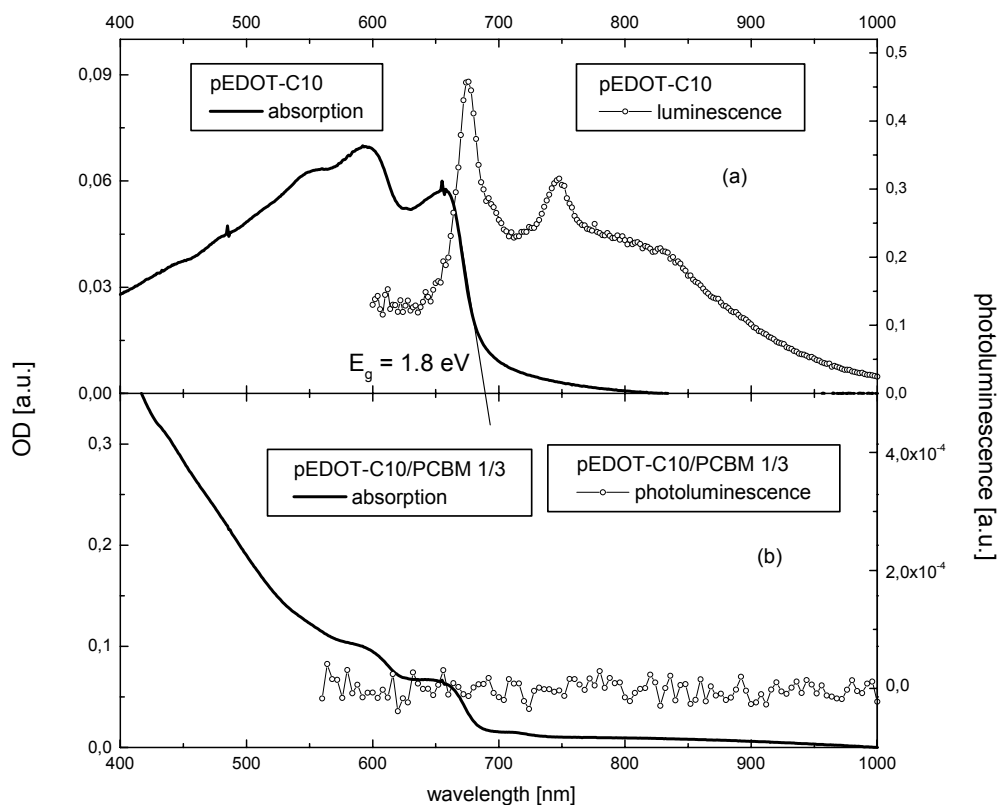


Figure 3.3:(a) Optical density (—) and luminescence (-o-) of a pEDOT -C10 film and (b) optical density (—) and photoluminescence (-o-) of pEDOT-C10/PCBM 1/3 film, films are spin cast from 1 % chlorobenzene solutions on cleaned glass substrates, the optical bandgap is estimated by the onset of the absorption; absorption is recorded at room temperature, luminescence at 100 K and excitation at 476 nm.

Several other spectroscopic data are known of this material. The photo induced absorption shows polaronic features after blending the polymer with PCBM. The light induced electron spin resonance confirms the presence of a radical species after illumination, assigned to the positive polaron of the polymer. From these results, photoinduced charge transfer can be concluded. Therefore, pEDOT-C10 should be suitable for bulk heterojunction solar cells.

Devices

The photovoltaic cells with pEDOT-C10/PCBM 1/3 as active layer were spin cast from a 1% chlorobenzene solution. Spin cast films are of high quality. No failures can be seen by eye. In the dark, the device shows rectifying behaviour, see figure 3.4, with a rectification of 10^3 at ± 1 V, which is rather high for polymer bulk heterojunction. After illumination on the solar simulator, a clear photoeffect can be observed.

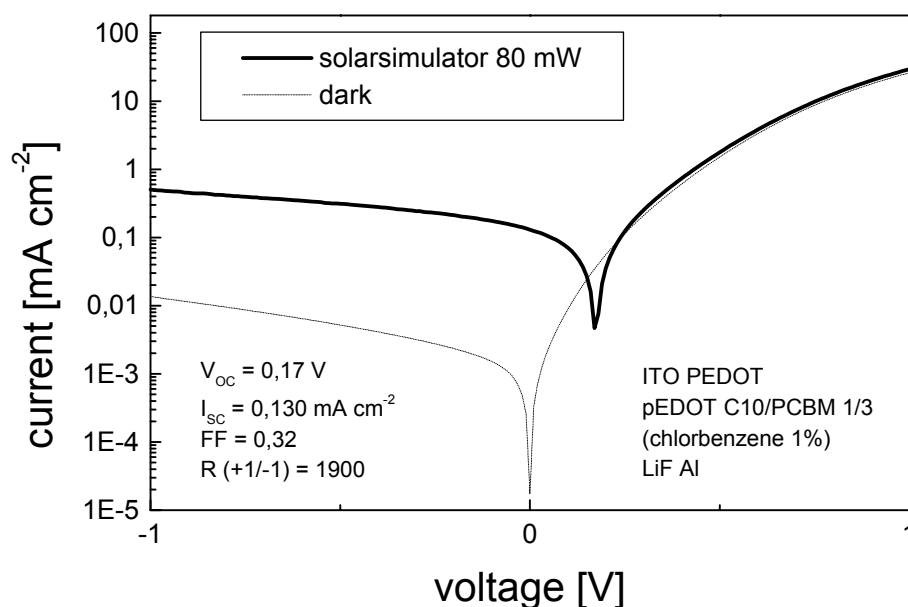


Figure 3.4: I-V curve in the dark (---) and on the solar simulator (—) of pEDOT-C10/PCBM 1/3 solar cell in standard configuration, active layer is spin cast from a 1 % chlorobenzene solution.

Figure 3.5 shows the external quantum efficiency compared with the amount of absorbed photons in transmission. The spectra fit well, but the shoulder of the absorption at 650 nm seems not to contribute to the photocurrent. The dependence of the short circuit current on the illumination intensity, shown in figure 3.6, scales with a power law exponent of 0.88. From

this value, partial influence of bimolecular recombination can be concluded. This may be a reason for the low short circuit current. Further reasons can be the poor absorption of the polymer and parasitic relaxation pathways beside charge transfer from polymer to the PCBM acceptor. The reason for the low voltage is not clear.

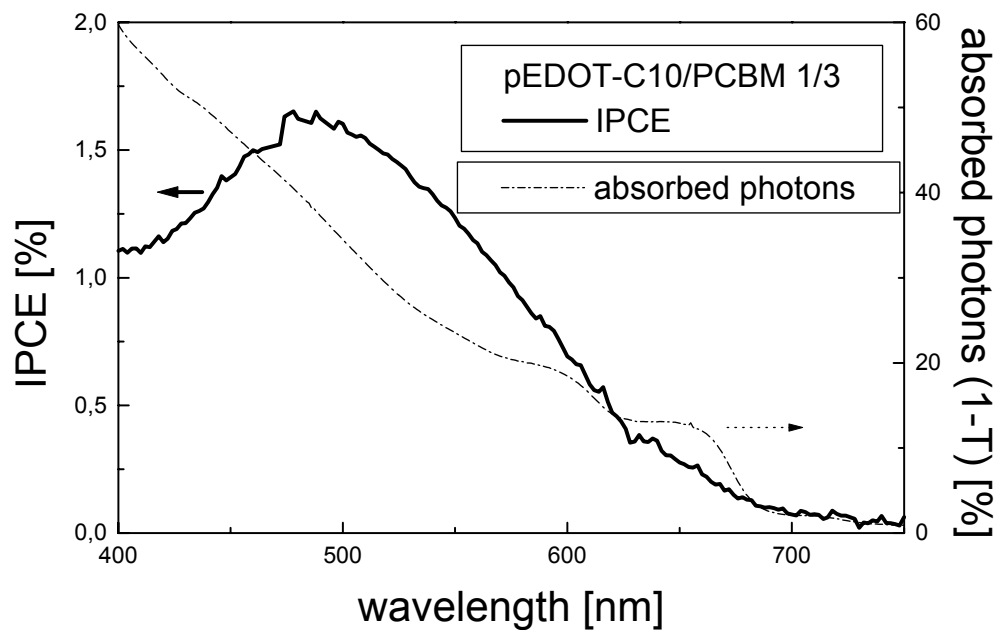


Figure 3.5: IPCE of pEDOT-C10/PCBM 1/3 solar cell (—) in standard configuration in comparison with the amount of absorbed photons in transmission of a film on glass (···).

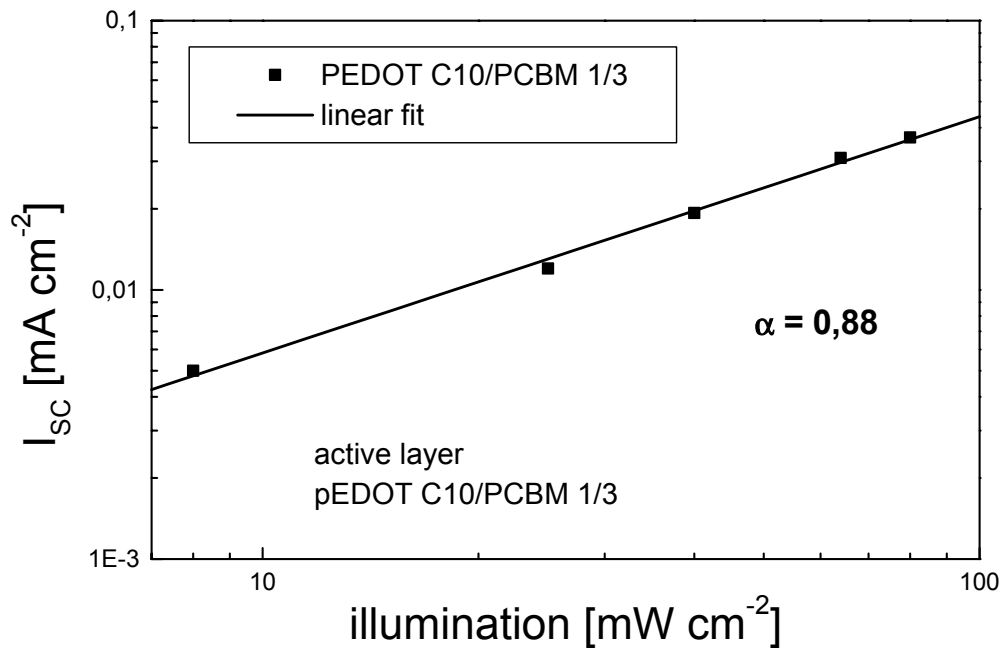


Figure 3.6: Dependence of the short circuit current (■) on the illumination of a pEDOT-C10/PCBM solar cell in standard configuration, fit is done by a power law dependence.

3.1.2 pEDOT-DOP

Spectroscopy

The copolymer poly-[(3,4-ethylenoxythiophene)-para-(2,5-dioctyloxy-phenylene)], abbreviated as pEDOT-DOP, is designed after the push-pull concept. Alternating of electron rich pEDOT units with electron deficient DOP units should lead to a reduced bandgap. The structure is shown in figure 3.1.

The absorption spectrum in chlorobenzene solution is shown figure 3.7. For the maximum at 450 nm, a molar extinction coefficient ϵ of $17760 \text{ l mol}^{-1} \text{ cm}^{-1}$ * is determined. The onset of the absorption is around 525 nm. The better comparable specific extinction coefficient is

* the monomer of both component, the eDOT and the DOP unit, drawn in figure 3.1, is taken as molecular unit ($M=472.2 \text{ g mol}^{-1}$)

calculated with $38 \text{ l g}^{-1} \text{ cm}^{-1}$, which is higher than for pEDOT-C10.

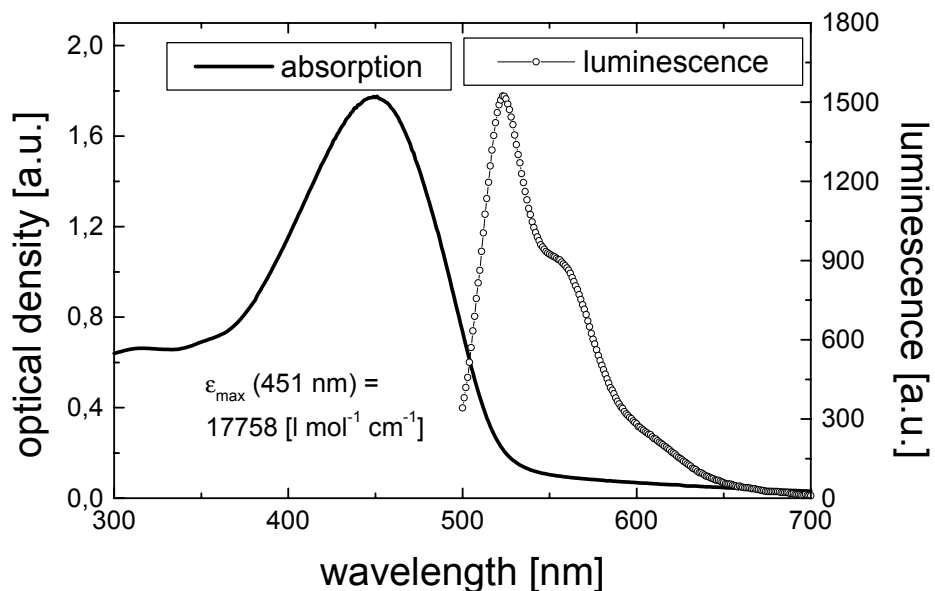


Figure 3.7: Optical absorption (—) and luminescence (-o-) of pEDOT-DOP in a $10^{-4} \text{ mol l}^{-1}$ chlorobenzene solution, the excitation wavelength for the luminescence measurements is 460 nm.

Thin films of the polymer and PCBM blend were spin cast from chlorobenzene. The absorption spectra of the pristine material and a 1:3 blend with PCBM are shown in figure 3.8. The thickness of the pristine polymer film is determined with 200 nm. At the absorption maximum at 490 nm, an absorption coefficient of 12000 cm^{-1} is determined. The onset of the absorption is at 565 nm. This correlates with a bandgap of 2.2 eV, which is in the range of MDMO-PPV. pEDOT-DOP has not a lower bandgap than MDMO-PPV, but even a higher than the EDOT-monomer. The absorption of the blend is mostly dominated by the fullerene.

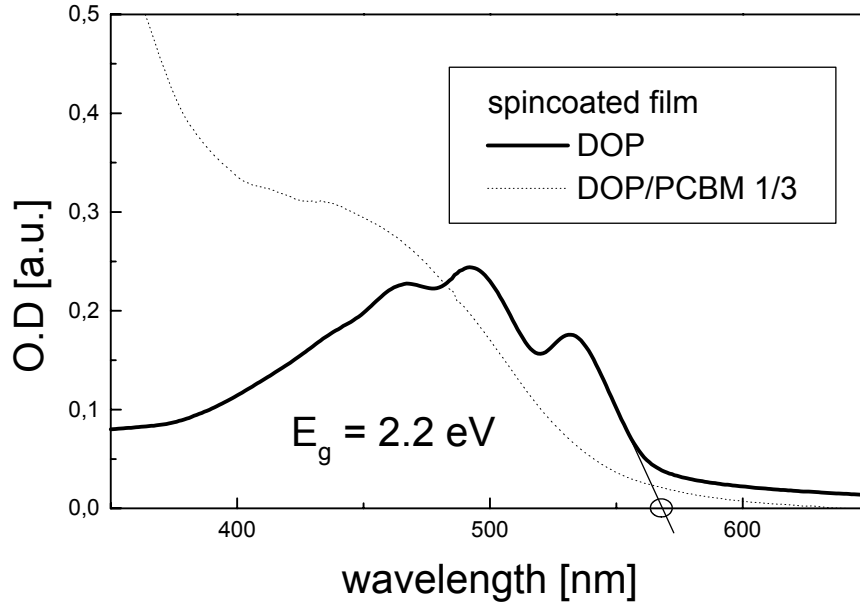


Figure 3. 8: Optical density of a pEDOT-DOP (—) and a pEDOT-DOP/PCBM 1/3 (····) film, films are spin cast from 1 % chlorobenzene solutions on cleaned glass substrates, the bandgap is estimated by the onset of the absorption.

Devices

Figure 3.9 shows the I-V characteristics of a pEDOT-DOP/PCBM 1/3 device. In the dark, low rectification value is observed. Under illumination, the diode shows a clear photoeffect and a short circuit current of 0.38 mA cm^{-2} . The open circuit voltage of 0.48 V is satisfying high for a non-optimised device. The IPCE, shown in figure 3.10, matches the absorption spectra quite well. Like mentioned above, the relative high bandgap does not bring any advantage to MDMO-PPV, and therefore this material was not optimised and considered any more during this work.

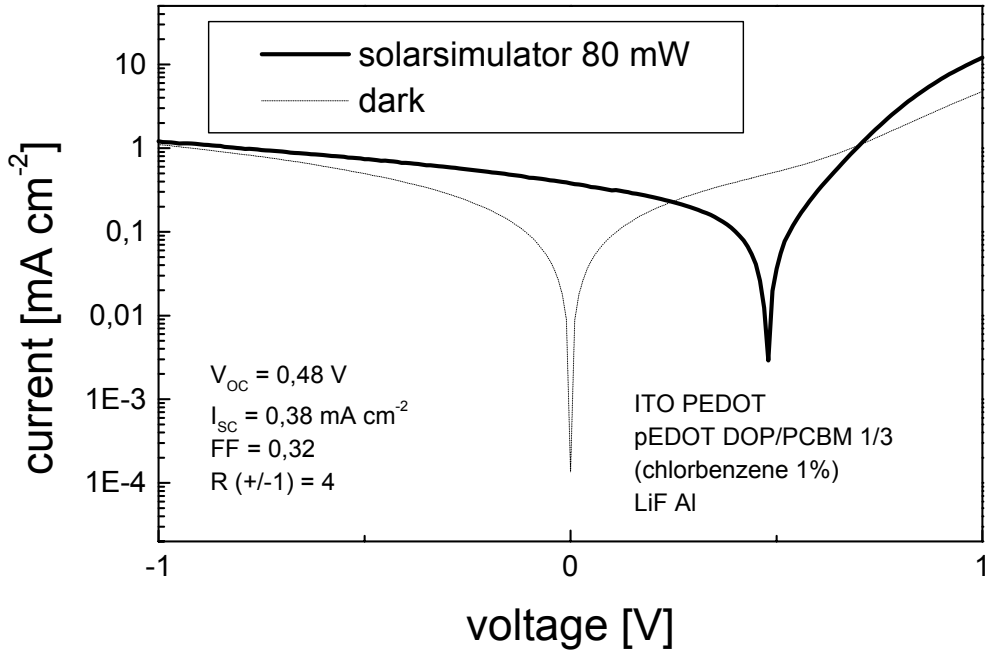


Figure 3.9: I-V curve in the dark (-----) and on the solar simulator (—) of pEDOT-DOP/PCBM 1/3 solar cell in standard configuration, active layer is spin cast from a 1 % chlorobenzene solution.

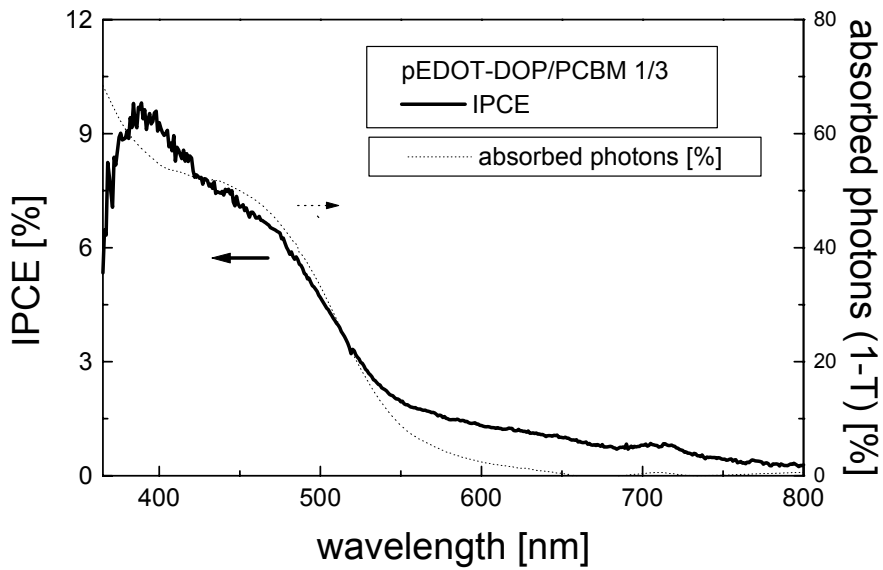


Figure 3.10: IPCE of pEDOT-DOP/PCBM 1/3 solar cell (—) in standard configuration in comparison with the amount of absorbed photons in transmission of a film on glass (···).

3.2 Isothionaphthalene-derivatives

These materials were synthesised by H. Meng in the group of Prof. F. Wudl at the university of Los Angeles. The materials were provided the university of Linz for spectroscopic characterisation and testing in solar cell application.

Polymers from isothionaphthalenes have to lowest bandgap with (~ 1.0 eV) reported for conjugated polymers up to now [63]. The condensed benzene ring minimizes the bond length alternation in the conjugated backbone making the interring bonds more quinoid character, which leads to a smaller bandgap [53]. Because of their low stability at ambient conditions, they were not considered for device application up to now.

A new derivative monomer has been synthesised, recently [64]. Beside the polymeric form of this monomer, different copolymers have been synthesised, too. The new polymers show improved stability and still low HOMO-LUMO transition energies. The structure of all three polymers is shown in figure 3.11. Spin casting of the films for spectroscopic measurements and devices was done under inert atmosphere.

The investigated materials show an unusual high electron spin resonance signal, which indicates the presence of a radical species. This species are probably positive polarons, which originates from the synthesis. All the presented results should be regard under this fact.

Hydrazine is known to reduce selectively conjugated polymers to their intrinsic semiconducting state. Further investigations of the are under way.

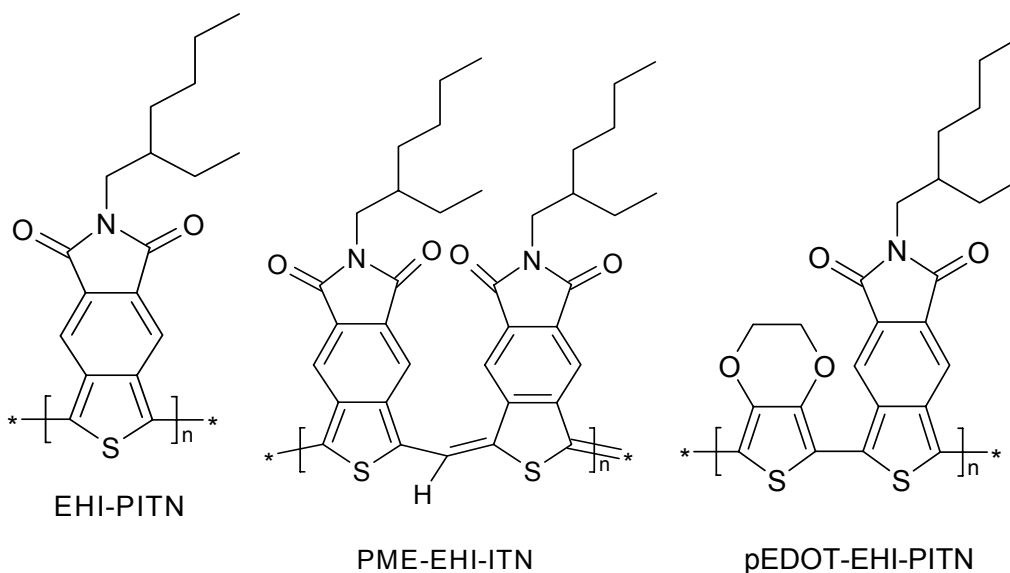


Figure 3.11: Chemical structure of EHI-PITN (Poly (benzo[c]thiophene-*N*-2'-ethylhexyl-4,5-dicarboxylic imide), pME-EHI-ITN (Poly(methine-benzo[c] thiophene-*N*-2'-ethylhexyl-4,5-dicarboxylic imide) and pEDOT-EHI-ITN (poly(3,4-ethylenedioxythiophene)-*N*-2'-ethyl-4,5-dicarboxylic-imide-benzo[c]thiophene).

3.2.1 EHI-PITN

Poly (benzo[c]thiophene-*N*-2'-ethylhexyl-4,5-dicarboxylic imide), abbreviated by EHI-PITN, is soluble in chloroform and in small amounts in dichlorobenzene. For all presented results in this work, chloroform solutions were used, because spin casting from dichlorobenzene results in too thin films.

The absorption and photoluminescence spectra of the pristine material, spin cast on glass, are shown in figure 3.12a. For the film thickness of approx. 200 nm, an optical absorption coefficient for the maximum at 788 nm of 8000 cm^{-1} is determined. The onset of the absorption is at 980 nm, which corresponds to 1.24 eV as estimation for the bandgap. No luminescence is observed within the sensitivity of the setup. The absorption spectrum of the blend with PCBM, figure 3.12b, is a superposition of both spectra. Also in the blend, no luminescence is observed.

For the devices, I-V curves are presented in figure 3.13. They show poor diode behaviour, indicated by low rectification and bad fill factor, and small currents.

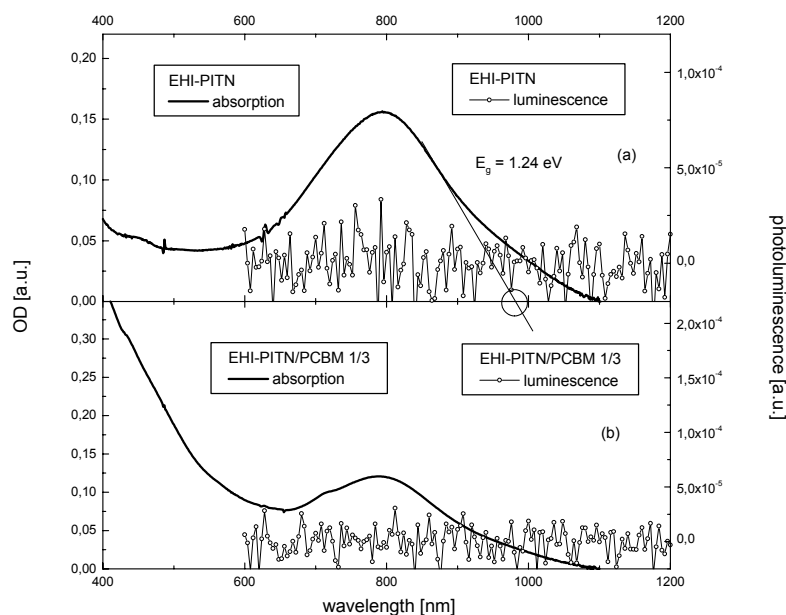


Figure 3. 12: (a)Optical density (—) and luminescence (-o-) of a EHI-PITN film and (b) optical density (—) and photoluminescence (-o-) of EHI-PITN/PCBM 1/3 film, films are spin cast from 1 % chlorobenzene solutions on cleaned glass substrates, the bandgap is estimated by the onset of the absorption; absorption is recorded at room temperature, luminescence at 100 K and excitation at 514 nm.

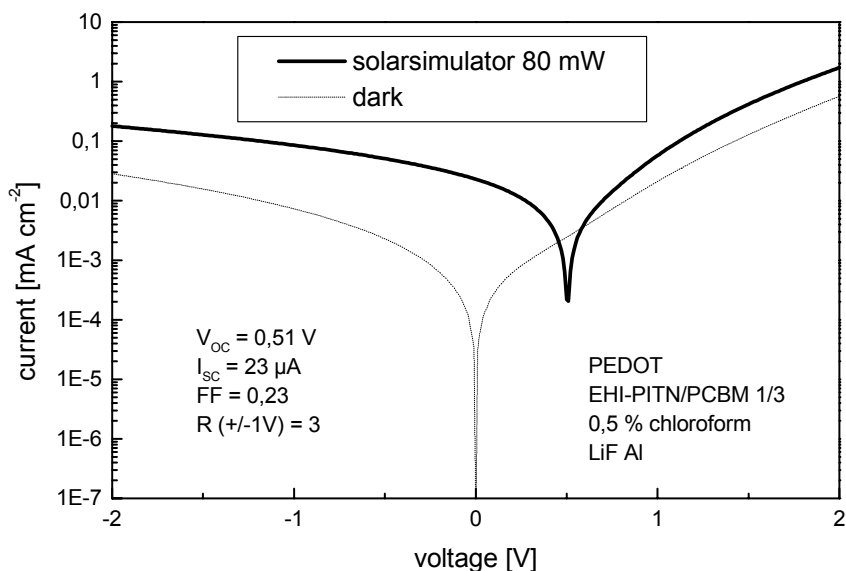


Figure 3. 13: I-V curve in the dark (-----) and on the solar simulator (—) of EHI-PITN/PCBM 1/3 solar cell in standard configuration, active layer is spin cast from a 0.5 % chloroform solution.

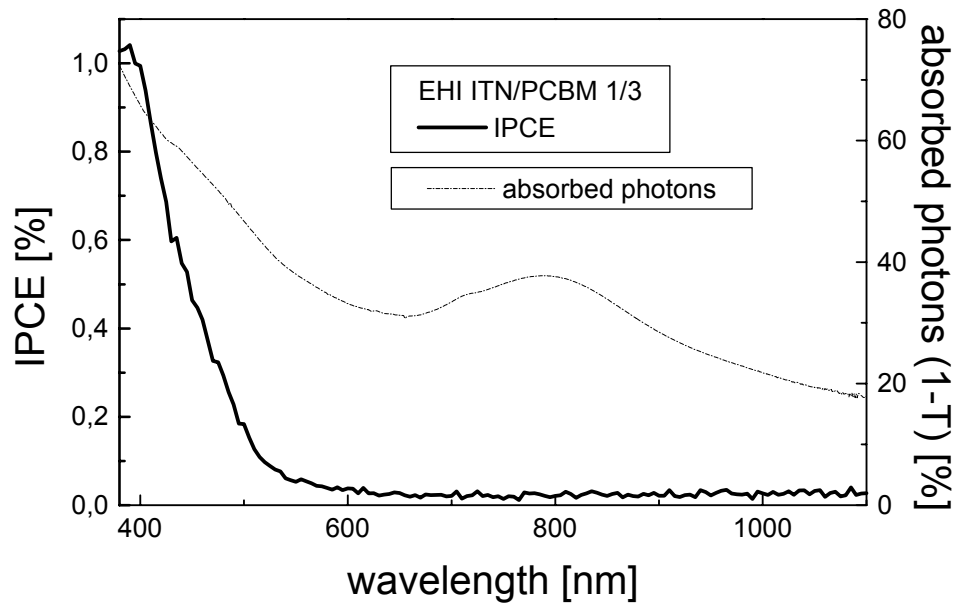


Figure 3. 14: IPCE of EHI-PITN/PCBM 1/3 solar cell (—) in standard configuration in comparison with the amount of absorbed photons in transmission of a film on glass (···).

The IPCE, presented in figure 3.14, shows no contribution of the polymer, the peak at 400 nm is caused by the PCBM absorption.

3.2.2 PME-EHI-PITN

The introduction of a methine linkage between the monomer units is a possible engineering way towards lower bandgap. Resulting from this, every other thiophene unit shows a chinoid-like structure instead of the aromatic one.

This concept was used for the EHI-ITN polymer. The structure of the resulting polymer Poly (methine-benzo[c] thiophene-*N*-2'-ethylhexyl-4,5-dicarboxylic imide, abbreviated as pME-EHI-ITN, is shown in figure 3.11. The material is soluble in chloroform in sufficient amounts. The optical absorption of a spin cast film from chloroform is shown in figure 3.15a. The maximum at 560 nm has an absorption coefficient of 6500 cm^{-1} . The film thickness is determined with 130 nm. The onset of the absorption is difficult to determine because of the extended tailing into the infrared. In comparison with absorption maximum of EHI-PITN, which is at 800 nm, it is shifted towards higher energies. The shift of the absorption maximum towards higher wavelength is in contrast to the expectation.

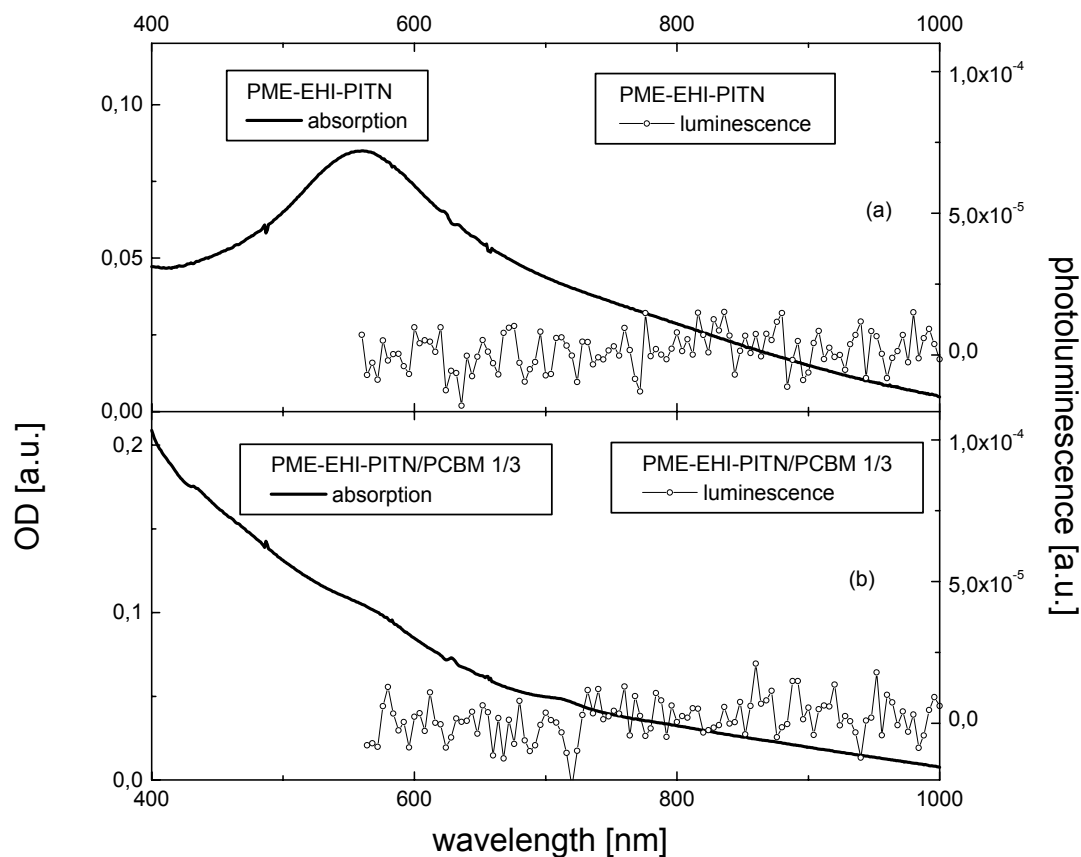


Figure 3. 15: (a) Optical density (—) and luminescence (-o-) of a PME-EHI-PITN film and (b) optical density (—) and photoluminescence (-o-) of a PME-EHI-PITN/PCBM 1/3 film, films are spin cast from 0.5 % chloroform solutions on cleaned glass substrates, the onset of the absorption is estimated with ~ 800 nm, which correspond with a bandgap of 1.55 eV; absorption is recorded at room temperature, luminescence at 100 K and excitation at 514 nm.

The absorption of the blend with PCBM, shown in figure 3.15b, is a linear superposition of the single spectra.

Solar cells are produced with an active layer of a PME-EHI-PITN/PCBM 1/3 blend, spin cast from chloroform. The recorded I-V curves are shown in figure 3.16. In the dark, the device shows a poor rectification of 8 at ± 1 V. Under solar simulator illumination, a clear photoeffect can be seen with an open circuit voltage of 0.44 V and a short circuit current of $37 \mu\text{A cm}^{-2}$. IPCE PCE measurements are presented in figure 3.17. The feature of the IPCE

spectrum does not follow the optical absorption of the blend and resembles more the absorption spectra of the pristine PCBM.

A contribution of the polymer to the photocurrent cannot be shown clearly. It is more likely, that the long wavelength contributions are originated by a forbidden excitation of PCBM.

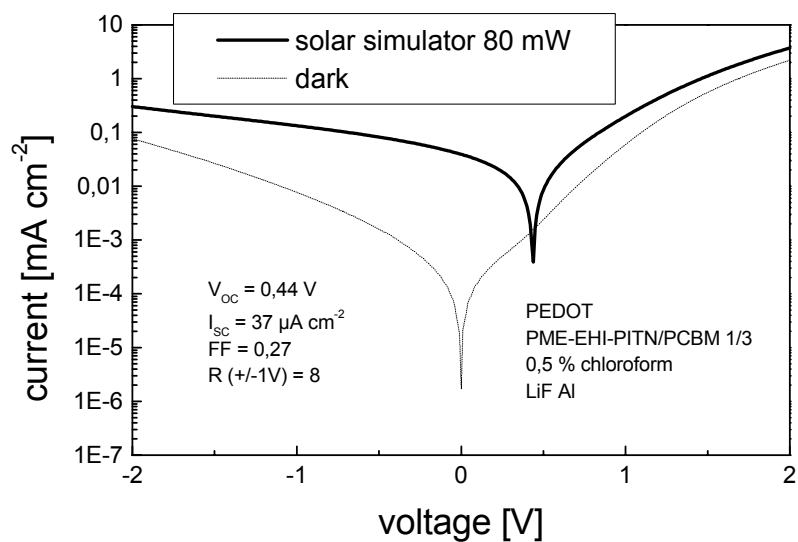


Figure 3.16: I-V curve in the dark (-----) and on the solar simulator (—) of PME-EHI-PITN/PCBM 1/3 solar cell in standard configuration, active layer is spin cast from a 0.5 % chloroform solution.

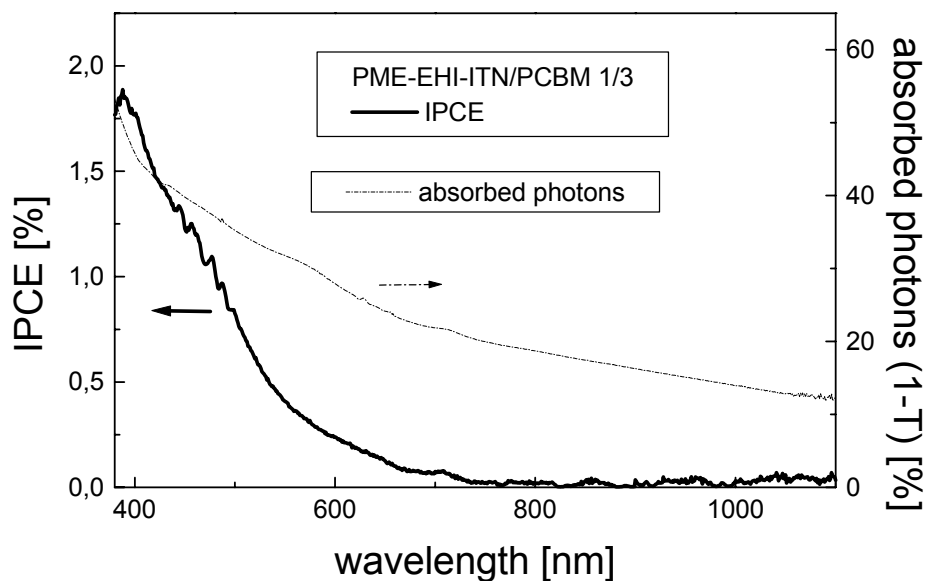


Figure 3. 17: IPCE of PME-EHI-PITN/PCBM 1/3 solar cell (—) in standard configuration in comparison with the amount of absorbed photons in transmission of a film on glass (....).

3.2.3 pEDOT-EHI-ITN

Copolymerisation of an electron rich unit like pEDOT and an electron deficient unit like the EHI-ITN, should lead to a reduction of the bandgap after the push-pull concept. The structure of the resulting polymer, poly (3,4-ethylenedioxythiophene)-N-2'-ethyl-4,5dicarboxylic-imide-benco[c]thiophene, pEDOT-EHI-ITN, is shown in figure 3.11.

The optical absorption is presented in figure 3.18a. The maximum at 808 nm has an coefficient of 10000 cm^{-1} ; the film thickness is approximately 80 nm. The onset of the absorption is determined at 1080 nm, corresponding with a bandgap of 1.15 eV. Compared to the EHI-PITN, the bandgap of the copolymer is reduced by nearly 100 meV. The absorption of the blend with PCBM is shown in figure 3.18. Neither in the pristine nor in the blend with PCBM, any photoluminescence is observed with the sensitivity of the setup.

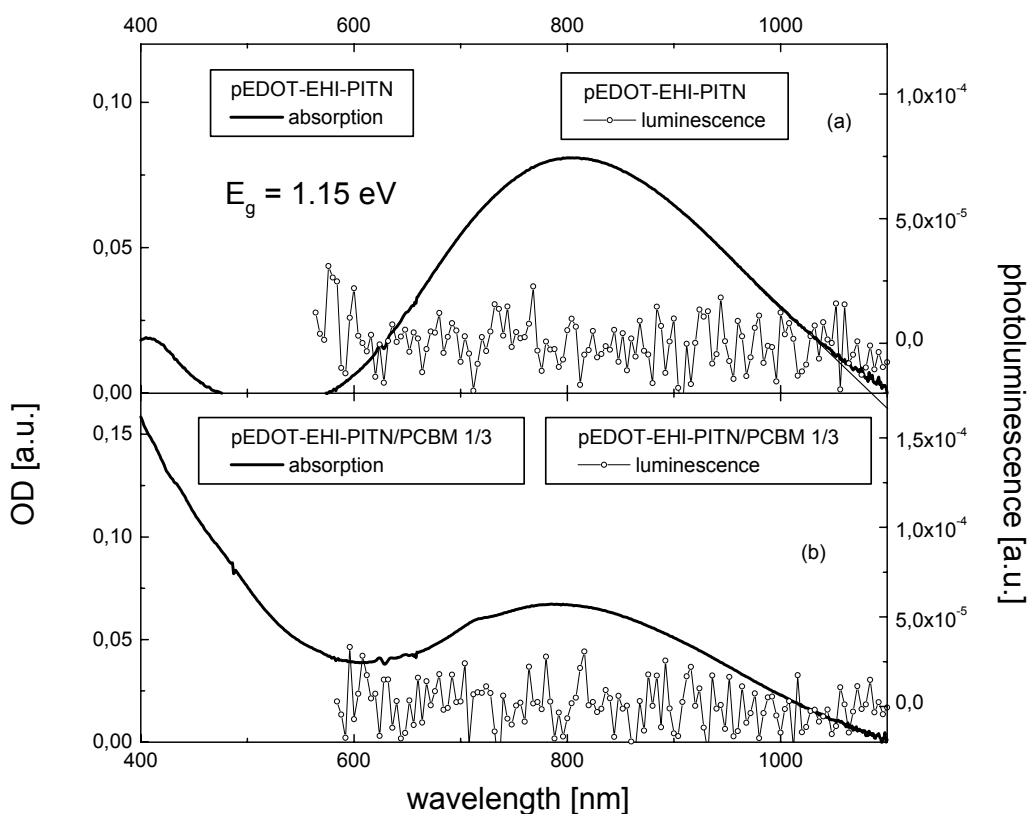


Figure 3. 18: (a) Optical density (—) and luminescence (---) of a pEDOT-EHI-PITN film and (b) optical density (—) and photoluminescence (---) of pEDOT-EHI-PITN/PCBM 1/3 film, films are spin cast from 0.5 % chloroform solutions on cleaned glass substrates, the bandgap is estimated by the

onset of the absorption; absorption is recorded at room temperature, luminescence at 100 K and excitation at 514 nm.

The I-V curves of the solar cell are shown in figure 3.19. The active layer is spin cast from chloroform. In the dark, the device show a good rectification of 46 at +/- 1 V, which is much higher than the corresponding solar cells of the other EHI-ITN derivatives. Under illumination, a strong photoeffect is observed with a surprising high short circuit current of 1 mA cm⁻². The open circuit voltage of 0.13 V is quite low.

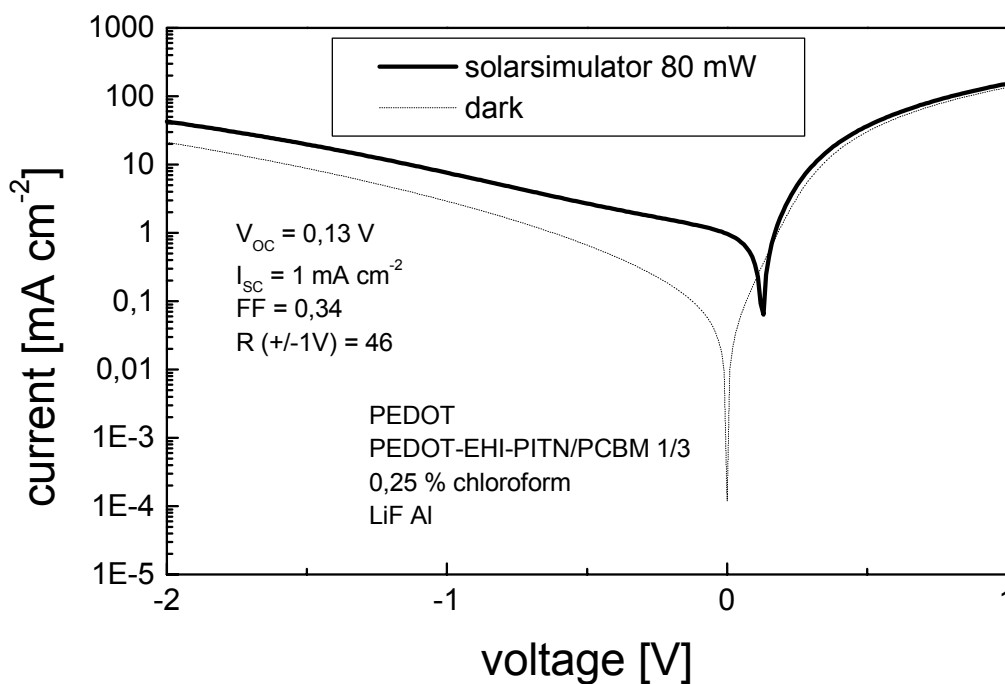


Figure 3. 19: I-V curve in the dark (-----) and on the solar simulator (—) of pEDOT-EHI-PITN/PCBM 1/3 solar cell in standard configuration, active layer is spin cast from a 0.25 % chloroform solution.

The IPCE, shown in figure 3.20, has a maximum around 450 nm with a broad shoulder at 700 nm and a long tailing to 1000 nm. The feature of the photocurrent matches nicely the absorption spectrum of the blend. Whereas the maximum originates from the PCBM absorption, in the shoulder and the tailing towards the infrared can be clearly assigned as contribution of the polymer. At 1000 nm, the IPCE is still roughly 0.5 %. To the best of my knowledge, photocurrent at 1.2 eV is the lowest value, which has been observed until now in polymer bulk heterojunction solar cells.

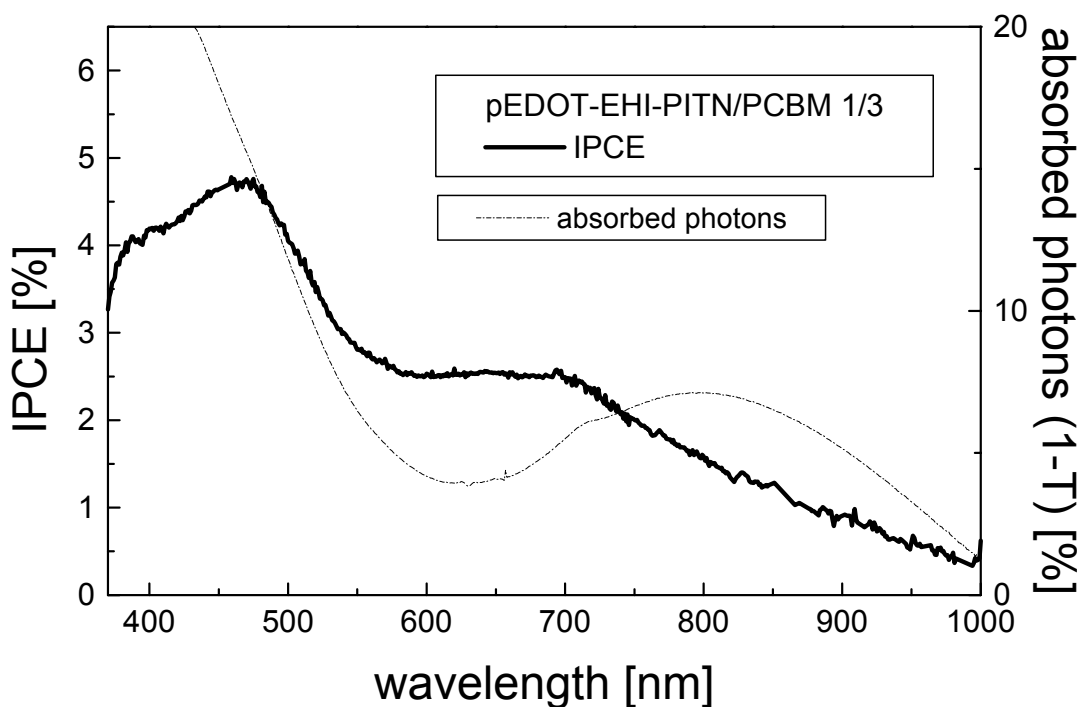


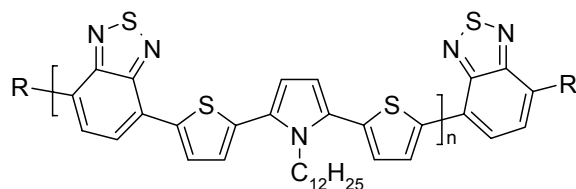
Figure 3.20: IPCE of pEDOT-EHI-PITN/PCBM 1/3 solar cell (—) in standard configuration in comparison with the amount of absorbed photons in transmission of a film on glass (···).

The reason of the low open circuit voltage is unclear up to now. Solar cells with a stronger accepting fullerene derivative do not show any increase in performance.

3.3 PTPTB

This material was designed and synthesized principally for photovoltaic application by the group of R.A.J. Janssen at the technical university of Eindhoven [65] and was provided to the university of Linz for spectroscopic characterization and testing in solar cell application. The same group showed also the photoinduced charge transfer from the polymer to PCBM by photoinduced absorption spectroscopy and the usability of the polymer in solar cell devices [66].

The conjugated polymer *Poly-N-dodecyl-2,5-bis(2'-thienyl)pyrrole-2,1,3-benzothiadiazole*, abbreviated as PTPTB, follows the push-pull concept by altering electron rich N-dodecyl-2,5-bis(2'-thienyl)pyrrole and electron deficient 2,1,3-benzothiadiazole groups. The structure can be seen in figure 3.21.



PTPTB

Figure 3.21: Chemical structure of PTPTB (*Poly-N-dodecyl-2,5-bis(2'-thienyl)pyrrole-2,1,3-benzothiadiazole*).

Spectroscopy

The optical absorption and luminescence of a dilute solution of PTPTB in toluene solution is shown in figure 3.22. The molar extinction coefficient for the peak at 534 nm is determined with $14200 \text{ l mol}^{-1} \text{ cm}^{-1}$ *. The specific absorption at the maximum is therefore $27 \text{ l g}^{-1} \text{ cm}^{-1}$. The onset of the absorption is estimated at 670 nm.

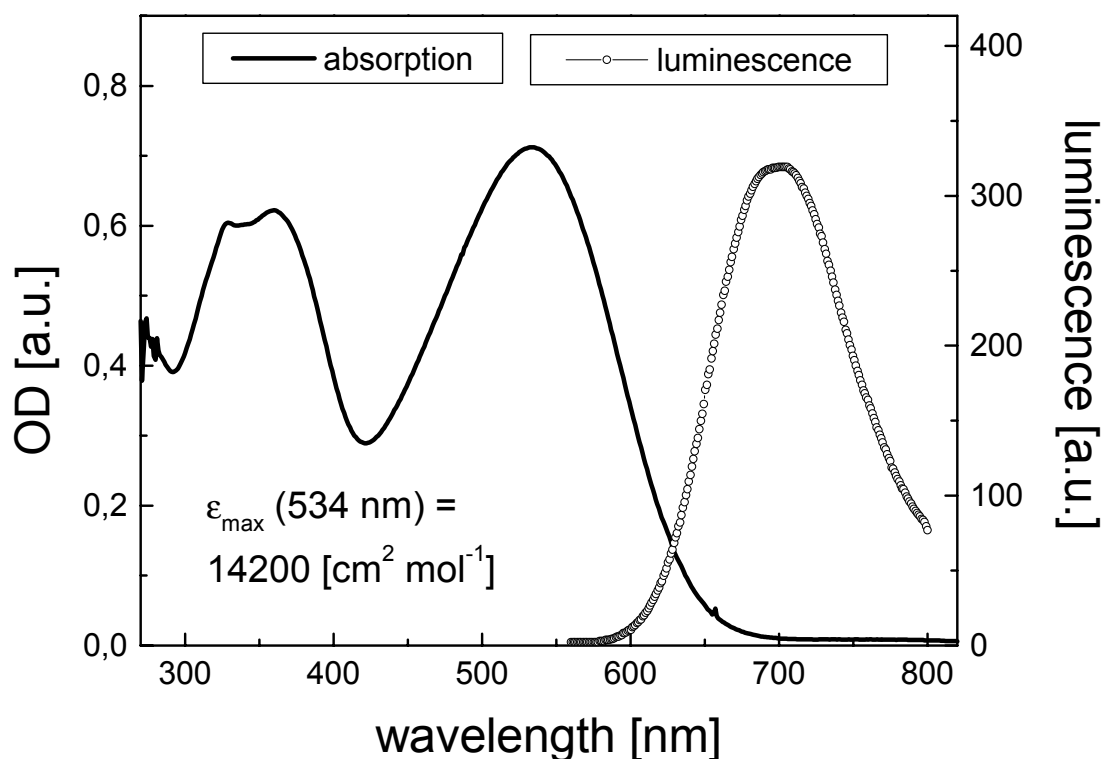


Figure 3. 22: Optical absorption (—) and luminescence (-o-) of PTPTB in a $5 \cdot 10^{-5} \text{ mol l}^{-1}$ toluene solution, the excitation wavelength for the luminescence measurement is 500 nm.

Films for spectroscopic measurements are spin cast from a 1 % chlorobenzene solution. The absorption and luminescence are shown in figure 3.23a for the pristine material and 3.23b for the mixture with PCBM. The absorption maximum of the polymer film is at 600 nm. This is a large shift in comparison to the solution. The absorption is a linear superposition of the single components, whereas the photoluminescence is quenched completely. This fact indicated photoinduced charge transfer of electrons from PTPTB to PCBM.

* as molecular unit, the monomer as drawn in figure 3.21 is taken ($M = 531 \text{ g mol}^{-1}$)

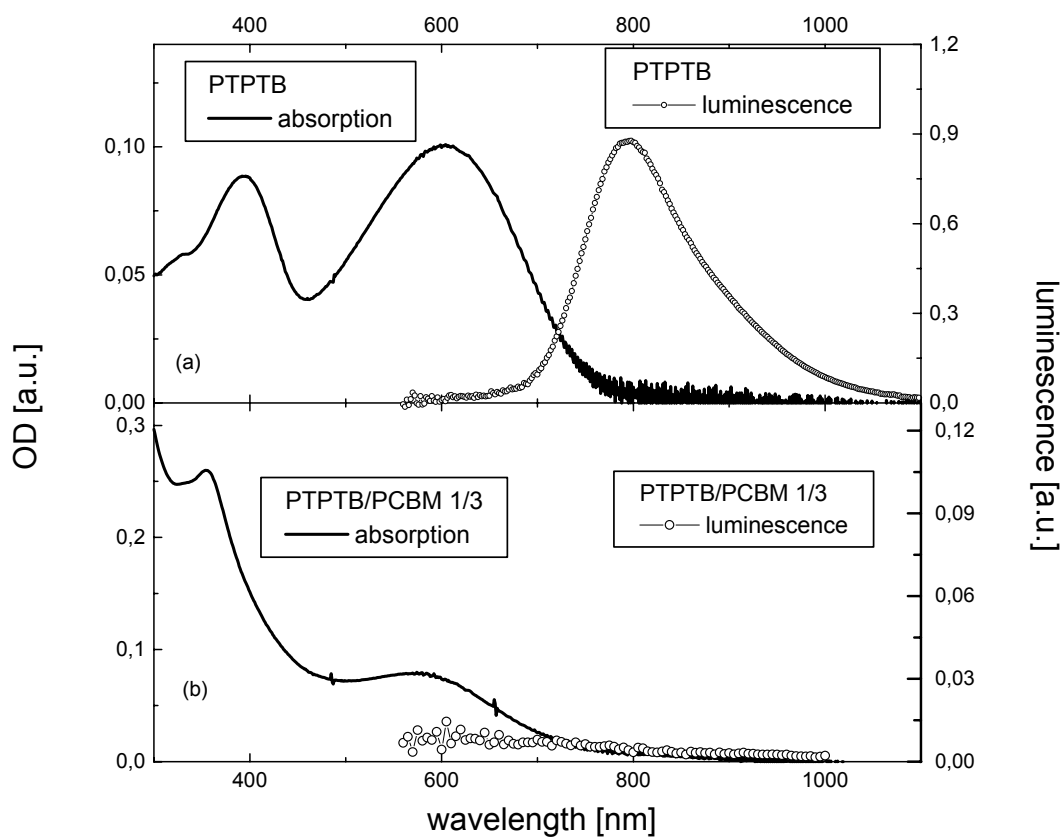


Figure 3. 23: (a) Optical density (—) and luminescence (-o-) of a PTPTB film and (b) optical density (—) and photoluminescence (-o-) of PTPTB/PCBM 1/3 film, films are spin cast from 1 % chlorobenzene solutions on cleaned glass substrates, the band gap is estimated by the onset of the absorption; all measurements were done at room temperature, for luminescence was the excitation at 476 nm.

Devices

Already first attempts as well as literature results shows the great potential of PTPTB for bulk heterojunction solar cells. Therefore, the parameters for device preparation are thoroughly tested. Several solvents are tested and the thickness of the active layer is varied.

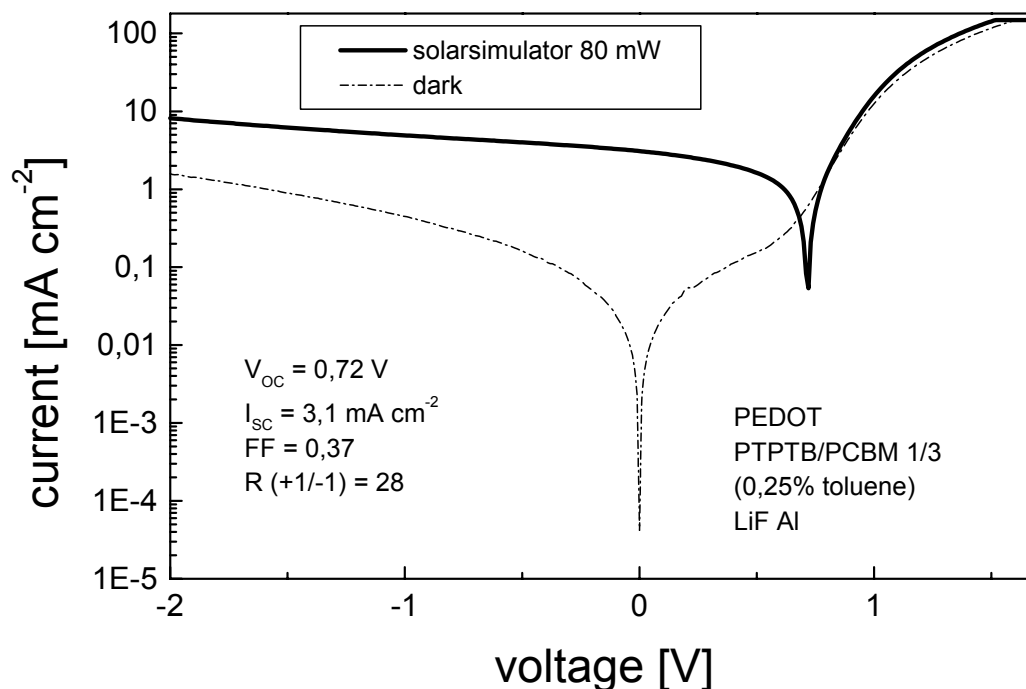


Figure 3. 24: I-V curve in the dark (-----) and on the solar simulator (—) of PTPTB/PCBM 1/3 solar cell in standard configuration, active layer is spin cast from a 0.25 % toluene solution.

The best results show devices, which are spin cast from toluene solution and with a relatively thin layer. The results for the optimized solar cells are shown in figure 3.24. In the dark, the I-V curve shows good rectifying behaviour. In forward direction, the onset for the current is around 0.7 V . Under solar simulator conditions, the device exhibits an intense photoeffect with an open circuit voltage of 0.72 V , which coincide with the injection current onset. Note, that the open circuit voltage in comparison to best MDMO-PPV devices is lowered by less than 100 mV after a reduction of the bandgap of more than 500 meV . The fill factor of 0.37 is higher than the often-observed values between 0.25 and 0.3 for poor diode behaviour. But it is still lower than for the best polymer solar cells. The overall power efficiency is around 1% .

The contribution of the PTPTB to the current can be clearly seen in the IPCE curve, shown in figure 3.25 in comparison with the amount of absorbed photons. The two spectra match well.

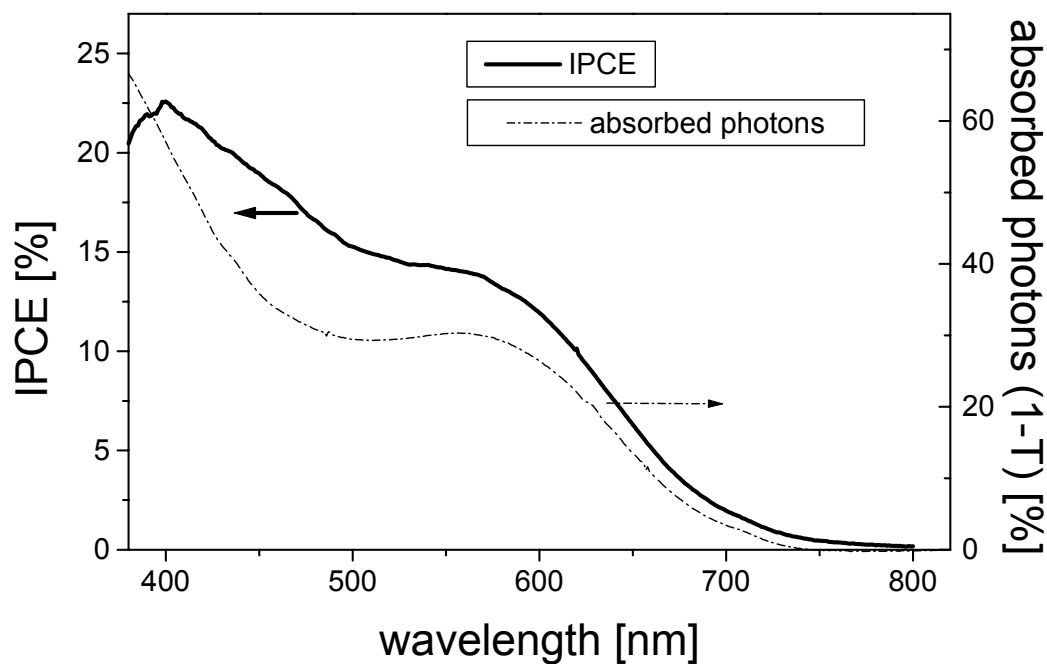


Figure 3. 25: IPCE of a PTPTB/PCBM 1/3 solar cell (—) in standard configuration in comparison with absorption spectrum in transmission of a film spin cast from the same solution on glass (···).

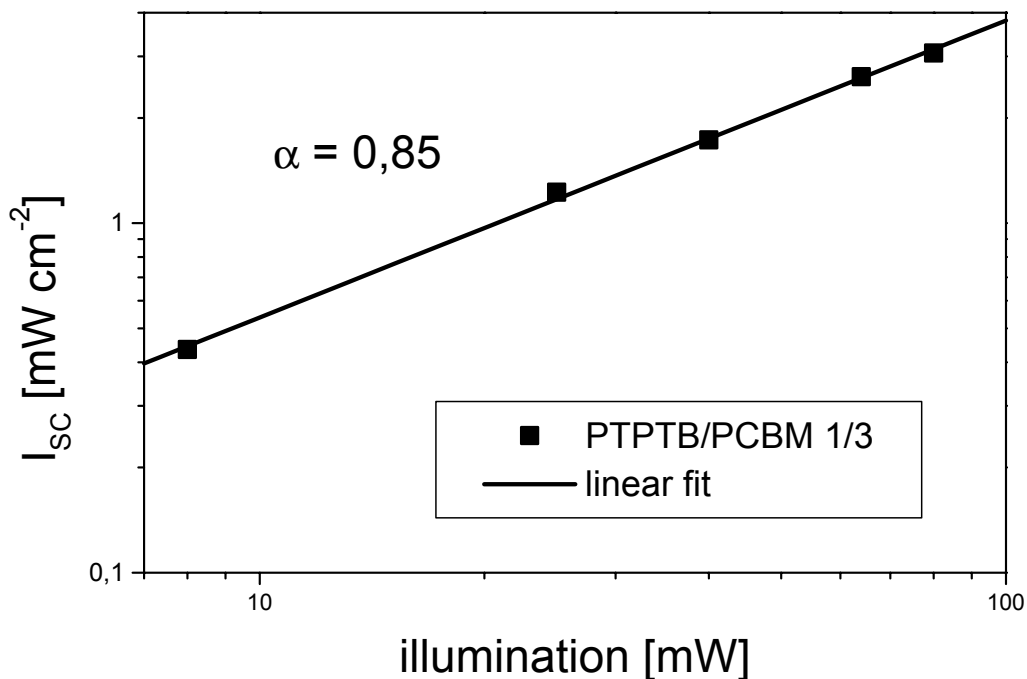


Figure 3. 26: Dependence of the short circuit current (■) on the illumination of a PTPTB/PCBM solar cell in standard configuration, linear fit is done by a power law dependence.

In order to understand the device operation in more detail, several characterization techniques are used for the device and the active layer. The short circuit current depends on the illumination, fitted by a power law, with $\alpha = 0.85$. For the data and linear fit see figure 3.26.

The sub linear behavior indicates partially contribution of bimolecular recombination, which lowers the device efficiency at higher illuminations. AFM picture, see figure 3.27, shows a rather rough surface with several spots, which shows a height up to 5 nm. As mentioned before, surface roughness is known to limit the power conversion of the solar cell.

The relative bad film quality may originate from short chain length of the polymer. As reported from the synthetic group, size exclusion chromatography shows chain length between 1-4. Short chain lengths are unfavorable for spin cast. Admixing of high molecular weight polymers like PMMA and PS, which has reported to improve the film quality without

influence the photovoltaic behavior for MDMO-PPV devices, does not show any improvement of whether the film quality nor the photovoltaic behavior.

For the low fill factor, several reasons may be relevant. Generally, the fill factor is indicating high serial resistances or low parallel resistances. Since high injection currents are observed in forward direction, significant influence of a serial resistance can be excluded. A low parallel resistance, or shunts, is more likely and in agreement with the bad film quality observed in AFM measurements.

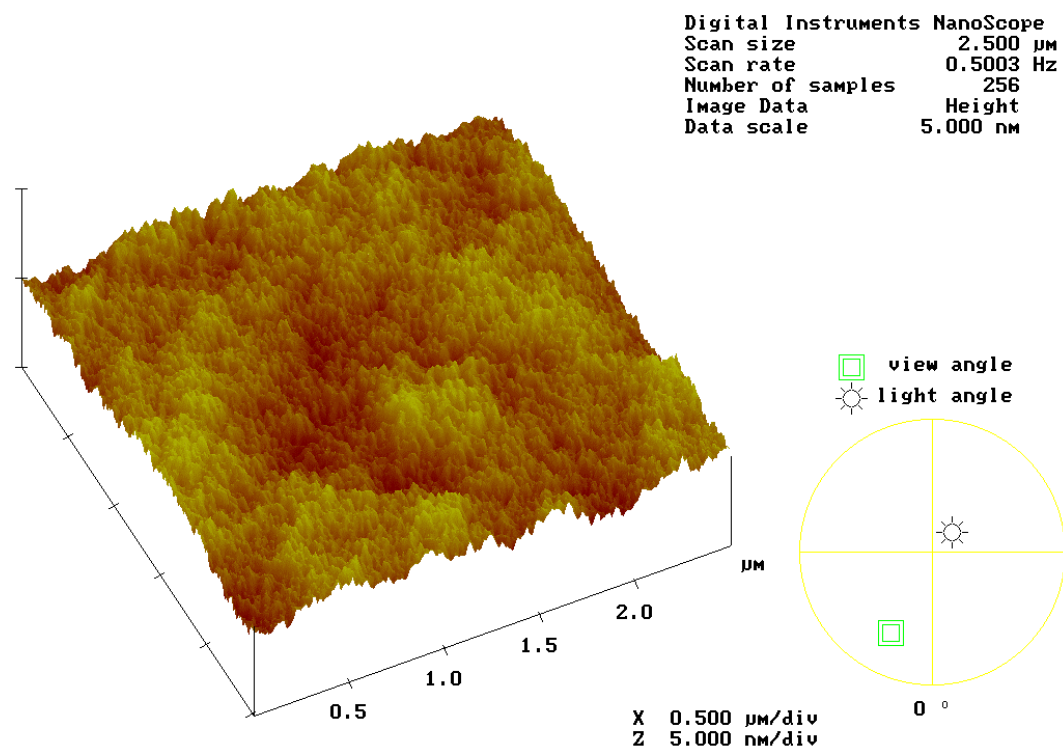


Figure 3. 27: AFM picture in tapping mode of the active layer of a PTPTB/PCBM 1/3 device, spin cast from 0.25 % toluene solution.

Electroluminescence from PTPTB

As reported in the introduction, LEDs from conjugated polymers are on the step to market introduction. In the numerous polymers presented in the literature giving electroluminescence, there is just a handful of polymer, which emits in the near infrared [67,68].

PTPTB films show photoluminescence peak at 800 nm with a tailing into the infrared. The question is now, if it is possible to obtain electroluminescence from PTPTB.

For this purpose, devices of pristine PTPTB with ITO/PEDOT and Ca electrodes are made to ensure balance of electron and hole injection in the device. Figure 3.28 shows light emission around 800 nm, which is in the same range than the photoluminescence of PTPTB. PTPTB shows electroluminescence and can therefore be successfully applied in LEDs. The onset of the electroluminescence with applied voltage coincide with the current injection, see figure 3.29. It should be point out here that the currents are quite high, in the range of 1 A cm^{-2} compared to the relative weak electroluminescence. Also the usage of LiF/Al electrodes instead of Ca give the same results, indicating the formation of a low barrier contact of LiF/Al to the polymer, as described in the introduction.

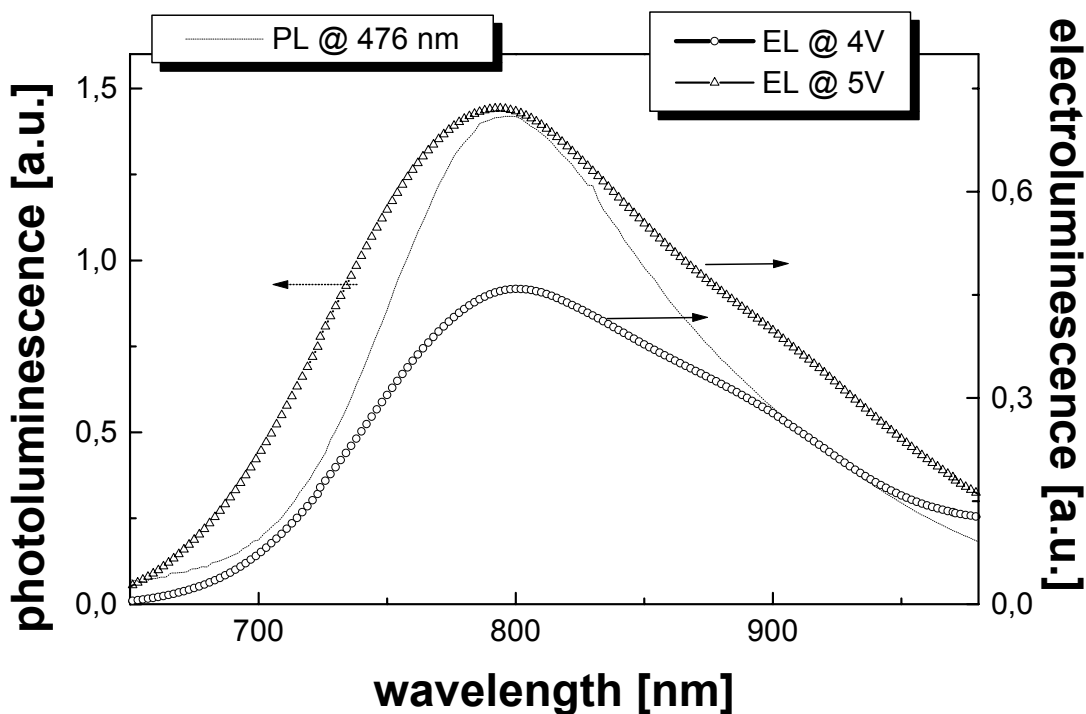


Figure 3. 28: Photoluminescence (---) of a PTPTB film, spin cast from a 1 % chlorobenzene solution, excitation at 476 nm and 40 mW and the electroluminescence from a pristine PTPTB device at 4V (-o-o-) and 5V (-□-□-); all spectra are corrected for the spectrometer sensitivities.

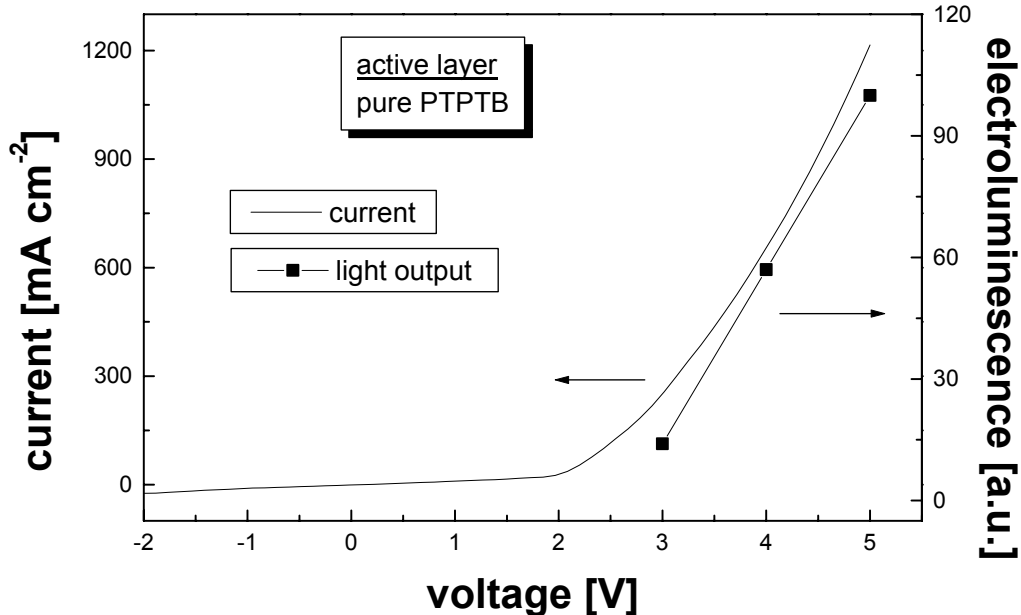


Figure 3.29: I-V curve (—) of a pristine PTPTB device, spin cast from a 1 % chlorobenzene solution, in comparison with its integrated electroluminescence (-■-■-)

Several techniques have been developed to increase electroluminescence yield of organic devices. The aim of all of them is to balance the amount of electron and hole in the active layer. This can be achieved by:

- (i) choice of contact materials,
- (ii) introduction of additional charge transport layers of
- (iii) sensitization with wide bandgap materials.

The last approach is very attractive for this work because it is the same idea as for the sensitization of solar cells: Creation of an exciton on a high bandgap material, which is then transferred to the material of lower bandgap. Unlike in solar cells, in LED's charge transport should be done by the wide bandgap material. Electrons and holes recombine on the wide bandgap material, creating excitons. These excitons are transferred to the low bandgap material and decay, showing the luminescence of the low bandgap material.

MDMO-PPV is chosen as the transport material. Besides its usage in organic photovoltaic, it is important as active layer in LEDs. Devices from MDMO-PPV show an intense electroluminescence 650 nm. This emission overlaps with the absorption of PTPTB, resonant

energy transfer, for example by a Foerster mechanism as described in the introduction, is likely.

Indication for energy transfer can be easily seen in photoluminescence studies. By exciting the wide bandgap material, the emission of the low bandgap material should be preferentially observed, whereas the emission of the wide bandgap material is quenched.

Different blends of MDMO-PPV/ PTPTB are spin cast from chlorobenzene solution. The optical density is measured and presented in figure 3.30a. The photoluminescence is shown in figure 3.30b. For a film containing 5 % PTPTB, the luminescence of the MDMO-PPV at 600 nm is quenched nearly completely, note the logarithmic scale on the y-axis. Instead, an intense peak around 780 nm is observed, origins from PTPTB. For comparison, the optical absorption is dominated by MDMO-PPV, whereas the PTPTB cannot be made out.

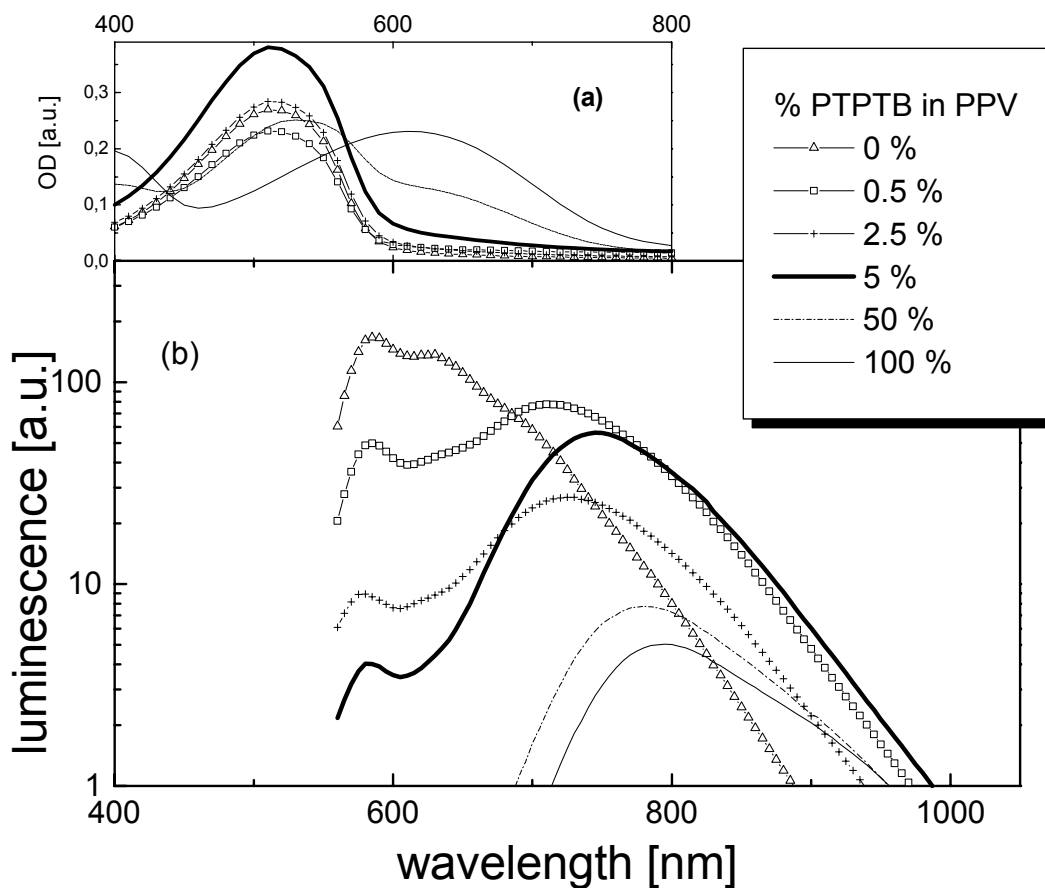


Figure 3. 30: (a) Optical density of different PPV/PTPTB mixtures, spin cast from chlorobenzene solutions on glass, (b) photoluminescence of the PPV/PTPTB films, excited at 514 nm; photoluminescence spectra are corrected for the detector sensitivity and the absorption at 514 nm.

LEDs are made with the MDMO-PPV/PTPTB mixtures and LiF/Al electrodes. The electroluminescence of these devices can be seen in figure 3.31. For an active layer containing 0.5 % of the low bandgap material, the electroluminescence spectrum is still dominated by the MDMO-PPV. But for the 5 % blend, the peak clearly shifts to 780 nm and the MDMO-PPV peak at 650 nm is quenched. The increasing of the PTPTB emission can be clearly seen by comparing the spectra of 5 % and the pristine PTPTB. For better comparison, the same plot is shown with logarithmic y-axis in the insert. The emission is increased more by nearly two orders of magnitude in the blend compared to pristine material. Considering the dilution of the material in the blend, the electroluminescence efficiency of PTPTB is increased by a factor of 1000.

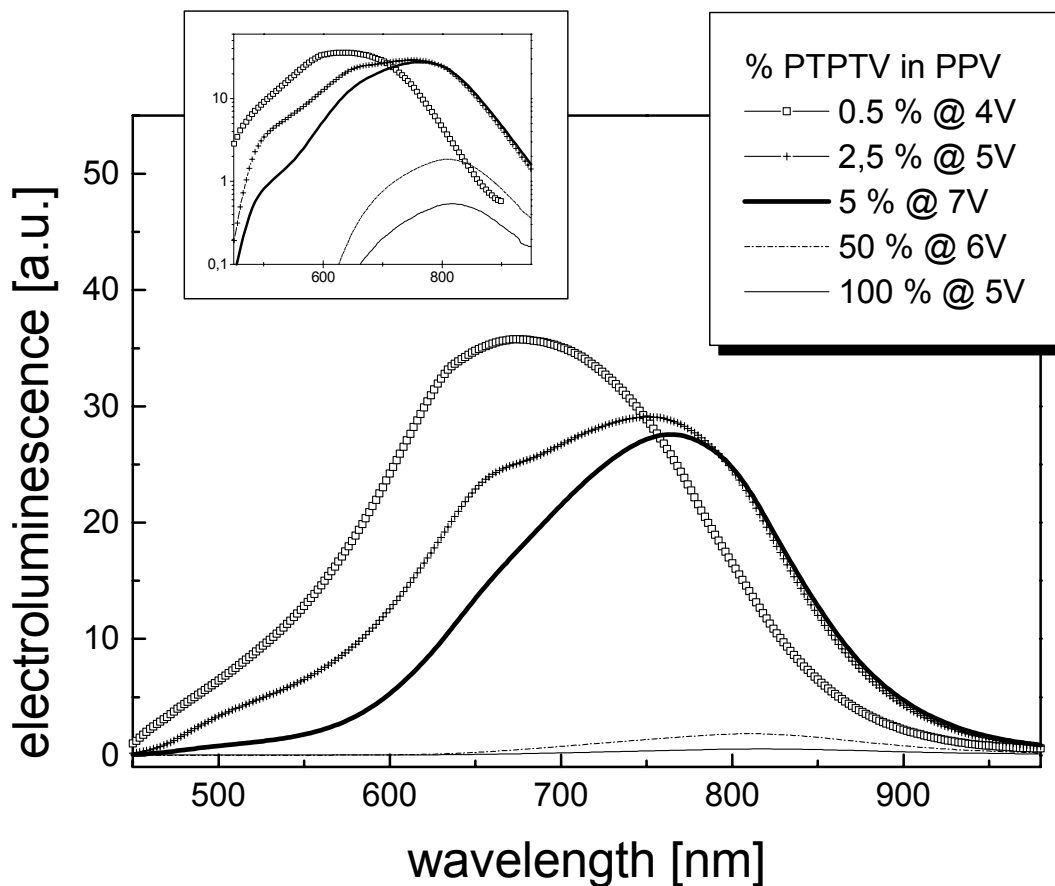


Figure 3. 31: Electroluminescence of devices with PPV/PTPTB mixtures as active layer, the absolute electroluminescence shows saturation at the given voltages. The insert shows the same data in a logarithmic plot, in order to show the weak electroluminescence of the pristine PTPTB.

4 Sensitization of Solar cells – Results and Discussion

4.1 Sensitization with MDMO-PPV

MDMO-PPV/PCBM solar cells show power conversion efficiencies up to 3 %, which are the highest efficiencies reported for polymer solar cells. After the encouraging results for sensitisation PTPTB with MDMO-PPV for LEDs, this idea is now applied for solar cells.

The excitation transfer from MDMO-PPV to PTPTB has been shown in the last chapter.

Devices

Active layers for the solar cells are spin cast from 0.3 % chlorobenzene solution, related on the polymer concentration: MDMO-PPV/ PTPTB/PCBM 0.5/0.5/4.

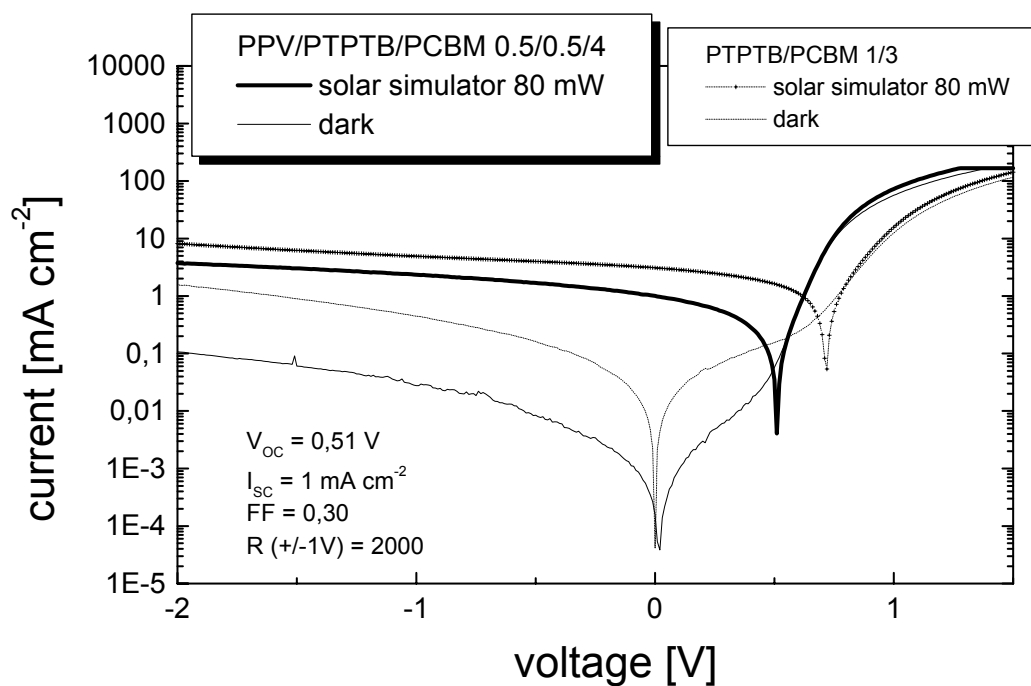


Figure 4.1: I-V curve of a device with PPV/PTPTB/PCBM 0.5/0.5/4 as active layer, spin cast from a 0.3 % chlorobenzene solution, under solar simulator 80 mW illumination (—) and in the dark (---); in comparison the I-V curve of an optimised PTPTB/PCBM device under solar simulator illumination (---) and in the dark (---).

Figure 4.1 shows the I-V curves of this device in comparison to a PTPTB/PCBM device. The injection current in forward direction is nearly an order of magnitude higher than in the corresponding PTPTB solar cell, although the cell is obviously thicker. On the onset for the current injection is shifted to lower bias. This facts lead to a rectification value of 2000 at +/- 1 V.

The open circuit voltage of the sensitised device is 0.51 V, which is more than 200 mV less than for the non-sensitized PTPTB device. This is in accordance with the shift of the current onset in forward direction. The reason for the short circuit current of 1 mA cm^{-2} is not understood. Also the fill factor, despite the high rectification, is rather poor. Further analysis of this device should help to understand the problems of this device.

In figure 4.2, the IPCE is compared with the amount of absorbed photons. Therefore, both polymers show a contribution to the photocurrent, but the PTPTB one is weaker than that of MDMO-PPV. The dependence of the short circuit current on the light intensity, presented in figure 4.3, shows in the power law fit a gradient of $\alpha = 0.78$. This behaviour is clearly sub linear and is interpreted as due to either recombination or excitons of charge trapping [42].

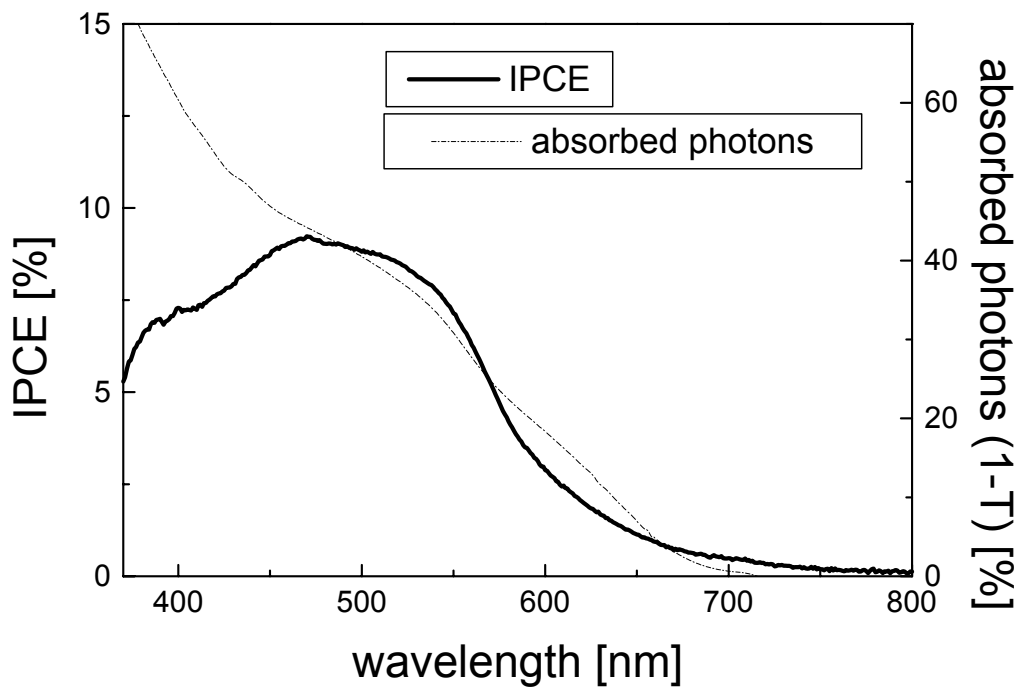


Figure 4.2: IPCE of a PTPTB/PPV/PCBM 0.5/0.5/4 solar cell (—) in comparison with absorption spectrum in transmission of a film spin cast from the same solution on glass (···).

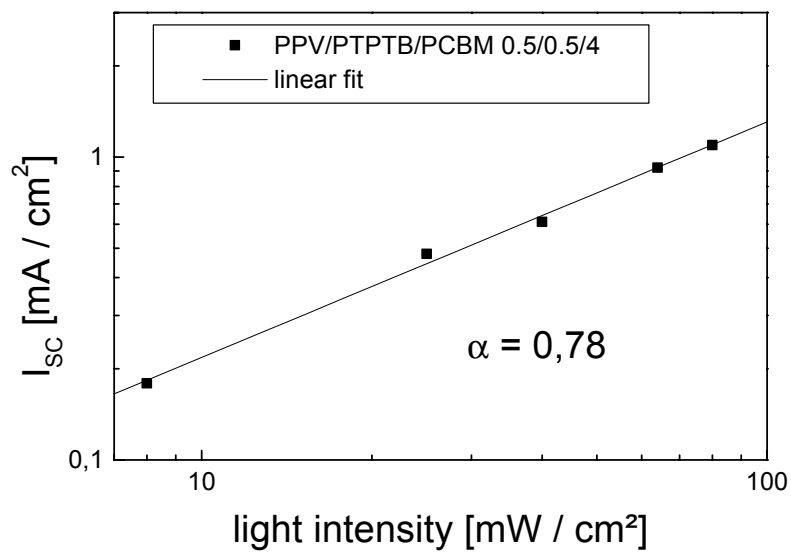


Figure 4.3: Dependence of the short circuit current (■) on the illumination of a PPV/PTPTB/PCBM 0.5/0.5/4 solar cell in standard configuration, linear fit is done by a power law dependence.

AFM picture of the active layer is shown in figure 4.4. It shows much spots up to a height of 15 nm. This is large and may be a hint on large-scale phase separation.

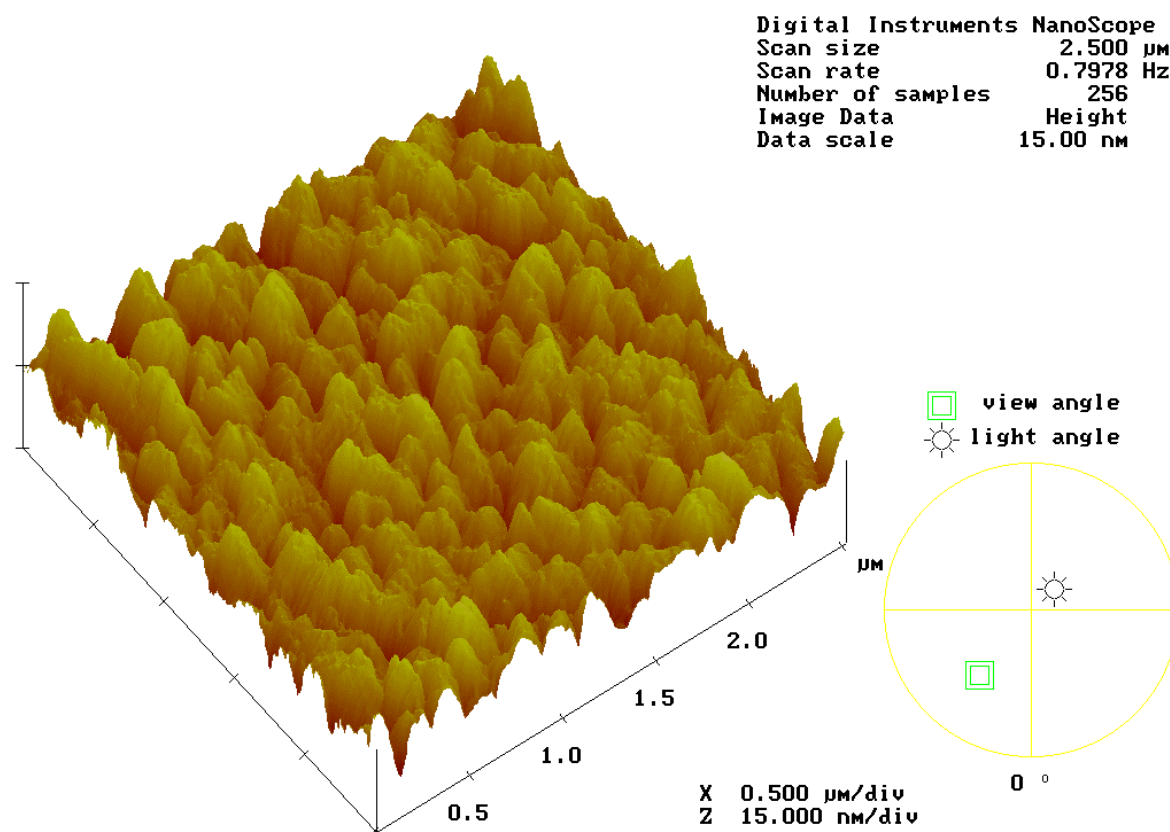


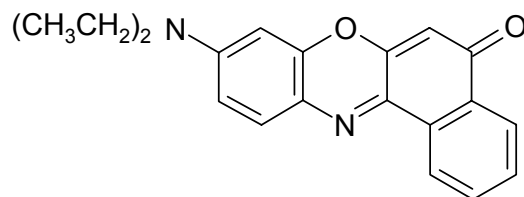
Figure 4. 4: AFM picture in tapping mode of the active layer of a PPV/PTPTB/PCBM 0.5/0.5/4 device, spin cast from 0.3 % chlorobenzene solution.

4.2 Sensitization with Nile Red

Sensitization with small dye molecules can increase the absorption of the active layer significantly.

Spectroscopy

9-(Dimethylamino)-5H-benzo[a]phenoxazin-5-one, named Nile Red, is a well-known dye from molecular biology and polymer LEDs [69], where it is used as emitting layer. Its structure is shown in figure 4.5. The overlap of the Nile Red photoluminescence and the PTPTB absorption should lead to energy transfer. The spectroscopic data will show the suitability to sensitize PTPTB solar cells after the proposed mechanism.



Nile Red

Figure 4.5: Chemical structure of Nile Red (9-(Diethylamino)-5H-benzo[a]phenoxazin-5-one).

Optical absorption and photoluminescence of Nile Red in dioxan solution are presented in figure 4.6, data are taken after reference [70]. The absorption peak is at 520 nm, the molar extinction coefficient is reported with $38000 \text{ l mol}^{-1} \text{ cm}^{-1}$. The molar mass is determined with 338 g mol^{-1} , hence, the specific absorption is $112 \text{ l g}^{-1} \text{ cm}^{-1}$. This is 5-10 times higher than the absorption coefficients for the polymer. It should be pointed out here, that the absorption coefficients may change with the solvent and the solution values does not necessarily describe the absorption in solid state. Nile Red shows a luminescence around 580 nm.

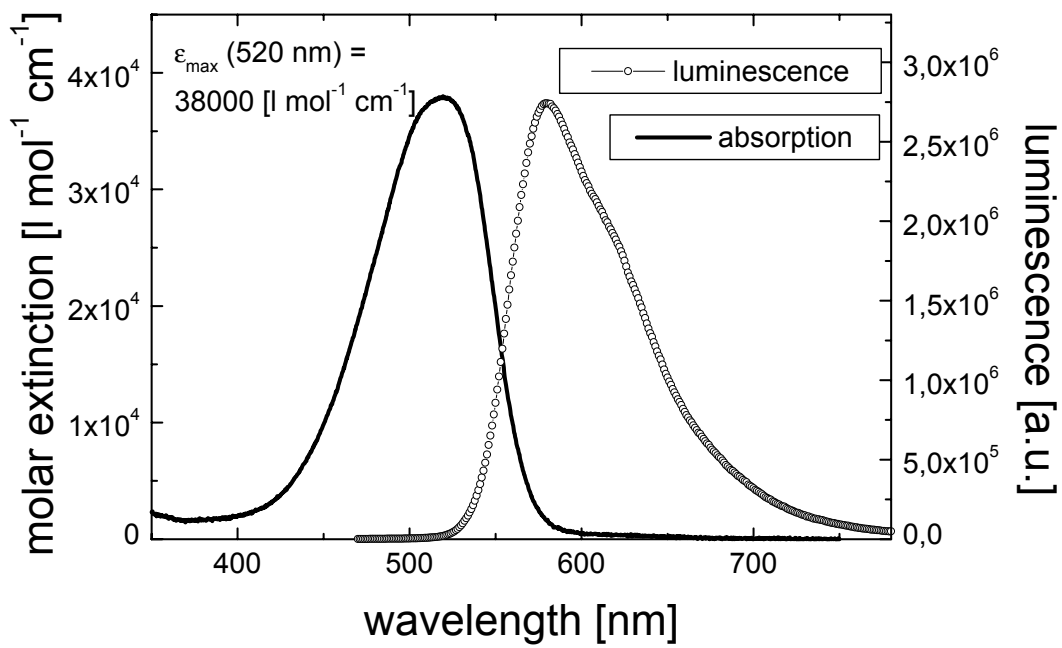


Figure 4.6: Optical absorption (—) and luminescence (-o-) of Nile red in dioxan solution, excitation for photoluminescence at 460 nm, after reference [70]

Nile red forms thin films neither by spin casting nor drop casting. Therefore, Polymethylmethacrylat PMMA is used as host materials. The spectroscopic data of Nile Red, dispersed in PMMA, are shown in figure 4.7a. The optical absorption and luminescence after addition of PCBM is shown in figure 4.7.b. Whereas the absorption is a linear superposition of the single spectra, the luminescence is quenched completely, indicating photoinduced charge transfer.

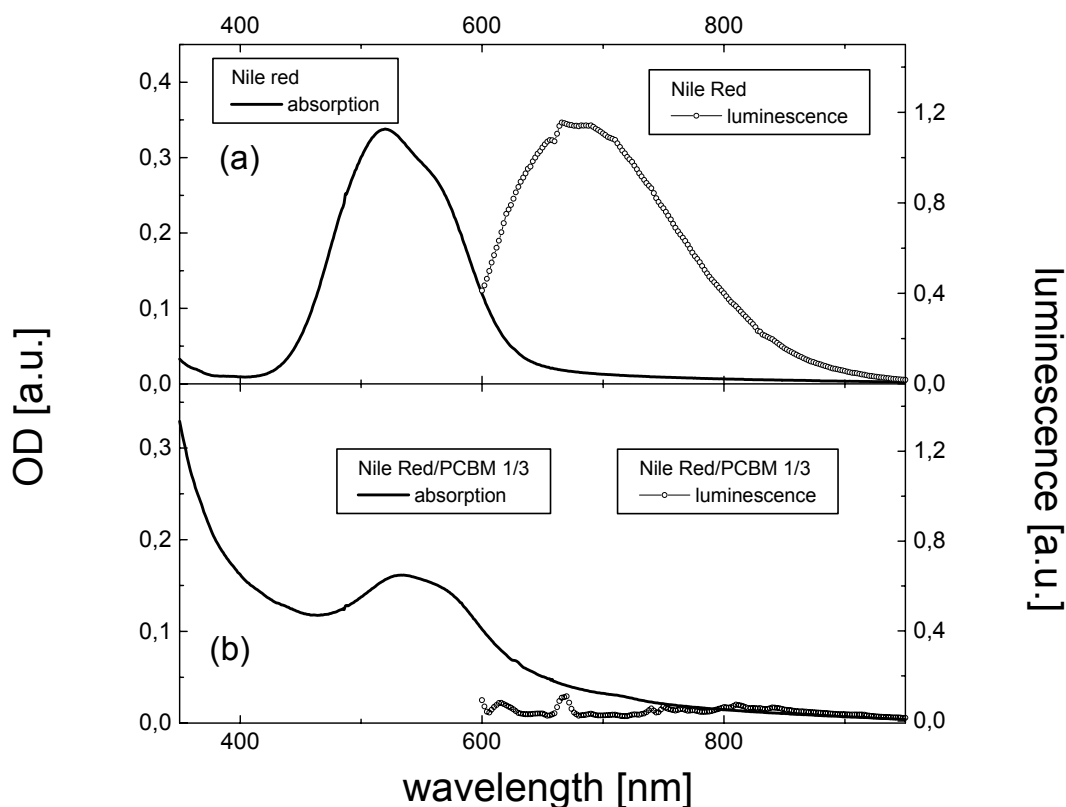


Figure 4.7: (a) Optical density (—) and luminescence (- -) of a Nile Red film and (b) optical density (—) and photoluminescence (- -) of Nile Red/PCBM 1/3 film, Nile Red is spin cast from 0.5 % toluene solution, using PMMA 1:1 as host polymer, Nile Red/PCBM from a 0.33 % toluene solution with PMMA 1:1 with respect to Nile Red. Absorption and luminescence is recorded at room temperature. Excitation for photoluminescence measurement is done with an Argon laser at 514 nm. PMMA does not show any absorption in this range (onset 350 nm).

The spectroscopic data of blends with PTPTB are presented in the figures 4.8a and 4.8b. The luminescence is shifted for a Nile Red/ PTPTB 5/1 blend from 680 nm for the pristine Nile Red to 750 nm. For the Nile Red/ PTPTB 1/ 10 blend, the Nile Red luminescence is quenched and the same feature as for pristine PTPTB is observed. The shift of the luminescence indicates energy transfer from Nile Red to PTPTB.

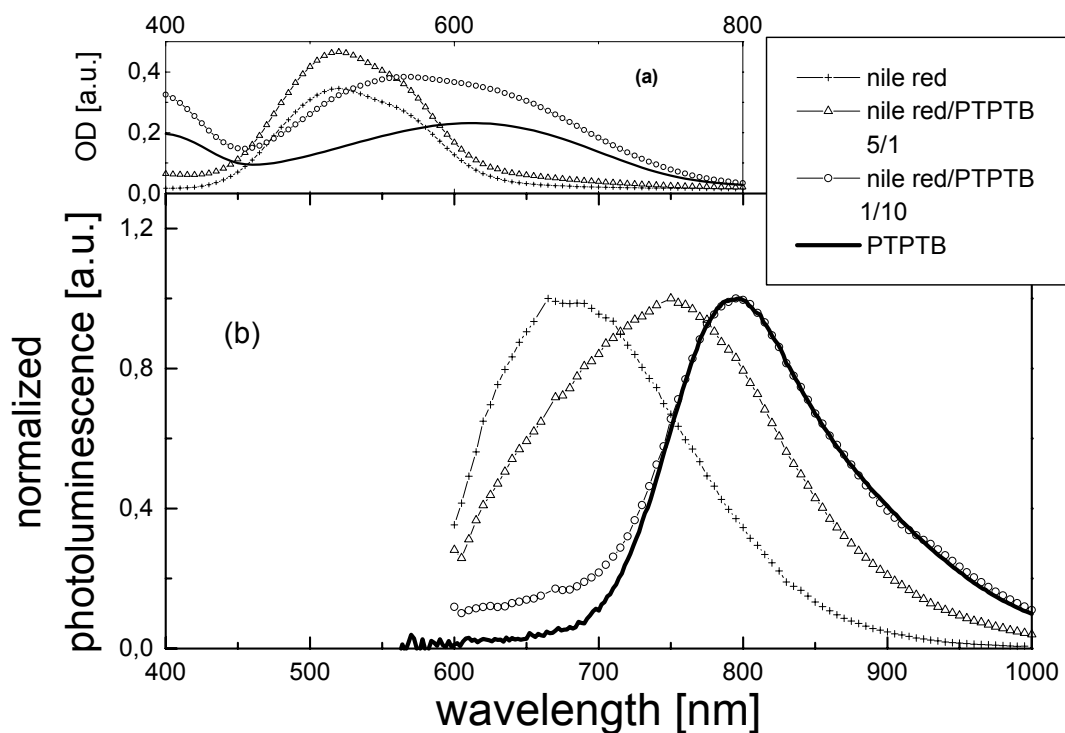


Figure 4.8: (a) optical absorption and (b) photoluminescence of Nile Red/ PTPTB mixture spin cast from toluene solution on glass. For the pristine Nile Red film, PMMA is used as host material. (-+-) Nile Red, (-Δ-) Nile Red/PTPTB 5/1, (-○-) Nile Red/ PTPTB 1:10 and (—) for pristine PTPTB luminescence is excited at 514 nm and the peak value is normalized to 1.

Devices

Solar cells from PTPTB/PCBM with the addition of 10 % Nile red are prepared. The I-V curves are shown in figure 4.9 in comparison with the not sensitised PTPTB device. In the dark, the onset of the current injection in forward direction is shifted by approximately 200 mV.

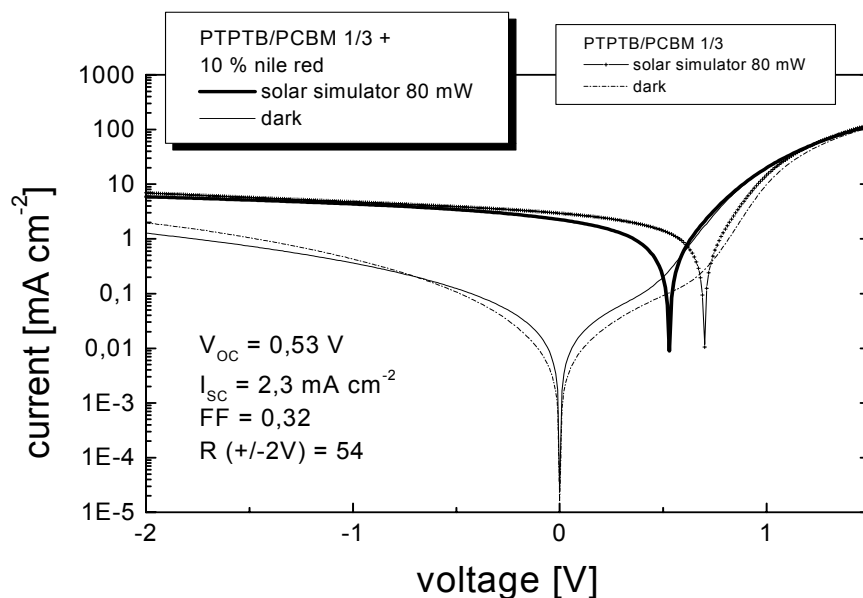


Figure 4.9: I-V curve of a device with PTPTB/PCBM 1/3 +10 % Nile red as active layer, spin cast from a 0.33 % toluene solution, under solar simulator 80 mW illumination (—) and in the dark (---); in comparison the I-V curve of an optimised PTPTB/PCBM device under solar simulator illumination (---) and in the dark (---).

For the illuminated cell, a clear photoeffect is observed. The open circuit is 530 mV, which reflects the lower voltage for current injection onset. The injection currents at +1.5 V are almost the same for both devices. The short circuit current of 2.3 mA cm⁻² is in the same range than for the not sensitised device.

The spectrally resolved photocurrent, presented in figure 4.10 in comparison with the amount of absorbed photons, shows its maximum at 550 nm and the onset at 750 nm. IPCE and absorption spectra fit well.

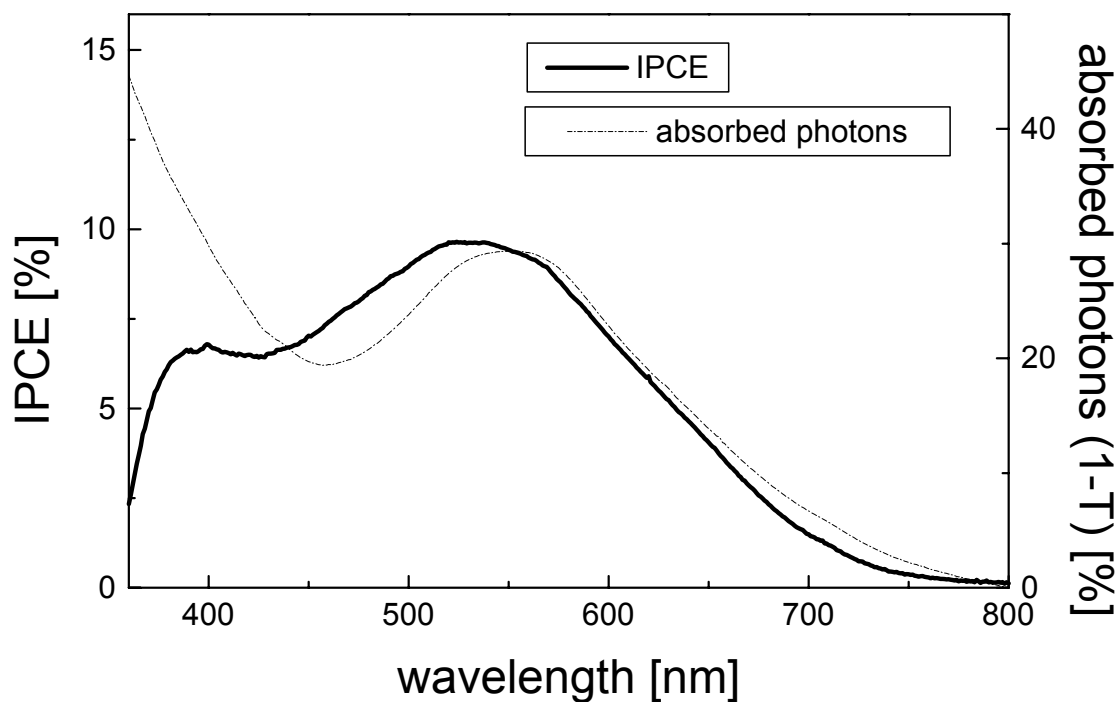


Figure 4.10: IPCE of a PTPTB/PCBM 1/3 + 10 % Nile red solar cell (—) in standard configuration in comparison with absorption spectrum in transmission of a film spin cast from the same solution on glass (---).

The dependence of the short circuit current on the illumination intensity, figure 4.11 shows a power law dependence with an exponent of 0.87. No saturation is observed in the range of the measurement. This value is in the same range and even slightly better than for the non-sensitized device.

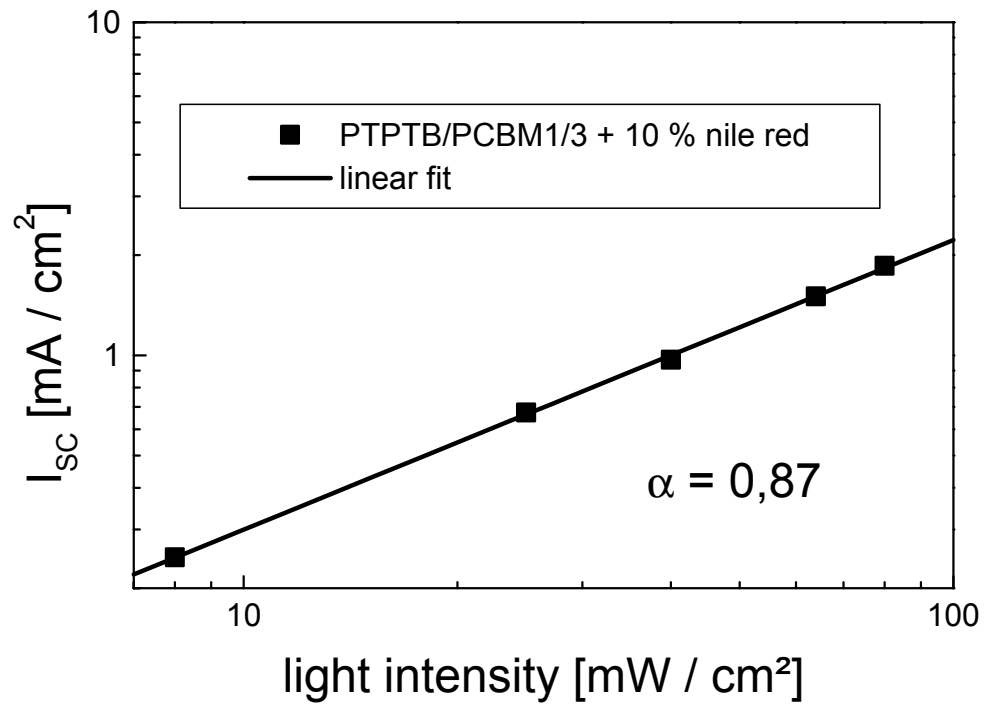


Figure 4. 11: Dependence of the short circuit current (■) on the illumination of a PTPTB/PCBM 1/3 + 10 % Nile red solar cell in standard configuration, linear fit is done by a power law dependence.

AFM picture, presented in figure 4.12, shows a rather smooth surface. The maximum height difference is in the order of 2 nm.

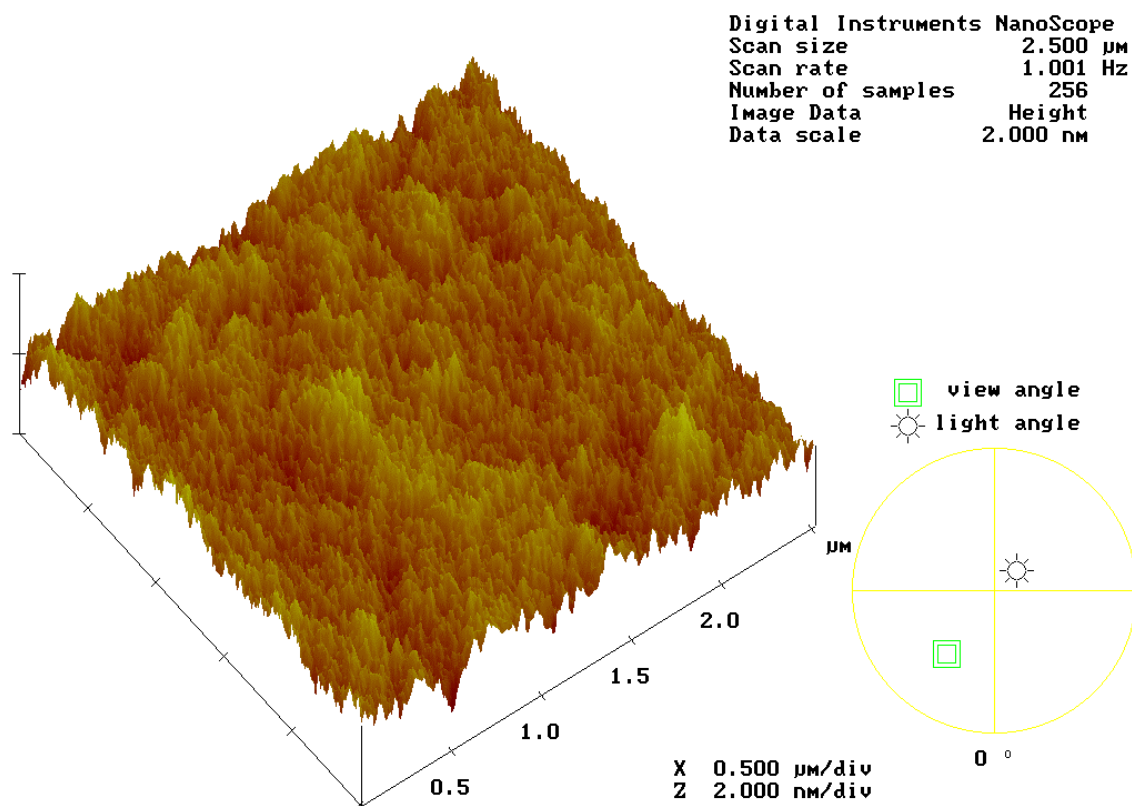


Figure 4. 12: AFM picture in tapping mode of the active layer of a PTPTB/PCBM 1/3 + 10 % Nile red device, spin cast from 0.33 % toluene solution

It can be clearly shown that the dye contributes to the photocurrent. The dye does not influence charge transport in the device and is miscible with the other components.

5 General Discussion

For conjugated polymers, energetic values of electron levels /bands are generally determined by electrochemistry. A collection of values of the used polymers is presented in table 5.1.

Table 5.1: List of the used materials with their optical parameters λ_{\max} , the maximum of the absorption, and E_{gap} , the bandgap, estimated with the onset of the optical absorption. E_{ox} and E_{red} are the oxidation and reduction values from electrochemistry cyclovoltametric measurements. Data are collected from different groups. For conversion into energy values versus vacuum, 4.9 eV vs. vacuum for the reference calomel electrode is taken.

Polymer	λ_{\max} [nm]	E_{gap} [eV] opt.	E_{ox} vs SCE	E_{red} vs SCE
PEDOT-DOP	494, (531)	2.15	-	-
PEDOT-C10	600, (660)	1.8	+0.2	-
PTPTB	585	1.6	+0.53	-1,24
EHI-ITN	797	1.2	+0.5	-0.8
PEDOT-EHI-ITN	804	1.1	+0.2	-1.0
PME-EHI-ITN	560	1.6	---	-1.1
PCBM		2.4	+1.2	

The first oxidation potential corresponds with the HOMO value, the first reduction potential with the LUMO value. It should be noted, that the electron band in solution and the solid state values might shift.

Figure 5.1 show the energy levels of the different LBP in comparison with MDMO-PPV, PCBM, ITO and Al. For MDMO-PPV, an offset to the LUMO of PCBM of 1 eV is observed, which is favourable for electron transfer. Also for pEDOT-C10, the energy difference is still more than 0.5 eV.

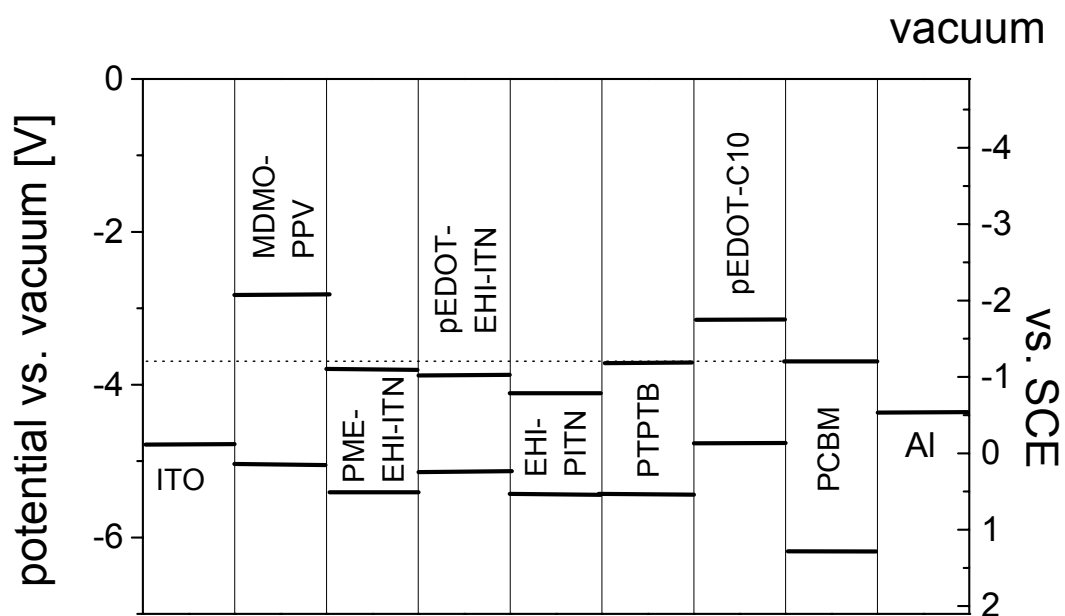


Figure 5. 1: Energy level diagram for the HOMO and LUMO levels different conjugated polymers, PCBM and ITO and Al in comparison; right axis is vs. vacuum, left axis vs. a saturated calomel electrode SCE. The vacuum level of the SCE is estimated with 5.9 eV

Table 5. 2: Photovoltaic parameters of bulk heterojunction solar cells with different low bandgap polymers.

Active layer	V_{OC} [V]	I_{SC} [mA cm^{-2}]	FF	R (+/- 1V)	η_e [%] AM1.5
PEDOT-C10/PCBM	0.17	0.13	0.32	1900	0.01
PEDOT-DOP/PCBM	0.48	0.38	0.32	4	0.08
EHI-PITN/PCBM	0.51	0.023	0.23	3	0.003
PME-EHI-PITN/PCBM	0.44	0.037	0.27	8	0.005
PEDOT-EHI-PITN/PCBM	0.13	1	0.34	46	0.06
PTPTB/PCBM	0.72	3.1	0.37	28	1.03

Table 5.2 compared the photovoltaic parameters of the different low bandgap solar cells.

Table 5.3 shows the photovoltaic parameters of the sensitized solar cells. .

Table 5. 3: Photovoltaic parameters of sensitized bulk heterojunction solar cells

Active layer	V_{OC} [V]	I_{SC} [mA cm^{-2}]	FF	R (+/- 1V)	η_e [%] AM1.5
PPV/PTPTB/PCBM	0.51	1	0.3	2000	0.20
PTPTB/PCBM +10 % Nile red	0.53	2.3	0.32	54	0.50

For the V_{OC} , the variations are not so clear. The thermodynamic limit of the V_{OC} has been discussed in the introduction. From the equivalent circuit can be seen that V_{OC} is the point, where the photocurrent is compensated through losses by the shunt resistance and the diode, i.e. it is the voltage where the dark current in the opposite direction become equal to the photocurrent.

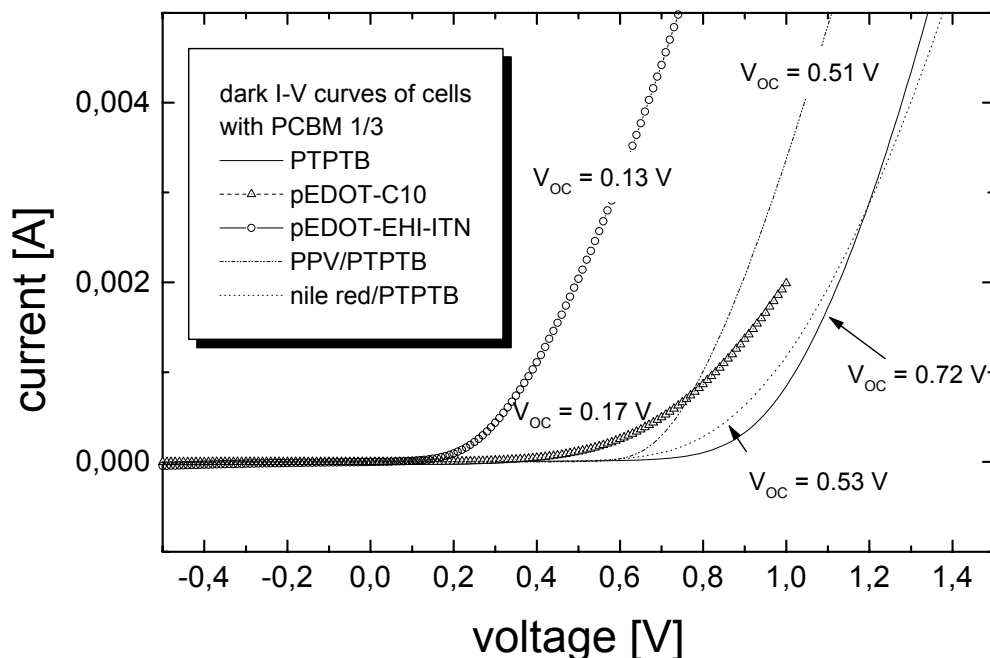


Figure 5. 2: I-V curves in the dark of different conjugated polymers/PCBM 1/3 bulk heterojunction solar cells; in comparison the open circuit voltages under 80 mW illumination, (—) PTPTB/PCBM 1/3, (-□-) pEDOT-C10/PCBM 1/3, (—○—) pEDOT-EHI-PITN, (—·—) MDMO-PPV/PTPTB/PCBM 0.5/0.5/4 and (-----) PTPTB/PCBM 1/3 + 10 % Nile red

The shift of the current injection toward lower voltages for the sensitized cells has been shown in figure 4.1 and 4.10. Figure 5.2 shows the dark I-V curves of different polymer solar cells; additionally the V_{OC} values under illumination are noted. The lower V_{OC} of the sensitized cells compared to the pristine ones is due to worsened diode behaviour and/ or shunt resistances.

6 Conclusion

Conjugated polymers with bandgaps below 2eV investigated here, show photoinduced charge transfer to PCBM. Blends of these materials can be successfully applied in bulk heterojunction solar cells. The open circuit voltage is not directly related on the bandgap of the polymer, therefore, low bandgap polymers can show similar V_{oc} like wide bandgap materials. Limitation of bandgap reduction is given by (i) closeness of the LUMO level of donor and acceptor, which is unfavourable for photoinduced charge transfer and (ii) by gap

between donor HOMO and acceptor LUMO, which limits the splitting of the quasi fermi levels.

PTPTB/ PCBM blend shows power conversion efficiencies above 1 %. Low film quality, caused by the relative short chain length, needs further improvement.

Sensitizing with wide bandgap materials contributes to the photocurrent. For efficient charge carrier collection, trap free hole current is required. Blending of small molecule dye and conjugated polymers can provide this. The V_{OC} is limited by the diode behaviour of the cells.

Electroluminescence from conjugated polymers in the near infrared is possible. The quantum yield can be significantly increased by sensitization with wide bandgap polymers.

7 References

- [1] Grünbuch der Europäischen Kommission: Komm. 2000 769
- [2] M. Green, K. Emery, K. Buecher, D.L. King, S. Igari, *Progress in Photovoltaics : Res. Appl* **5**, 51 (1997);
for current updates see also: http://www.pv.unsw.edu.au/eff/eff_tab1.html
- [3] D. Meissner, *Photon 2*, 34-37 (1999)
- [4] C.J. Brabec, F. Padinger, N.S. Sariciftci, J.C. Hummelen, *Journal of Applied Physics* **85**, No.9, 6886 (1999)
- [5] F. Padinger, C.J. Brabec, T. Fromherz, J.C. Hummelen, N.S. Sariciftci, *Opto-Electronics Review* **8**, No.4, 280 (2000)
- [6] C.J. Brabec, F. Padinger, J.C. Hummelen, R.A.J. Janssen, N.S. Sariciftci, *Synthetic-Metals*. **102**, No.1-3, 861 (1999)
- [7] M. Granström, K. Petritsch, A.C. Arias, A. Lux, M.R. Andersson, R.H. Friend, *Nature* **395**, 257 (1998)
- [8] S. E. Shaheen, C. J. Brabec, N. S. Sariciftci, *Applied Physics Letters* **78**, No.6, 841 (2001)
- [9] C.J. Brabec, S.E. Shaheen, C. Winder, N.S. Sariciftci, P. Denk, "The Effect of LiF/Metal Electrodes on the Performance of Plastic Solar Cells" submitted to: *Applied Physics Letters*
- [10] C.J. Brabec, N. S. Sariciftci, J. C. Hummelen, *Advanced Functional Materials* **11**, No.1, 15 (2001)
- [11] G.G. Wallace, P.C. Dastoor, D.L. Officer, C.O. Too, *Chemical Innovation* **30**, 1, p.14 (2000)
- [12] H. Gerischer, H. Tributsch, *Berichte der Bunsengesellschaft für Physikalische Chemie* **72**, (1968)
- [13] D.O Reagen, M. Graetzel, *Nature* **353**, p. 737 (1991)
- [14] D. Wöhrle, D. Meissner, *Advanced Materials* **3**, No.3, 129 (1991)
- [15] C.W. Tang, *Applied Physics Letters* **48**, No. 2, 183 (1986)
- [16] T. Tsuzuki, Y. Shirota, J. Rostalski, D. Meissner, *Solar Energy Materials and Solar Cells* **61**, 15, p.1 (2000)
- [17] J.H. Schön, C. Kloc, E. Bucher, B. Batlogg, *Nature* **403**, No.6768, p.408 (2000)
- [18] J.H. Schön, Ch. Kloc, B. Batlogg, *Applied Physics Letters* **77**, 16, 2473 (2000)
- [19] J.H. Schön, Ch. Kloc, E. Bucher, B. Batlogg, *Synthetic Metals* **115**, p177 (2000)

- [20] H. Antoniadis, B.R. Hsieh, M.A. Abkowitz, S.A. Jenehke, M. Stolka, *Synthetic Metals* **62**, p.265 (1994)
- [21] W. Rieß, S. Karg, V. Dyakonov, M. Meier, M. Schwoerer, *Journal of Luminescence* **60**, p. 906 (1994)
- [22] N.S. Sariciftci, L. Smilowitz, A. J. Heeger, F. Wudl, *Science* **258**, 1474 (1992)
- [23] L. Smilowitz, N.S. Sariciftci, R.Wu, C. Gettinger, A.J. Heeger, F. Wudl, *Physical-Review-B-(Condensed-Matter)* **47**, No.20, p.13835 (1993)
- [24] N.S. Sariciftci, D. Braun, C. Zhang, V.I. Srdanov, A.J. Heeger, G. Stucky, F. Wudl, *Applied Physics Letters* **62**, 585 (1993)
- [25] J.J.M. Halls, K. Pichler, R.H. Friend, S.C. Moratti, A.B. Holmes, *Applied Physics Letters* **68**, No.22, 3120 (1996)
- [26] G. Yu, J. Gao, J.C. Hummelen, F. Wudl, A.J. Heeger, *Science* **270**, 1789 (1995)
- [27] G. Yu, A.J. Heeger, *Journal of Applied Physics* **78**, No.7, 4510 (1995)
- [28] J.C. Hummelen, B.W. Knight, F. LePeq, F. Wudl, *Journal of Organic Chemistry* **60**, 532 (1995)
- [29] L. Chen, D. Godovsky, O. Inganäs, J.C. Hummelen, R.A.J. Janssen, M. Svensson, M.R. Andersson, *Advanced Materials* **12**, No. 18, p. 1367 (2000)
- [30] C.Y. Yang, A.J. Heeger, *Synthetic Metals* **83**, p.85 (1996)
- [31] C.J. Brabec, H. Johannson, F. Padinger, H. Neugebauer, J.C. Hummelen, N.S. Sariciftci, *Solar Energy Materials and Solar Cells*, **61**, No1; 19-33 (2000)
- [32] C.J. Brabec, N.S. Sariciftci, Chapter 15 in “Semiconducting Polymers” edited by G. Hadziannou and P. F. van Hutten, (2000), p. 515-560
- [33] HOMO = Highest Occupied Molecular Orbital
LUMO = Lowest Unoccupied Molecular Orbital
- [34] N.S. Sariciftci, A.J. Heeger, Chapter 8 in “*Handbook of Organic Conductive Molecules and Polymers*” Vol.1, Edited by H.S. Nalwa 1997 John Wiley & Sons,
- [35] C.J. Brabec, G. Zerza, G. Cerullo, S. De-Silvestris, S. Luzatti, J.C. Hummelen, S. Sariciftci, *Chemical Physics Letters* **340**, No. 3-4, p.232 (2001)
- [36] G. Lanzari, S. Froloy, M. Nisoli, P.A. Lane, S. De-Silvestri, R. Tubino, F. Abbate, Z.V. Vardeny, *Synthetic Metals* **84**, No. 1-3, p.517 (1997)
- [37] J.J. Dittmer, E.A. Marseglia, R.H. Friend, *Advanced-Materials* **12**, No.17, 1270 (2000)
- [38] J.J. Dittmer, R. Lazzaroni, P. Leclere, P. Moretti, M. Granstrom, K. Petritsch, E.A. Marseglia, R.H. Friend, J.L Bredas, H. Rost, A.B. Holmes, *Solar Energy Materials And Solar Cells* **61**, No.1, 53 (2000)

- [39] I.D. Parker, *Journal of Applied Physics* **75**, No.3, 1656 (1994)
- [40] N.S. Sariciftci, D. Braun, C. Zhang, V. I. Srdanov, A. J. Heeger, G. Stucky, F. Wudl, *Applied Physics Letters* **62**, p.585
- [41] J.J.M Halls, C.A. Walsh, N.C. Greenham, E.A. Marseglia, R.H. Friend, S.C. Moratti, A.B. Holmes, *Nature* **376**, No.6540, 498 (1995)
- [42] L.S. Roman, M.R. Andersson, T. Yohannes, O. Inganäs, *Advanced Materials* **9**, No.15 (1997)
- [43] G.Yu, K.Pakbaz, A.J. Heeger, *Applied Physics Letters* **64**, p.3422 (1994)
- [44] J.H. Burroughes, D.D.C. Bradley, A.R. Brown, R.N. Marks, K. Mackay, R.H. Friend, P.L. Burns-PL, A.B. Holmes, *Nature* **347**, No.6293, p.539 (1990) das, M. Lögdlund, W.R. Salaneck, *Nature* **397**, p.121 (1999)
- [45] R.H. Friend, R.W. Gymer, A.B. Holmes, J.H. Burroughes, R.N. Marks, C. Taliani, D.D.C. Bradley, D.A. Dos Santos, J.L. Br ???
- [46] C.J. Brabec, A. Cravino, D. Meissner, N.S. Sariciftci, T. Fromherz, M. T. Rispens, L. Sanchez, J.C. Hummelen, On the Origin of the Open Circuit Voltage of Plastic Solar Cells, accepted by *Advanced Functional Materials* (2001)
- [47] L. S. Hung, C. W. Tang, and M. G. Mason, *Applied Physics Letters* **70**, 152 (1997)
- [48] S.E. Shaheen, G.E. Jabbour, M.M. Morrell, Y. Kawabe, B. Kippelen, N. Peyghambarian, M.F. Nabor, R. Schlaf, E.A. Mash, and N.R. Armstrong, *Journal of Applied Physics* **84**, 2324 (1998)II
- [49] Jörn Rostalski Dissertation Rheinisch-Westfälischen Technischen Hochschule Aachen „Der photovoltaisch aktive Bereich molekularer organischer Solarzellen“ (1999)
- [50] J.Ronstalski, D. Meissner, *Solar Energy Materials and Solar Cells* **63**, p.37 (2000)
- [51] S.Kuran, A. Stakr-Hauser, S. Roth, Handbook of Organic Conductive Molecules and Polymers, Vol.2, Edited by Hari Singh Nalwa Chapter 1, p.13-32, 1997 John Wiley & Son
- [52] R.E. Peierls, Quantum Theory of Solids (Oxford Univeristy Press, London, 1955)
- [53] J.L. Brédas, A.J. Heeger, F. Wudl, *Journal of Chemical Physics* **85**, _No.8, p.4673 [1986]
- [54] J. Roncali *Chemical Review* **97**, 173-205 (1997)
- [55] Kiesboms et al., “Synthesis, Electric and Optical Properties of Conjugated Polymers” in *Handbook of Advanced Electronic and Photonic Materials and Devices* **8** (Conducting Polymers), Edited by Hari Singh Nalwa., p.38-47 (2000)

- [56] L.Chen, L.S.Roman, D.M.Johansson, M. Svensson, M.R.Andersson, R.A.J.Janssen O.Inganäs, *Advanced Materials* **12**, No.15 1110 (2000)
- [57] K. Petritsch, J.J. Dittmer, E.A. Marseglia, R.H. Friend, A. Lux, G.G. Rozenberg, S.C. Moratti, A.B. Holmes, *Solar Energy Materials and Solar Cells* **61**, No.1, 63 (2000)
- [58] L. Sicot, C. Fiorini, A. Lorin, P. Raimond, C. Sentein, J.M. Nunzi, *Solar Energy Materials & Solar Cells* **63**, p. 49 (2000)
- [59] A.A. Zakhidoc, K. Tada, K. Yoshino, *Synthetic Metals* **71**, p.2113 (1995)
- [60] A.Fujii, A.A. Zhakjidov, V.V. Borovkov, Y.Ohmori, K. Yoshino, *Japanese Journal of Applied Physics Part 2* **35**, No.11, p.1438 (1996)
- [61] J.J.M. Halls, J. Cornil, D.A. dos Santos, R. Silbey, D. -H. Hwang, A.B. Holmes, J. L. Bredas, R.H. Friend, *Physical Review B* **60**, No. 8, p.5721 (1999)
- [62] T. Förster. *Discuss. Faraday Soc.* **27** (1959), p. 7
- [63] F. Wudl, M. Kobayashi, A.J. Heeger, *Journal of Organic Chemistry* **49**, p3382 (1984)
- [64] H. Meng, F. Wudl *to be published* "Tuning Low Band Gap Control of Highly Stable Isothiophennaphtalene Conjugated Polymers"
- [65] A. Dhanabalan, P.A. Van-Hal, J.K.J. Van-Duren, J.L.J. Van-Dongen, R.A.J. Janssen, *Synthetic-Metals* **119**, No.1-3, 169 (2001)
- [66] J.K.J. van Duren, A. Dhanabalan, P.A. van Hal, R.A.J. Janssen, "Low-bandgap polymer photovoltaic cells" to be published
- [67] M.Berggren, O.Inganäs, G.Gustafsson, J.Rasmusson, M.R.Andersson, T.Hjertberg, O.Wennerström, *Nature* **372**, 444 (1994)
- [68] D. R. Baigent, P. J. Hamer, R. H. Friend, S. C. Moratti, A. B. Holmes, *Synthetic Metals* **71**, 2175 (1995)
- [69] J. Kido, H. Shionoya, K. Nagai, *Applied Physics Letters* **67**, 2281 (1995)
- [70] Fuh, J. Li, A. Corkan, J. S. Lindsey, *Photochemistry and Photobiology* **68**, 141 (1998)

Eidesstattliche Erklärung:

Ich erkläre an Eides statt, dass ich die vorliegende Diplomarbeit selbstständig und ohne fremde Hilfe verfasst, andere als die angegebenen Quellen und Hilfsmittel nicht benutzt bzw. die wörtlich oder sinngemäß entnommenen Stellen als solche kenntlich gemacht habe.

Linz, September 2001

Winder Christoph

Die vorliegende Diplomarbeit entstand zwischen Oktober 2000 und September 2001 am Forschungsinstitut für Organische Solarzellen der Technisch-Naturwissenschaftlichen Fakultät der Universität Linz unter Betreuung von Prof. Dr. N. S. Sariciftci und Dr. Christoph Brabec.

Curriculum Vitae

Linz, September 2001

Angaben zu meiner Person

- Geboren am 27.12.1975 in Bregenz
- Familienstand: verheiratet

Schulbildung

- 1982-1986 VS Hörbranz
- 1986-1994 Gymnasium BG Bregenz Blumenstrasse, neusprachlicher Zweig
- 1994 -2001: Studium an der JK Universität Linz; Technische Chemie und WiTech

Praxis

- Juli- September 1998: 10 wöchiges Praktikum bei der *Fluka Chemie AG* in Buchs SG, Schweiz
- August- Oktober 1999, Februar 2000: Projektmitarbeiter am *Institut für physikalische Chemie* im Rahmen des EU Joule III-Projektes
- August- September 2000: 8-wöchiges Praktikum bei *Omicron Surface Science Ltd* in East Grinstead, Großbritannien
- Studienjahr 2000/2001: Tutor für Physikalische Chemie Übungen an der Universität Linz

Weitere Arbeitgeber

- Sommer 1991- 1993: Fa. Revital Baugesellschaft, 6850 Feldkirch
- Sommer 1994- 1997: Post und Telekom Österreich

Interessen

- Wissenschaftlich: Photovoltaik, Umwelttechnologie, neue Materialien
- Privat: Musik, Reisen, Sport

Sprachkenntnisse

Englisch: fließend und verhandlungssicher,

Französisch: für den Anstand

Curriculum Vitae

Linz, September 2001

Personal Data

- Born on the 27th of December 1975 in Bregenz, Austria
- Martial status: married

Education

- 1982-1986 primary school Hörbranz
- 1986-1994 Grammar school BG Bregenz Blumenstrasse, branch: modern language
- 1994 -2001: studies at the university of Linz, *technical chemistry* and *technical chemistry and management*

Related Experience

- July- September 1998: traineeship at the *Fluka Chemie AG* in Buchs SG, Switzerland
- August-October 1999, February 2000: project collaborator at the *institute for physical chemistry*
- August- September: IAESTE traineeship at *Omicron Surface Science Ltd* in East Grinstead, Great Britain
- 2000/2001: students tutor for physical chemistry at the university of Linz

Further Employer

- Summer 1991- 1993: Fa. Revital Baugesellschaft, 6850 Feldkirch
- Summer 1994- 1997: Post und Telekom Österreich

Interests

- Scientific: photovoltaics, new materials, environmental protection
- Private: music, traveling, sports

Foreign Languages

English: business fluent

French: for policy and manners

List of Publications

- The Influence of Ordering on the Photoinduced Charge Transfer in Composites of Phenyl-type substituted Polythiophenes with Methanofullerenes
C.J. Brabec, C.Winder, M.Scharber, N.S. Sariciftci, M.R.Andersson, O.Inganäs, J.C.Hummelen
Mat. Res. Symp. Proc. Vol. **598**, B 3.24.1-6 (2000)
- Influence of Disorder on the Photoinduced Excitations in Phenyl Substituted Polythiophenes
C.J. Brabec, C.Winder, M.Scharber, N.S. Sariciftci, J.C.Hummelen, M.R.Andersson
Accepted by *Journal of Chemical Physics*
- A Soluble Low-Bandgap Polymer for Near-IR Optoelectronic Devices
C.J.Brabec, Christoph Winder, N.Serdar Sariciftici, Jan.C.Hummelen, Anantharaman Dhanabalan, Paul A.van Hal, René A.J.Janssen
Submitted to *Applied Physics Letters*
- The Effect of LiF/Metal Electrodes on the Performance of Plastic Solar Cells
Christoph J. Brabec, Sean E. Shaheen, Christoph Winder, N. Serdar Sariciftci
Accepted by *Applied Physics Letters*
- Christoph Winder, Christoph J. Brabec, N. Serdar Sariciftci, Rene. A. J. Jansser, Jan. C. Hummelen “Sensitization of Low Bandgap Polymer Bulk Heterojunction Solar Cells” accepted by *thin film solid*

Contribution to Conferences

- “The Influence of Ordering on the Photoinduced Charge Transfer in Composites of Phenyl-type substituted Polythiophenes with Methanofullerenes”
C.J. Brabec, C. Winder, M. Scharber, N.S. Sariciftci, M.R. Andersson, O. Inganäs, J.C. Hummelen, MRS 99 Boston, Poster Contribution
- “Sensitization of Low Bandgap Polymer Bulk Heterojunction Solar Cells” C. Winder, C. J. Brabec, G. Matt, N. S. Sariciftci, J. C. Hummelen, R. A. J. Janssen
EMRS 2001 spring meeting Strassbourg, Poster session P/P2.34
- “Device Operation of Conjugated Polymer/Fullerene Bulk Hetero-Junction Solar Cells” G. Matt, T. Munters, T. Fromherz, C. Winder, D. Vanderzande, J.C. Hummelen, N.S. Sariciftci, C.J. Brabec, MSS10 2001 Linz